0-315-03708-3

National Library of Canada — Bibliothèque nationale du Canada

Canadian Theses Division — Division des thèses canadiennes

Ottawa, Canada K1A 0N4

51603

PERMISSION TO MICROFILM — AUTORISATION DE MICROFILMER

• Please print or type — Écrire en lettres moulées ou dactylographier

Full Name of Author — Nom complet de l'auteur

KRZYSZTOF LUCJAN WENSLAW

Date of Birth — Date de naissance

Jan. 19-th, 1950

Country of Birth — Lieu de naissance

POLAND

Permanent Address — Résidence fixe

607E Michener Park, Edmonton, Alta T6H 5A1

Title of Thesis — Titre de la thèse

Flow Characteristics in Two Successive Pipe Elbows

University — Université

Univ. of Alberta

Degree for which thesis was presented — Grade pour lequel cette thèse fut présentée

M.Sc.

Year this degree conferred — Année d'obtention de ce grade

1981

Name of Supervisor — Nom du directeur de thèse

J.S. Kennedy & C.M. Rodkiewicz

Permission is hereby granted to the NATIONAL LIBRARY OF CANADA to microfilm this thesis and to lend or sell copies of the film.

The author reserves other publication rights, and neither the thesis nor extensive extracts from it may be printed or otherwise reproduced without the author's written permission.

L'autorisation est, par la présente, accordée à la BIBLIOTHÈQUE NATIONALE DU CANADA de microfilmer cette thèse et de prêter ou de vendre des exemplaires du film.

L'auteur se réserve les autres droits de publication; ni la thèse ni de longs extraits de celle-ci ne doivent être imprimés ou autrement reproduits sans l'autorisation écrite de l'auteur.

Date

~~Dec~~ Dec. 9-th / 1980

Signature

Krzysztof

NL-91 (4/77)

National Library of Canada
Collections Development Branch

Canadian Theses on
Microfiche Service

Bibliothèque nationale du Canada
Direction du développement des collections

Service des thèses canadiennes
sur microfiche

NOTICE

The quality of this microfiche is heavily dependent upon the quality of the original thesis submitted for microfilming. Every effort has been made to ensure the highest quality of reproduction possible.

If pages are missing, contact the university which granted the degree.

Some pages may have indistinct print especially if the original pages were typed with a poor typewriter ribbon or if the university sent us a poor photocopy.

Previously copyrighted materials (journal articles, published tests, etc.) are not filmed.

Reproduction in full or in part of this film is governed by the Canadian Copyright Act, R.S.C. 1970, c. C-30. Please read the authorization forms which accompany this thesis.

THIS DISSERTATION
HAS BEEN MICROFILMED
EXACTLY AS RECEIVED

AVIS

La qualité de cette microfiche dépend grandement de la qualité de la thèse soumise au microfilmage. Nous avons tout fait pour assurer une qualité supérieure de reproduction.

S'il manque des pages, veuillez communiquer avec l'université qui a conféré le grade.

La qualité d'impression de certaines pages peut laisser à désirer, surtout si les pages originales ont été dactylographiées à l'aide d'un ruban usé ou si l'université nous a fait parvenir une photocopie de mauvaise qualité.

Les documents qui font déjà l'objet d'un droit d'auteur (articles de revue, examens publiés, etc.) ne sont pas microfilmés.

La reproduction, même partielle, de ce microfilm est soumise à la Loi canadienne sur le droit d'auteur, SRC 1970, c. C-30. Veuillez prendre connaissance des formules d'autorisation qui accompagnent cette thèse.

LA THÈSE A ÉTÉ
MICROFILMÉE TELLE QUE
NOUS L'AVONS REÇUE

Ottawa, Canada
K1A 0N4

NL-339 (Rev. 8/80)

THE UNIVERSITY OF ALBERTA

FLOW CHARACTERISTICS IN TWO SUCCESSIVE PIPE ELBOWS

BY

© KRZYSZTOF L. WENSLAW

A THESIS

SUBMITTED TO THE FACULTY OF GRADUATE STUDIES

IN PARTIAL FULFILMENT OF THE REQUIREMENTS FOR THE DEGREE

OF MASTER OF SCIENCE

DEPARTMENT OF MECHANICAL ENGINEERING

EDMONTON, ALBERTA

SPRING, 1981

THE UNIVERSITY OF ALBERTA

RELEASE FORM

NAME OF AUTHOR KRZYSZTOF L. WENSLAW

TITLE OF THESIS FLOW CHARACTERISTICS IN TWO SUCCESSIVE PIPE ELBOWS

DEGREE FOR WHICH THESIS WAS PRESENTED MASTER OF SCIENCE

YEAR THIS DEGREE GRANTED 1980

Permission is hereby granted to THE UNIVERSITY OF ALBERTA LIBRARY to reproduce single copies of this thesis and to lend or sell such copies for private, scholarly or scientific research purposes only.

The author reserves other publication rights, and neither the thesis nor extensive extracts from it may be printed or otherwise reproduced without the author's written permission.

(signed) K.Wenslaw

PERMANENT ADDRESS:

607 E Michener Park

Edmonton, Alberta

T6H 5A1

DATED Jan. 14/1981

THE UNIVERSITY OF ALBERTA

FACULTY OF GRADUATE STUDIES AND RESEARCH

The undersigned certify that they have read, and recommend to the Faculty of Graduate Studies and Research, for acceptance, a thesis entitled "FLOW CHARACTERISTICS IN TWO SUCCESSIVE PIPE ELBOWS" submitted by Krzysztof Lucjan Wenslaw in partial fulfilment of the requirements for the degree of Master of Science.

J.S. Kennedy
Supervisor

C.A. Rodling
Supervisor

M. Gyarmathy

Date September 23, 1980

ABSTRACT

The behavior of steady flow in two successive 90° pipe elbows of large dimensionless curvature (a/R = 0.357) has been investigated experimentally. The flow has been established in terms of the dimensionless parameters: the Reynolds (or Dean) number, Re or D, the non-dimensional length of the spacer between the elbows, L', and the angle between the elbows' planes of curvature, Ψ.

The influence of the dimensionless variables on the laminar secondary flow has been shown for the case of uniform velocity profile at the entrance and the types of the secondary flow patterns have been classified. Also the association of the flow types to the two basic flow structures, observed when the elbows have formed the U shape and the S shape, has been given.

The positions of the separation lines and the reattachment lines have been measured and presented as functions of the dimensionless variables, both for the uniform velocity profile and the fully developed flow at the entrance.

The flow inside the separation zones (backflow), the influence of the second elbow on the flow upstream and the transition to turbulence also have been observed.

ACKNOWLEDGEMENTS

The author wishes to express his thanks and acknowledgements to the following:

- Dr.J.S.Kennedy and Dr.C.M.Rodkiewicz for their guidance and supervision of the thesis, also for proof reading the manuscript for grammar and spelling.
- The Mechanical Engineering Machine Shop for technical assistance.

TABLE OF CONTENTS

CHAPTER		PAGE
I.	INTRODUCTION	
	1.1 Introductory Remarks	1
	1.2 Literature Survey	2
	1.3 Objectives of the Thesis	10
II.	DIMENSIONLESS PARAMETERS	
	2.1 Introductory Remarks	11
	2.2 Dimensionless Parameters	12
III.	APPARATUS	
	3.1 Apparatus Description	15
	3.2 Flow Visualisation	17
	3.3 Apparatus Limitations	18
IV.	EXPERIMENT	
	4.1 Experimental Range	27
	4.2 Experimental Procedure	28
	4.3 Presentation of Results	30
V.	SOME OBSERVED FLOW PHENOMENA	
	5.1 Secondary Flow and Influence of the Second Elbow	35
	5.2 Separation	37
	5.3 Turbulence	43
VI.	SECONDARY FLOW PATTERNS	
	6.1 Introductory Remarks	79
	6.2 "U" Configuration ($\Psi = 0°$)	81
	6.3 "S" Configuration ($\Psi = 180°$)	81
	6.4 Flow Patterns for $0° < \Psi < 180°$	82

TABLE OF CONTENTS (continued)

CHAPTER		PAGE
VII.	CONCLUSIONS	
	7.1 Summary	115
	7.2 Suggestions for Further Work	116
REFERENCES		117
APPENDIX	TABLES OF RESULTS FOR SECTION 5.2	121

LIST OF TABLES

Table	Description	Page
1	Apparatus Data	21
2	Cross-Sections and Dye Pipes Positions	25
3	Secondary Flow Patterns - Flow Types with a Long Spacer ($L' > 0.85$)	86
4	Secondary Flow Patterns - Flow Types with a Short Spacer ($L' \leq 0.85$)	86
A.1	Dependance of L_1 on Ψ and Re for a Uniform Velocity Profile and $L' = 0$	87
A.2	Dependance of L_1 on Ψ and Re for a Uniform Velocity Profile and $L' = 0.85$	122
A.3	Dependance of L_1 on Ψ and Re for a Uniform Velocity Profile and $L' = 1.8$	123
A.4	Dependance of L_1 on Ψ and Re for a Uniform Velocity Profile and $L' = 3.15$	124
A.5	Dependance of L_3 on Ψ and Re for a Uniform Velocity Profile and $L' = 0$	125
A.6	Dependance of L_3 on Ψ and Re for a Uniform Velocity Profile and $L' = 0.85$	126
A.7	Dependance of L_3 on Ψ and Re for a Uniform Velocity Profile and $L' = 1.8$	127
A.8	Dependance of L_3 on Ψ and Re for a Uniform Velocity Profile and $L' = 3.15$	128
A.9	Dependance of L_5 on Ψ and Re for a Unoform Velocity Profile and $L' = 0$	129
		130

LIST OF TABLES (continued)

Table	Description	Page
A.10	Dependance of L_5 on Ψ and Re for a Uniform Velocity Profile and L' = 0.85	131
A.11	Dependance of L_5 on Ψ and Re for a Uniform Velocity Profile and L' = 1.8	132
A.12	Dependance of L_5 on Ψ and Re for a Uniform Velocity Profile and L' = 3.15	133
A.13	Dependance of L_1 on L', Ψ and Re for a Fully Developed Velocity Profile	134
A.14	Dependance of L_3 on L', Ψ and Re for a Fully Developed Velocity Profile	135
A.15	Dependance of L_5 on L', Ψ and Re for a Fully Developed Velocity Profile	136

LIST OF FIGURES

Figure		Page
1	Apparatus Layout	20
2	Apparatus - Elbows ($\Psi = 90°$; $L' = 3.15$)	23
3	Apparatus - General View ($\Psi = 0°$)	23
4	Apparatus - Elbows ($L' = 0$)	24
5	Apparatus - General View ($\Psi = 180°$)	24
6	Mirrors and Camera Positions	26
7	Coordinate System	32
8	Notation of Elbows and Cross - Sections	33
9	Standard Cross - Sections Presentation, Dye Pipe Locations at Cross - Sections and Flow Symbols	34
10	Influence of the Second Elbow on the Flow in the Spacer	46
11	Separation and Vortex Formation on a Circular Cylinder and Flow in the Boundary Layer Near a Point of Separation	47
12	Separation in a Two - Dimensional Elbow	47
13	First Separation as a Function of Reynolds Number	48
14	Vortices Due to the Second Separation	49
15	Second Separation - Dye Motion	50
16	Backflow Streamlines in the First Separation	51
17	Backflow in the Spacer	52

LIST OF FIGURES (continued)

Figure		Page
18	First Separation - Dye Motion Due to the Backflow	53
19	Backflow in the First Elbow	54
20	First Separation - Reattachment Line	54
21	Second Separation as a Function of Reynolds Number	55
22	First Separation Line Position versus Reynolds (Dean) Number as a Function of Angle Ψ for a Uniform Velocity Profile and L' = 0	56
23	First Separation Line Position versus Reynolds (Dean) Number as a Function of Angle Ψ for a Uniform Velocity Profile and L'=0.85	57
24	First Separation Line Position versus Reynolds (Dean) Number as a Function of Angle Ψ for a Uniform Velocity Profile and L'=1.8	58
25	First Separation Line Position versus Reynolds (Dean) Number as a Function of Angle Ψ for a Uniform Velocity Profile and L'=3.15	59
26	First Separation - Reattachment Line Position versus Reynolds (Dean) Number as a Function of Angle Ψ for a Uniform Velocity Profile and L'= 0	60
27	First Separation - Reattachment Line Position versus Reynolds (Dean) Number	

LIST OF FIGURES (continued)

Figure		Page
	as a Function of Angle Ψ for a Uniform Velocity Profile and L'= 0.85	61
28	First Separation - Reattachment Line Position versus Reynolds (Dean) Number as a Function of Angle Ψ for a Uniform Velocity Profile and L'= 1.8	62
29	First Separation - Reattachment Line Position versus Reynolds (Dean) Number as a Function of Angle Ψ for a Uniform Velocity Profile and L'= 3.15	63
30	Second Separation Line Position versus Reynolds (Dean) Number as a Function of Angle Ψ for a Uniform Velocity Profile and L'=0	64
31	Second Separation Line Position versus Reynolds (Dean) Number as a Function of Angle Ψ for a Uniform Velocity Profile and L'=0.85	65
32	Second Separation Line Position versus Reynolds (Dean) Number as a Function of Angle Ψ for a Uniform Velocity Profile and L'=1.8	66
33	Second Separation Line Position versus Reynolds (Dean) Number as a Function of Angle Ψ for a Uniform Velocity Profile and L'=3.15	67
34	First Separation Line Position versus Reynolds (Dean) Number as a Function of Angle Ψ for a Fully Developed Velocity Profile	

LIST OF FIGURES (continued)

Figure		Page
	and L' = 0	68
35	First Separation Line Position versus Reynolds (Dean) Number as a Function of Angle Ψ for a Fully Developed Velocity Profile and L'= 3.15	69
36	First Separation-Reattachment Line Position versus Reynolds (Dean) Number as a Function of Angle Ψ for a Fully Developed Velocity Profile and L'= 0	70
37	First Separation-Reattachment Line Position versus Reynolds (Dean) Number as a Function of Angle Ψ for a Fully Developed Velocity Profile and L'= 3.15	71
38	Second Separation Line Position versus Reynolds (Dean) Number as a Function of Angle Ψ for a Fully Developed Velocity Profile and L'= 0	72
39	Second Separation Line Position versus Reynolds (Dean) Number as a Function of Angle Ψ for a Fully Developed Velocity Profile and L'= 3.15	73
40	Fully Laminar Flow with the Backflow	74
41	Laminar Vortices Produced by the First Separation	74
42	Laminar Flow Center (Re = 1407)	75

LIST OF FIGURES (continued)

Figure		Page
43	Instabilities Produced by the First Separation	75
44	Laminar Disturbances at the Outer Curvature of the First Elbow	76
45	Instabilities Produced by the Second Separation	76
46	Laminar Flow Center (Re = 2221)	77
47	Instabilities Outside the Laminar Center	77
48	"U" Configuration Instabilities (Re = 1507)	78
49	"U" Configuration Instabilities (Re = 2200)	78
50	Flow Type A0 - Left Coil (DP-Ko)	88
51	Flow Type A0 - Two Coil Structure	89
52	Flow Type A0 - Left Coil (DP-A⊙)	90
53	Flow Type B0 - Lower Coils	91
54	Flow Type B0 - Upper Coils	92
55	Flow Type B1 - Upper Coils	93
56	Flow Type B1 - Lower Coils	94
57	Flow Type B1 - Right Coils	95
58	Basic Flow Types	96
59	Area of the Flow Types Existence	97
60	Flow Type A1 - Left Coil	98
61	Flow Type A1 - Two Coil Structure	99
62	Flow Type A1 - Left Coil and Final Vortex	100
63	Flow Type A2 - Lower Left Coil and Backflow	101

LIST OF FIGURES (continued)

Figure		Page
64	Flow Type A3 - Upper Right and Lower Left Coils	102
65	Flow Type A2 - Upper and Lower Right Coils, Final Vortex	103
66	Flow Type A3 - Right Coils and Final Vortex	103
67	Flow Type A2 - Lower Left Coil and Final Vortex	104
68	Flow Type A3 - Left Coils and Final Vortex	104
69	Flow Type AB - Lower Coils	105
70	Flow Type AB - Lower Right Coils	106
71	Flow Type AB - Lower Left Coil, Two Coils Structure in the Spacer and Final Vortex	107
72	Flow Type B2 - Large ψ	108
73	Flow Type B2 - Lower Right Coil and Final Vortex	109
74	Flow Type B2 - Lower Left Coil	110
75	Flows Type B2 - Different ψ	111
76	Flow Type B2 - Lower Left Coil and Final Vortex	112
77	Flow Type B2 - Lower Right Coil	113
78	Final Vortex	114

LIST OF SYMBOLS

a	radius of the pipe
D	Dean number ; $D = 2\ Re\ (2a/R)^{\frac{1}{2}}$
d	diameter of the pipe ; $d = 2a$
d_p	internal diameter of the pipe for the experiments with a uniform velocity profile
K	Dean constant ; $K = \frac{1}{2}\ Re^2\ a/R$
L	length of a spacer
L'	dimensionless lenght of a spacer
L_1	separation line position due to the separation in the first elbow and a spacer or the second elbow, measured parallel to a spacer axis from the cross - section 1 (positive value if downstream)
L_3	reattachment line position for the separation which originates at L_1, usually in the first elbow, measured parallel to a spacer axis from the cross - section 3 (positive value if downstream)
L_5	separation line position due to the separation in the second elbow and/or the outlet pipe, measured parallel to the outlet pipe axis from the cross - section 5 (positive value if downstream)
L'_1, L'_3, L'_5	dimensionless values of the L_1, L_3 and L_5 measured in degrees of an elbow angle (angle θ) from a cross-section of reference along an elbow axis or as the dimensionless values : L_1/d, L_3/d, L_5/d from this cross - section along a spacer or the outlet pipe

LIST OF SYMBOLS (continued)

L_p	length of the tube for the experiments with a uniform velocity profile
p	static pressure
Q	volumetric flow rate
R	radius of curvature
r	radial distance in a plane cross - section of an elbow
Re	Reynolds number ; $Re = Ud/\nu$
U	mean axial velocity
u	relative axial velocity (total axial velocity = U+u)
v	peripheral component of velocity
w	radial component of velocity
θ	angle between a bend section and the bend inlet
λ_c, λ_s	resistance coefficients of a curved and a straight pipe, respectively ; defined by: λ = 2d (change of pressure) / ρU^2 (pipe length)
μ	dynamic viscosity of fluid
ν	kinematic viscosity of fluid
ρ	density of fluid
ϕ	angle in a plane cross - section of an elbow
Ψ	angle between the curvature planes of the elbows

LIST OF ABBREVIATIONS

(used in figures and tables only)

A to O	dye pipe symbols (see Table 2)
C.C.1, C.C.2	center of curvature, first or second elbow
DP-	dye pipe
I.C.1, I.C.2 or I	inner curvature, first or second elbow
O.C.1, O.C.2 or O	outer curvature, first or second elbow
i	inner } dye pipe
l	left } dye pipe
o	outer } dye pipe
r	right } dye pipe
X1 to X7	cross - section symbols (see Table 2)

CHAPTER 1

INTRODUCTION

1.1 Introductory Remarks

Problems associated with fluid motion through two or more elbows, have attracted a good deal of attention recently, mainly because of their possible relevance to many engineering or physiological situations. For example, a pipe line in practical use often has many bent portions located close to one another and the flows through these elbows are affected by their relative positions. In this case, the total bend loss is not equal to the sum of the individual elbow losses as would be the case if the elbows were located separately sufficiently far apart in a pipe line. This is due to the mutual interference of the elbows on the flow.

Another possible application of this work is the blood flow in the cardiovascular system: two 90° elbows with no spacer and angle $\Psi = 15°$ can simulate the human aortic arch. In contrast to the interests of engineering, where the increase in resistance due to curvature is of principal interest, a knowledge of the velocity distribution is required for the study of the cardiovascular system. Through a knowledge of the velocity distribution, the distribution of injected substances and the effects of the distribution of wall shearing stress on the formation of arterial lesions may be better understood.

1.2 Literature Survey

Only a few studies on the subject of fluid flow in pipes with two or more bends combined have been carried out, but much attention has been directed to the more general, and theoretically simpler problem associated with the fluid motion through a curved tube.

The first investigation of loss of head in a coiled tube was done by Eustice (1911), who carried out color band experiments and classified the flows as laminar, double helical and turbulent. Because of the elliptical cross-section of the tube used (due to the bending process employed) the results obtained for head loss were of little practical significance.

The theoretical behavior of the steady motion of a viscous fluid in a curved tube having a circular cross-section, was first considered by Dean (1927, 1928). In this analysis it was found necessary to assume that the dimensionless curvature of the pipe (ratio a/R) is small. In the first approximation (by Fourier - series analysis method) to the Navier-Stokes equations (Dean, 1927) the relation between the rate of flow and the pressure gradient was found to be independent of the curvature of the tube, but in a higher order analysis, (Dean 1928, fourth approximation) the reduced flow due to curvature was determined to be a function of a single constant $K=\frac{1}{2}Re^2a/R$. The problem of determining the relation between flow rate and pressure gradient in any curved pipe of small dimensionless curvature therefore

reduced to that of finding a single function f(K). Dean showed that his analysis was in good qualitative agreement with Eustice's (1911) experiment, reliable for values of K less than 576, and gave an equation for the axial pressure drop. This analysis cannot be used to determine the velocity distribution which is important in many engineering problems.

White (1929) continued the experimental investigation of laminar motion in a curved pipe for fully developed entrance profile and small dimensionless curvature. In his paper an empirical equation for the axial pressure drop in a coiled pipe was suggested. Also, limitations on the application of Dean's theory and a comparison with Eustice's experiment were given. White concluded, that even with the small dimensionless curvature of a pipe (a/R=1/50) flow was fully laminar up to Re=6000. This result was experimentally verified by Taylor (1929) by repetition of the Eustice experiment, but with focus on turbulence (three pipes of small dimensionless curvature were used).

Adler (1934) showed that the ratio of the resistance coefficients for the curved and a straight pipe of the same radius, depends only on K (the constant introduced by Dean) as long as the motion is laminar.

Based on the White, Taylor, and Adler experiments, several attempts have been made to extend the solution over the entire range of laminar flow.

Barua (1963) deduced from experimental results that

for large K, motion outside the boundary layer is mostly confined to planes parallel to the plane of symmetry of the pipe. This concept led to the prediction that the effect of curvature is to increase the resistance coefficient of the curved pipe relative to that of the same pipe if it was straight, according to the empirical formula

$$\frac{\text{res. coeff. curved pipe } \lambda_c}{\text{res. coeff. straight pipe } \lambda_s} = 0.0918\, K^{\frac{1}{2}} + 0.509$$

Barua's solution was obtained using the momentum integral method.

Topakoglu (1967) gave a systematic method for determining an approximate solution (with required accuracy) for steady laminar flow in a curved pipe. Using the assumption that the stream-function and the normal component of the velocity vector may be expanded in a power series in terms of the curvature of the pipe he obtained an expression for the rate of flow in a curved pipe.

McConalgue & Srivastava (1968) extended Dean's work and adopted a parameter $D=2Re(2a/R)^{\frac{1}{2}}$. Solutions obtained numerically by Fourier analysis, were given over the range D=96 to 605.72, the value D=96 corresponding to the upper limit K=576 of Dean's work. Truesdell and Adler (1970) obtained results up to D=3578 by a method based on finite-difference approximations to the governing partial differential equations. By a similar method, Greenspan (1973) obtained a numerical solution covering the whole range of D for laminar flow, that is, for $0 < D \leq 5000$. In his paper, calculations

applied to the particular model studied by Dean and McConalgue & Srivastava and velocity profiles for different D were given. However, as was pointed out by Yao & Berger (1975) the numerical viscosity inherent in the finite-difference scheme may be different than the actual viscosity and therefore the results may not be valid for large D.

Earlier, Ito (1969), based on assumptions similar to those used by Barua (1963), investigated theoretically the laminar flow in a curved pipe and derived a formula for the friction factor. Also a comparison of his calculated results with the experimental results of Adler (1934) and Ito (1959) was given.

By the method of successive approximations, Sankaraiah & Rao (1973) solved the equation of flow obtained in terms of a secondary flow stream function and an axial velocity component (as suggested by Dean). The first five approximations were computed and the solution obtained was used to determine the axial velocity distribution, secondary flow patterns, axial pressure drop and pressure distribution along the pipe wall. A semiemprical equation was obtained for axial pressure drop and the theoretical results were compared with the available experimental data.

Collins & Dennis (1975) attempted to establish an asymptotic structure for the behavior of the numerical solutions as $D \to \infty$. The solutions were obtained by the method of forward and backward differences and corrected. The complete range covered by McConalgue & Srivastava (1968) and

Greenspan (1973) was considered and the results were found to be generally consistent with the former but quantitatively different from the latter, although many of the general trends were qualitatively similar. The results obtained were in good agreement with their experiments.

Smith (1976) investigated the influence of curvature on fluid flow for a pipe that starts bending uniformly after an initial straight section. The Reynolds number and dimensionless curvature were assumed to be large and small, respectively. Smith's theory was also extended to larger length scale, larger D and to various velocity profiles.

Patankar et al (1974) applied a calculation procedure (finite-differences marching technique) to three-dimensional parabolic flows to predict the velocity and temperature fields in helically coiled pipes, in the developing and fully developed regions. Results were compared with experimental data and showed good agreement. Also, the effects of Dean's number on the friction factor were presented. Only the small dimensionless curvatures ($a/R \leqslant 0.07$) were considered.

Murata et al (1976) investigated theoretically the laminar flow through pipes of circular cross-section, but with locally varying curvature of the centre line. The analysis is applicable to any two-dimensional curved pipe, when the centre-line dimensionless curvature is small.

Time dependent fully developed flow in curved pipes was analysed by Lyne (1970), Zalosh & Nelson (1973), Smith (1975) and Singh et al (1978).

All of the theoretical investigations mentioned above were carried out with the assumption of small dimensionless curvature of a pipe ($0 < a/R < 1/50$). This assumption allowed the investigators to neglect terms of order a^2/R^2 and significantly simplified the calculations, but for practical applications, even for pipes of small dimensionless curvature, results obtained in this way were sometimes unsatisfactory (see McConalgue & Srivastava 1968, Greenspan 1973 and Collins & Dennis 1975). Although any solution obtained with the above assumption would not be valid for bends of large dimensionless curvature, some investigators have applied it to an entry region of curved pipe.

By the method of matched asymptotic expansion, Singh (1974) obtained the solution for flow development in a curved tube near the inlet for conditions of constant dynamic pressure at the entrance (application-blood flow in an aorta) and uniform velocity profile. This solution, however, breaks down at a distance of the order $(aR)^{\frac{1}{2}}$, corresponding physically to the point beyond which the effect of the centrifugal force, initially small, becomes as important as inertia and viscous forces within the boundary layer.

Yao & Berger (1975) investigated flow with large D as it developed from a uniformly distributed velocity at the entrance to a fully developed profile. Barua's results for the fully developed flow were adopted as down-stream conditions.

These theoretical considerations were inspected experi-

mentally by Agrawal et al (1978) applying laser anemometry for the measurements of the axial velocity and the component of the secondary velocity (parallel to the plane of curvature). They dealt with the laminar flow of a Newtonian fluid in the entry region of a curved pipe of curvatures 1/20 to 1/7, covering Dean's numbers from 138 to 679. The experimental axial velocity profiles were compared with those constructed from the theoretical analysis of Singh (1974) and Yao & Berger (1975). The quantitative agreement between theory and experiment was found to be poor. However, some of the features observed in the experiment were in qualitative agreement with the theoretical solution of Yao & Berger.

Singh (1978), continuing his study of the problem with particular reference to the ascending aorta, investigated the oscillatory flow of viscous fluid in the entrance to the curved pipe. He neglected arterial wall elasticity, the taper of the aorta and the influence of the branches.

A different approach, more important from the point of view of this work because of possible application to the large curvature elbows, was presented by another group of investigators. They carried out a theoretical analysis of an inviscid flow without body forces, which significantly reduced the mathematical difficulties. First, Squire & Winter (1949, 1951) showed theoretically that secondary flows could occur in a bend through which a perfect (inviscid) fluid is flowing as a result of a non-uniform distribution of velocity

at the entrance to the bend.

Hawthorne (1950) applied Squire & Winter's conclusion to a more general theoretical investigations of the rotational flow. It was found that the secondary flow was not spiral but oscillatory, and that the direction of the circulation changed periodically. Hawthorne showed also that the secondary circulation remains unchanged along the streamline if the direction of acceleration (or pressure gradient) lies in the plane containing the velocity vector and the normal to the Bernoulli surface.

Later, Horlock (1953) described some experiments on the secondary flows in curved pipes, dealing in particular with the effects of reversal of curvature on the pattern of the streamlines.

Recently, Murakami & Shimizu (1978) extended Horlock's analysis for three large dimensionless curvature elbows combined in series and compared the results with experiments. The investigators predicted three types of swirling flows to occur: oscillatory, spiral and suspended. Experiments were carried out for fully developed turbulent profile ($Re=10^5$), different Ψ angles and different lenths of the spacers between the elbows.

Due to the difficulty of obtaining even approximate theoretical solutions, some investigators have focused their attention, for practical purposes, on purely empirical work. Those included are Beij (1938), Crane Ltd. (1942), Pigott (1950), Ito (1959, 1960) and others.

The hydraulic losses and flow patterns in pipes with two bends combined for fully developed turbulent profile were investigated by Murakami & Shimizu (1977).

1.3. Objectives of the Thesis

The aim of this thesis is to provide a better understanding of the flow of fluid through the 90° elbows located close to one another. The variable parameters will be:

- the Dean number
- the length of the spacer between the elbows
- the angle between the planes of curvature of the elbows

Qualitative and quantitative results of the separation and reattachment positions will be produced for two cases: a constant pressure tank or a fully developed flow at the inlet. Also qualitative results of the observations of the turbulence and secondary flow patterns will be given and illustrated by photographs.

CHAPTER II

DIMENSIONLESS PARAMETERS

2.1 Introductory Remarks

As has been mentioned, a theoretical approach presents very serious computational difficulties. Moreover, there are no effective simplifying assumptions useful in the case being considered. Neglecting the fluid viscosity (e.g. Horlock 1956, Murakami & Shimizu 1978), is acceptable for high Reynolds number flows and/or non-uniform velocity profile flow, but for the case being considered, this simplification leads to a direct contradiction with the existence of secondary flow. Similarly, the assumption that viscous forces exist in the inlet pipe only (for a non-uniform velocity distribution at the inlet to the first elbow) is also unsatisfactory because the inlet pipe is relatively short and therefore the flow development is not completed before the inlet to the first elbow, even for the lowest Reynolds numbers. But the rapid increase of the boundary layer thickness in the inlet pipe also indicates the continuation of this process inside the elbow and the importance of the viscosity forces.

Additionally, the large dimensionless curvature of the elbows means that terms of the orders (a/R) and $(a/R)^2$ are equally important and the methods used by Dean (1927, 1928), McConalgue & Srivastava (1968), Greenspan (1968) and others may not be adopted for this study.

For the reasons described above this thesis will focus

on the expirimental study of the water flow in two composite pipe elbows with special application to the blood flow in the human aortic arch, assuming that the blood in large arteries behaves like a Newtonian fluid.

2.2 Dimensionless parameters

The purpose of this section is to establish a set of dimensionless parameters fully describing the system and concerned with the conditions under which flows of different fluids (e.g. water and blood) in two geometrically similar elbow systems are dynamically similar.

The physical quantities which determine the geometry and the flow in the two elbows, are:

i. geometry: radius of curvature R and internal diameter of the elbows d; mutual positions of the elbows (length of the spacer L and angle between the curvature planes of the elbows Ψ)

ii. flow: mean velocity U ; properties of the fluid (density ρ and viscosity μ) ; the representative linear dimension of the system (diameter of pipe d)

It can be proved by the condition of dynamic similarity or by the method of indices (Schlichting 1968) that there exists a unique dimensionless combination of the four quantities: Q, μ , ρ and d - the Reynolds number Re, which provides the conditions under which flows of different fluids about two geometrically similar bodies (in this case- in two geometrically similar elbow systems), and with identical in-

itial flow direction display geometrically similar streamlines (are dynamically similar), when only frictional and inertia forces are important.

For geometrical similarity, the linear parameters must also be expressed in a dimensionless form. This can be done by referring them to the representative linear dimension of the system, the diameter d. Introducing also $L' = L/d$ and taking into account that the angle Ψ is dimensionless by definition, the following set of the dimensionless parameters, fully describing the system, have been obtained:

$$R/d, L', \Psi, Re$$

As has been mentioned in Section 2.1, Dean (1928) showed that the dynamic similarity of the fully developed flow in a single bend of small dimensionless curvature depends on a non-dimensional parameter, called Dean's number by McConalque & Srivastava , which is a function of the Reynolds number and the geometrical parameters of the bend. Although in this case the flow is not fully developed and the dimensionless curvature of the elbows is large, both Reynolds and Dean numbers will be used in present work, for convenience of the reader. It should be noted, that because of the fixed geometry used in this investigation, the Dean number is the Reynolds number multiplied by a constant.

It must be mentioned also that there exist at least three definitions of the Dean number. They are as follows:

McConalgue & Srivastava (1968), Greenspan (1973)

$$D = 2\,Re\,(2a/R)^{\frac{1}{2}} \qquad (2.1)$$

Singh (1974), Yao & Berger (1975)

$$D = Re\,(a/R)^{\frac{1}{2}} \qquad (2.2)$$

Schlichting (1968)

$$D = \tfrac{1}{2}\,Re\,(a/R)^{\frac{1}{2}} \qquad (2.3)$$

The definition (2.1) which is the most widely used, will be employed in this thesis.

Finally, the set of the dimensionless variables includes:

- Reynolds (Dean) number, Re (D)
- Dimensionless spacer length, L'
- Angle between the curvature planes of the elbows, Ψ

CHAPTER III

APPARATUS

3.1 Apparatus Description

The purpose of the experimental model was to enable the study of the flow characteristics in two successive pipe elbows and relate it to blood flow in the aortic arch. For this reason, the dimensions of the elbows and the lengths of the inlet and outlet pipes, were chosen to be close to the average values obtained from measurements made on humans of the ascending aorta, the aortic arch, and the section of the aorta downstream from this arch (McDonald 1960, Singh et al 1978). The aorta is an elastic tube that stems from the left ventricle of the heart, curving in a complicated three-dimensional way with branchings to the head and upper limbs. In this investigation, the aorta has been modelled using two elbows with a straight pipe at the inlet and a straight pipe at the outlet. As a first approach to the problem the three dimensional model employed ignores the influence of branches, the taper of the aorta, the arterial wall elasticity and the pulsating character of the blood flow. The various length spacers have been introduced between the elbows to make the model more universal and the results obtained more general and useful.

As can be seen in Figure 1, some additional devices have been necessary to provide the working conditions for the model. To obtain the uniform velocity profile at the inlet to the first elbow, city water was supplied to the clo-

sed, watertight inlet tank. For the uniform velocity profile, the long copper tube was used, but due to supply difficulties the internal diameter of this tube d_i differed slightly from the diameter of the elbows (see Table 1) and an adapter had to be used. Therefore the velocity profile produced during these tests cannot be considered to be fully parabolic, but as being very close to it. The required length of this pipe was calculated on the basis of the formula, (Daugherty & Ingersoll 1954)

$$L_p = 0.058\, d_p\, Re \qquad (3.1)$$

and provided fully developed laminar flow at the outlet of the pipe up to Re = 1918.

To avoid thermal effects the water temperature was maintained at the same level as the room temperature by mixing hot and cold water. The flow rate was controlled and the safe, low pressure in the supplying pipe was maintained using the flow control valves. The flow rate was coarsely measured by the flow meter and precisely using the scaled flow rate measurement tank and a stopwatch.

The outlet unit, containing the outlet tank, the flow rate measurement tank and the bottom tank, were mounted on casters, to enable easy changes of the angle Ψ. This angle was changed by loosening the vertical screws pressing the elbows together, located in the steel housing of the elbows, and rotating the unit about the vertical axis of the spacer. Additionally, the outlet tank located at the unit could be moved vertically to keep the outlet pipe in the horizontal

position, when the spacer length was changed.

Apparatus data are provided in Table 1. The general views and the details of the apparatus are shown in Figures 2 through 5 inclusive.

3.2 Flow Visualisation

The flow was made visible by injecting water colored with a dark-blue dye using dye pipes located at various points from the inlet tank to the outlet pipe. For the exact dye pipe locations see Table 2. The first dye pipe, marked A, was mounted (see Figures 1, 3, & 4) such that it could be located at any point before the entrance to the inlet pipe in the inlet tank. That is, it was possible to introduce the dye mixture at any point of the entrance. All other dye pipes were fixed perpendicularly to the main direction of flow in the walls of the elbows, spacer and the outlet pipe (see Figures 2 & 4). Due to the fixed position of the dye pipes located in the elbows walls, two, three, or four dye pipes were located at the same cross-section and were marked left, right, outer and inner.

Dye pipes being in use during a certain experiment were connected to the container supplying the dye mixture and all other dye pipes were closed.

The dye motion in the elbows was observed and photographed, and to obtain the true three-dimensional pattern of the flow, two small variable position mirrors were used (see Figure 6). The vertical position of the mirrors was

in accordance with the needs of the experiment being conducted. Since the elbows were made by matching the two halves then joining them together with the connecting plane coinciding with the plane of curvature of the elbows, care was taken to position the mirrors to eliminate possible optical effects created by this joint, see Figure 6.

3.3 Apparatus Limitations

The actual dimensions of the elbows chosen here introduced certain limitations to the experimental procedure which will be described in Chapter IV. This is related to the relatively small diameter, from the experimental point of view, that has prevented the locating inside the elbows or pipes of any pitot tubes or other velocity measuring devices of the diameter larger than approximately 1 mm. This means that for low velocity flows the dynamic force driving a pressure sensitive device connected to a pitot tube will be very low. For example, for the more advantageous case of potential water flow with a velocity of 4.5 cm/s, the average velocity for Re = 500 (D = 2535) in this experiment, the dynamic force on the 1 mm diameter pitot tube and the dynamic pressure head, using the Bernoulli equation, would be approximately 0.8×10^{-6} N and 0.1 mm of water, respectively. These numbers are lower for viscous flow and decrease rapidly as the flow velocity decreases (0.005 mm H_2O for 1 cm/s). To investigate secondary flow velocities, which are at least one order of magnitude smaller than the main flow velocities,

the necessary sensitivity of the device measuring the differential pressure must be better than 0.001 mm H_2O. No device has been found to satisfy this condition - the very sensitive condenser-type sensors, designed to work with gases, require a special interfacing device for use with water, which reduces the sensitivity to the point where it is of no use.

For the reasons noted above, the qualitative dye motion observations of the flow patterns could not be confirmed by independent pitot tube measurements. Also the more modern technique of laser or hot-wire anemometry have not been applied, mainly due to time limitations.

The flow visualisation technique used has introduced further limitations, in that secondary flow patterns could only be observed in the range of Reynolds number from 400 to 1400 (Dean numbers 676 to 2366). Below this range the observations were made impossible by the dye dispersion and the long time required for the flow stabilization, and above the range by the disturbances produced by separation zones.

The dye method also required the continuous use of city water, which was associated with presence of air bubbles, visible on some figures.

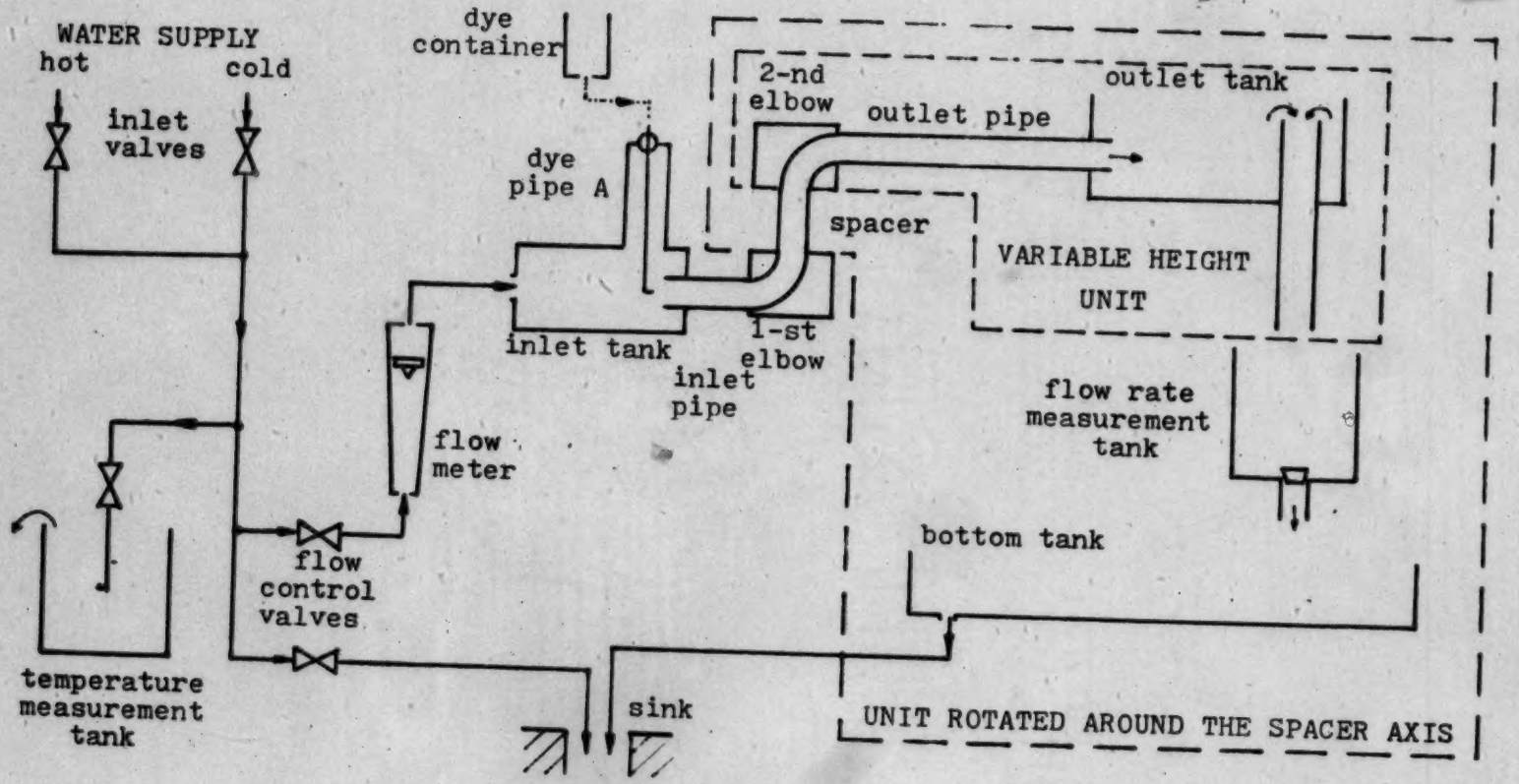

Figure 1 Apparatus Layout

Table 1

Apparatus Data

Internal diameter of the pipe and the elbows	d	31.75 mm
Radius of curvature of pipe centre-line	R	44.45 mm
Dimensionless curvature	a/R	0.357
Relation between the Reynolds and Dean numbers		$D = 1.69\ Re$
Spacer lengths	L	0; 27 mm; 57 mm; 100 mm
Dimensionless spacer lengths	L'	0; 0.85; 1.8; 3.15
Inlet pipe length		51 mm
Outlet pipe length		508 mm
Inlet tank dimensions (length x width x height)		305 mm x 305 mm x 124 mm
Outlet tank dimensions (length x width x depth)		610 mm x 202 mm x 203 mm
Length of the long inlet pipe (for fully developed flow)	L_i	3664 mm
Internal diameter of the pipe as above	d_i	32.94 mm
Effective adapter length		28.6 mm
Distance from the water level in the outlet tank to the outlet pipe axis		approx. 75 mm
Temperature of water		22°C

Table 1

continued

Kinematic viscosity of water	ν	0.95×10^{6} m^2/s
Material of the elbows and the tanks		plexiglass
Diameter of the pipes injecting the dye mixture		1 mm
Camera / lens		Canon F 1/FD 55 mm
Close-up lenses		58 mm: 450; 240
Film		Kodak Tri - X
Lighting		Fluorescent

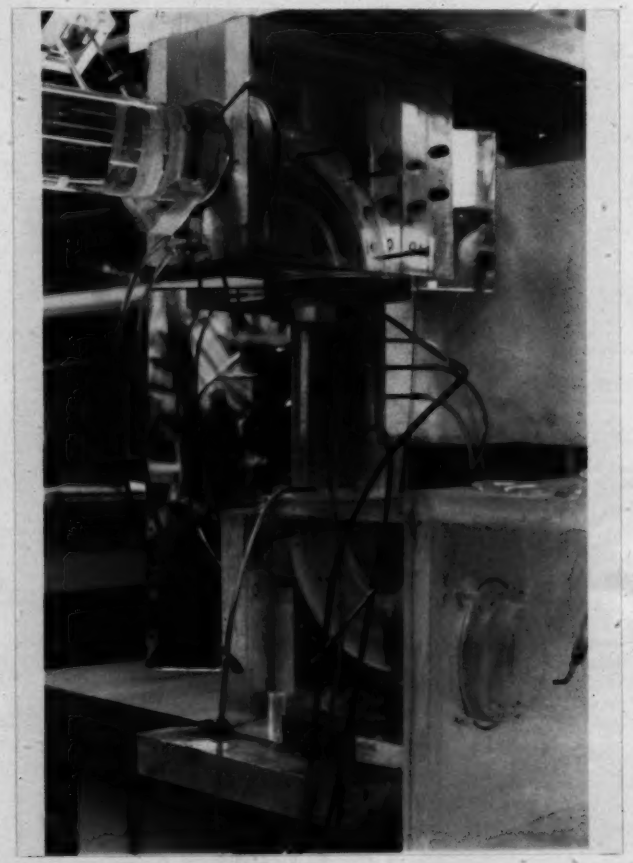

Figure 2 Apparatus - Elbows (Ψ = 90° ; L'= 3.15)

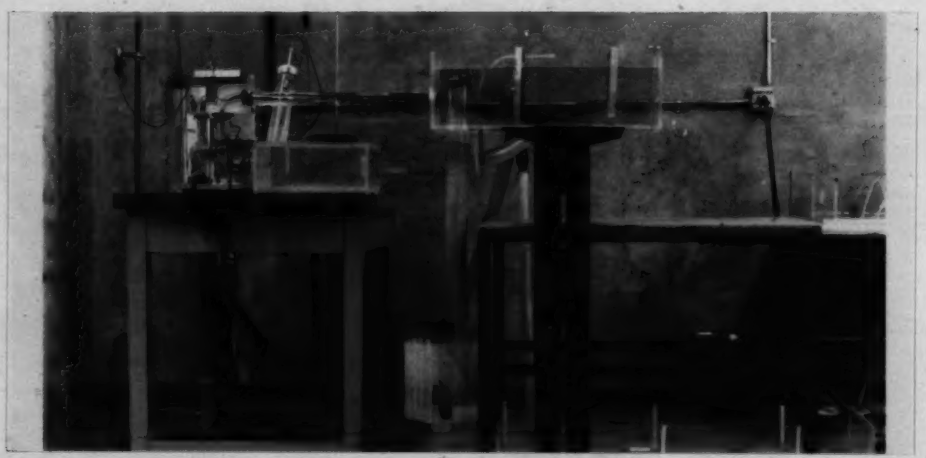

Figure 3 Apparatus - General View (Ψ = 0° ; L'= 3.15)

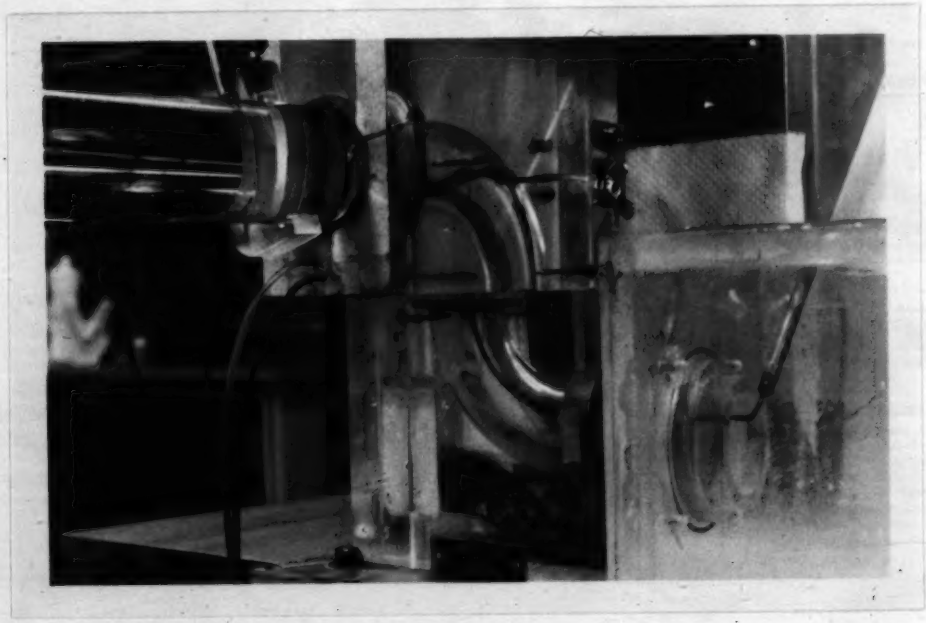

Figure 4 Apparatus - Elbows ($\Psi = 90°$; $L' = 0$)

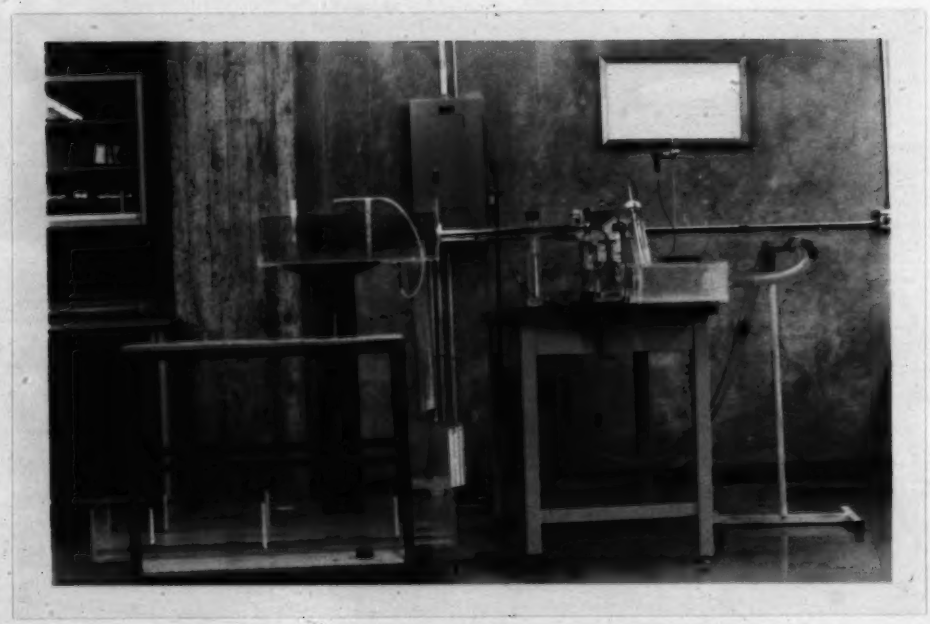

Figure 5 Apparatus - General View ($\Psi = 180°$; $L' = 3.15$)

Table 2

Cross-Sections and Dye Pipes Positions

X-S.	DYE PIPES*	EXACT POSITION	NOTES
	A	upstream tank	movable - any position at x-section available
	B1&Br	1-st elbow inlet	
	C1&Cr	3 mm before 1-st elbow outlet	
1		1-st elbow outlet	when L'= 0, X1=X2=X3
	D_{α}-J_{α}	spacer **	rotated with spacer
2		spacer mid-point	when L'= 0, X1=X2=X3
3		2-nd elbow inlet	
	Ki,Ko,K1,Kr	13 mm before 2-nd elbow inlet	
4	L1,Lr	2-nd elbow mid-point	
5		2-nd elbow outlet	
	Mi,M1,Mr	11 mm behind 2-nd elbow outlet	
6	N_{α}	42 mm behind 2-nd elbow outlet	can be rotated with outlet pipe around this pipe axis
7	O_{α}	166 mm behind 2-nd elbow outlet	

* for the dye pipes nomenclature see Figure 9

**Dye Pipes in Spacers (distance from X1 in mm):

DYE PIPE		D	E	F	G	H	I	J
SPACER LENGHT	3.15	14	25	40	52	63	78	89
	1.8	13	21	29	38	48		
	0.85	11	19					

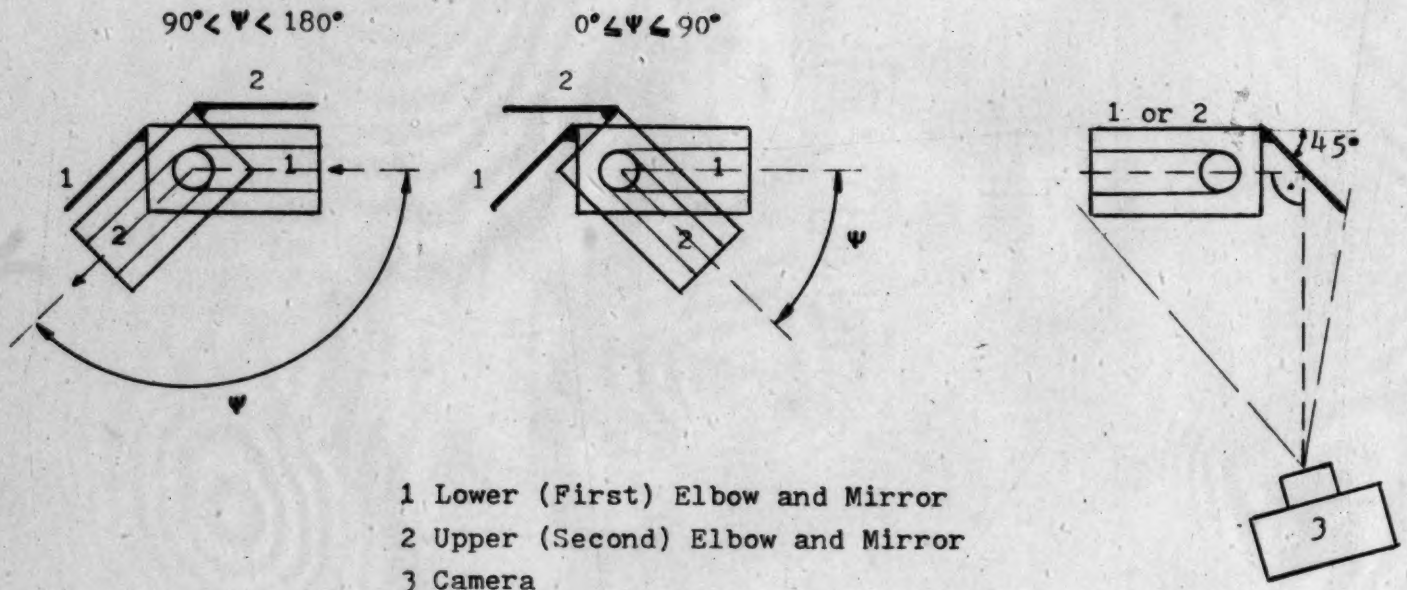

1 Lower (First) Elbow and Mirror
2 Upper (Second) Elbow and Mirror
3 Camera

Figure 6 Mirrors and Camera Positions

CHAPTER IV

EXPERIMENT

4.1 Experimental Range

As can be concluded from Section 1.2, no references on experimental flow pattern investigations in two successive pipe elbows or bends with Reynolds numbers lower than 10^5 have been found. In the present work, due to the apparatus limitations mentioned in Section 3.3, only the lower part of this unreported range was investigated: the flow pattern investigation covered the range of the Reynolds numbers from 400 to 1400 (Dean numbers from 646 to 2366) and the separation investigation covered the range Re from 400 to 2500 (D from 676 to 4225). The upper limit of the former was restricted by the turbulent disturbances, but the upper limit for the latter was extended to the higher flow velocities because for this case the turbulence did not disturb the observations. Selection of the flow velocities for the illustrated photos was made based on the factors leading to the good quality pictures, but due to the weak dependance of the flow patterns on the Reynolds (Dean) number over the range investigated, this approach seems to be correct.

To provide a satisfactory number of measurement points, the position of the separation lines and the reattachment lines were measured for 8 or 9 different flow rates.

The upper limit of the next variable, the dimensionless spacer length L', was chosen equal 3.15 on the basis of observations showing no observable relationship between the

flow characteristics and the spacer length for values of L' larger than 3.15. For the purpose of the separation position measurements, in the case of the uniform velocity profile, all four spacer lenths were used. The experiments with the fully developed flow at the inlet required fewer spacer lengths. The measurements using only two of them, L' = 0 and L' = 3.15, have provided enough data for conclusions and comparisons.

The last dimensionless variable, the angle Ψ, was varied between 0° and 180°. The quantitative results of the separation measurements were obtained for the values of the angle Ψ: 0°, 45°, 90°, 135° and 180° for the constant pressure tank and for 15°, 90° and 180° for the fully developed flow at the inlet.

4.2 Experimental Procedure

The procedure of the experiment was separated into two major parts. For both of them the water temperature was precisely adjusted to match the surrounding air temperature (22°C), the apparatus was systematically flushed with a strong jet of water to remove air bubbles and the flow rate was coarsely controlled by the valves and the flowrator meter, and precisely measured using the flow rate measuring tank and stopwatch. Also, in the both cases, a few minutes of time was required for the flow to stabilize after any change of the flow setting (up to 10 min for the lowest flows).

The first procedure was applied to all qualitative observations, such as the flow pattern investigation. Conducting this procedure, all variable parameters were changed within the ranges described in the previous section and the dye mixture was injected at different dye points using the trial-and-error method, until a detailed understanding of the observed effects had been reached. Next, the flow was photographed for certain apparatus settings, chosen to obtain the best photographic results.

A different procedure was applied to the quantitative observations of the separation positions. In this case for the apparatus settings given in the previous section, the dye mixture was injected by the dye pipe located in the area where separation probably existed. After a few minutes, required for the dye stabilization, the distances between the extremal upstream dye positions and the reference cross-sections, L_1 and L_5, were measured as the separation lines positions. The reattachment point position was found by looking for the place where the injected dye mixture moves in both directions simultaneously: upstream and downstream. In this case the dye pipes located in a spacer downstream from the separation line position were used. Due to the vortices existing behind the separation zone, especially for the higher flow velocities, and the experimental procedure employed, the numerical results obtained for the reattachment point position should be treated as approximated.

All numerical results were recalculated in order to

obtain dimensionless values, L_1', L_2', and L_3'.

4.3 Presentation of Results

In this thesis the results are presented mainly in the form of graphs and tables (numerical results), and sketches and photographs (qualitative results). Most of them follow immediately the proper section of the text, except the tables of the separation position measurements which are located in Appendix for reference.

The basis for the interpretation of the sketches and photographs are Figures 7 & 8, where the information about the cross-sections' observation points and the cross-sections' locations is given (for the exact cross-sections' locations see also Table 2). The illustrative material also contains the data of the dye pipes in use and the symbols of the flow perpendicular to the observer. For interpretation, see Table 2 and Figure 9. Additionally, the following notes should be kept in mind:

- the velocities v and w are at least one order of magnitude lower than the average flow velocity U
- in certain cases when the dye mixture was injected with large initial momentum to investigate the flow inside the pipe, the jet effect must be taken into account when the photographs are studied
- in practice, it was impossible to obtain pictures of the second elbow and the outlet pipe cross-sections photographed from the cross-sections observation point shown in Figure 8;

instead the camera was located as shown in Figure 6 or behind the outlet tank (final vortex pictures) which means the photographs obtained are the reverse, around the vertical axis, of what would have been obtained using the observation point of Figure 8

- the "outer curvature" and the "inner curvature" of the elbows are defined in Figure 8 (see picture in the upper right corner).

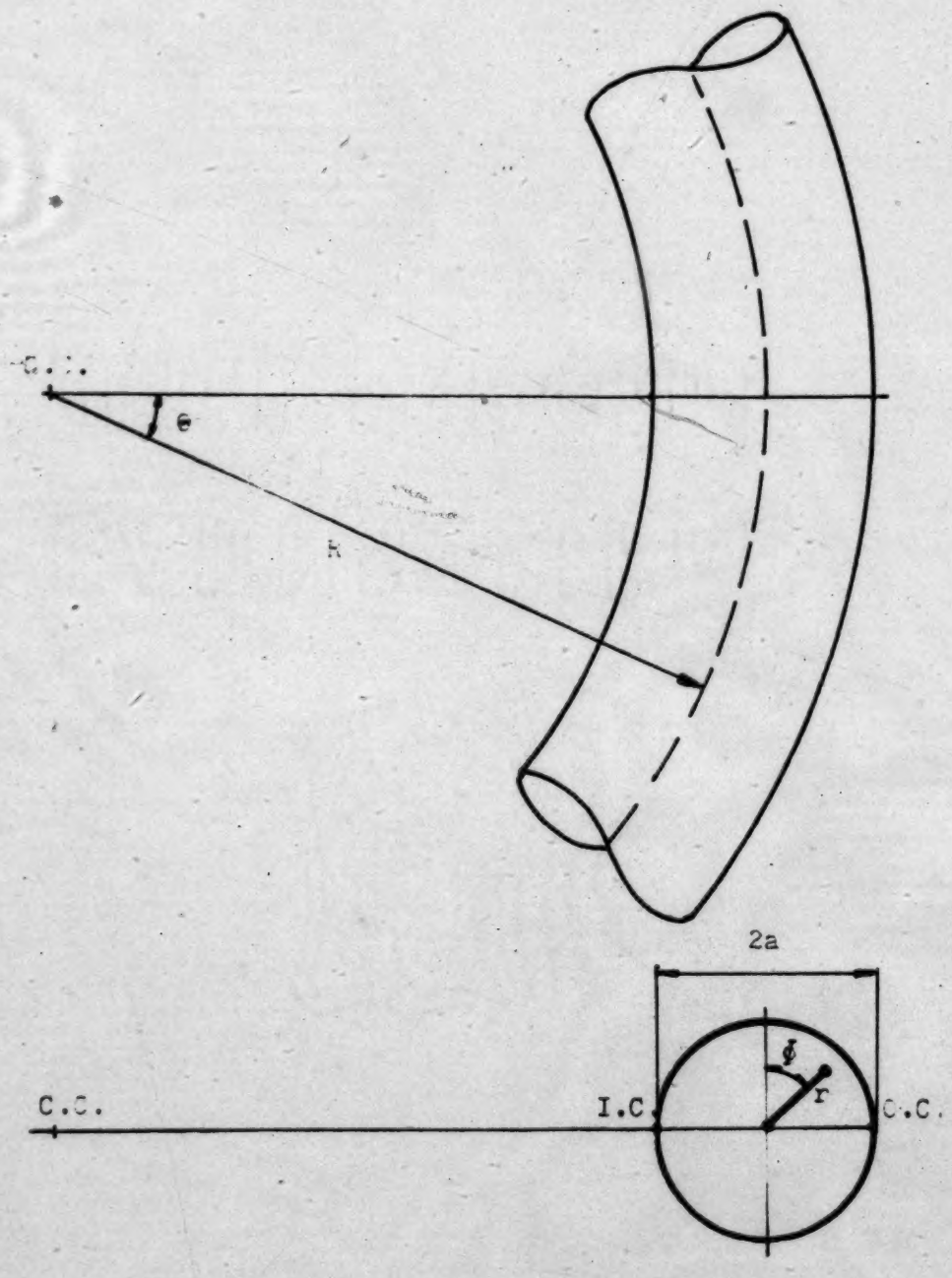

Figure 7 Coordinate System

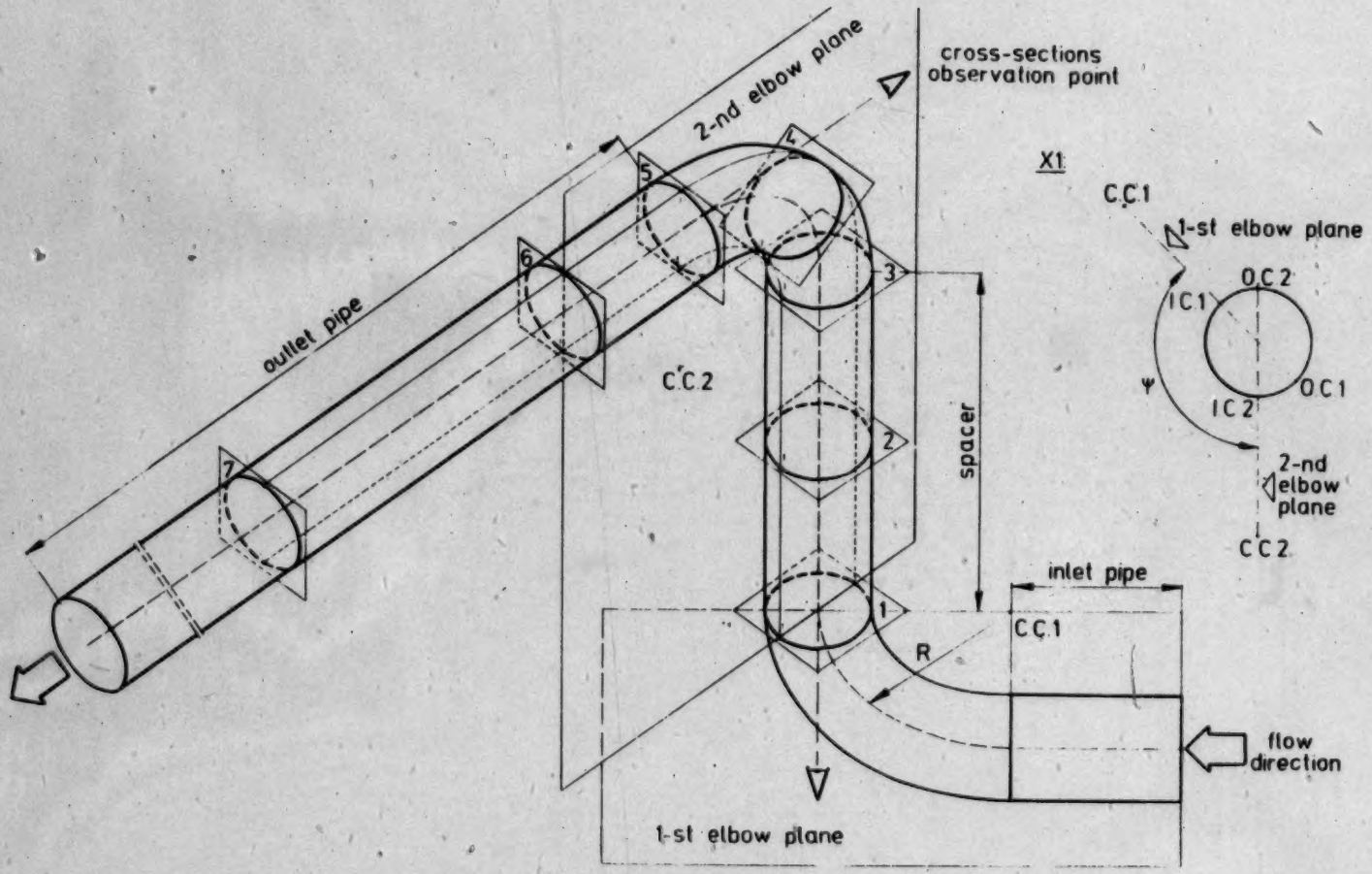

FIG 8 NOTATION OF ELBOWS AND CROSS-SECTIONS

FIRST ELBOW
DP's-B and C

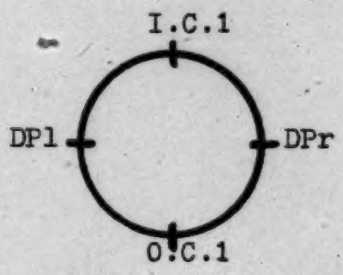

SECOND ELBOW
DP's-K,L and M

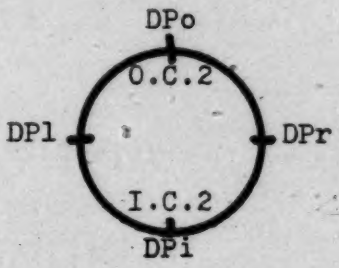

SPACERS AND OUTLET PIPE
DP's-D_α to J_α and N_α, O_α

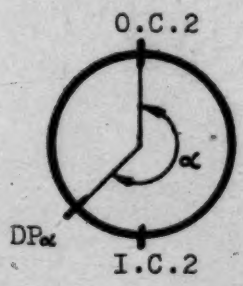

INLET TANK, POSITION
SHOWN GRAPHICALLY (DP-A)

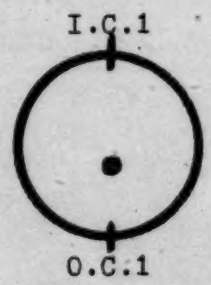

Note: For the observation positions of the above cross-sections see Figure 8

observation point

flow direction

perpendicular flow symbol

low sheaf stress and / or separation zone

Figure 9 Standard Cross-Sections Presentation, Dye Pipes Locations at Cross-Sections and Flow Symbols

CHAPTER V

SOME OBSERVED FLOW PHENOMENA

5.1 Secondary Flow and Influence of the Second Elbow

The general character of fluid motion in a bend is well known (Singh 1974): as the fluid enters the bend from the reservoir, a boundary layer similar to that in a straight pipe develops at the wall. Thus the region consists of two parts: (i) a thin layer near the wall where the viscous forces are balanced by the inertia forces and the centrifugal force has a second-order effect near the inlet and (ii) an inviscid core in which the centrifugal force due to the circular motion of the main body of the fluid along the pipe is balanced by the pressure gradient directed towards the centre of curvature. However, as the flow develops downstream the bend, the curvature effects become as important as the viscous effects and the inertia forces in the boundary layer, which in turn influence the flow in the core due to fluid particles displacement. The secondary flow of the fluid due to curvature consists of the transverse flow of the slower-moving fluid particles in the boundary layer from the outside of the bend towards the inside and the cross-flow of faster-moving fluid particles from inside to the outside of the bend. Thus, the secondary boundary layer behaves as a reservior receiving the fluid moving towards the outer curvature, and also acts as a source because of the fluid leaving it at the inner curvature.

If a sufficiently long coiled pipe has a constant radius and a constant cross-section, the current flow eventually becomes fully developed, that is, the velocities do not vary with distance along the pipe axis. Although, in view of the convective mass transfer due to secondary flow, the developing flow requires a much shorter entrance length to become fully developed in comparison to a straight tube, as was found by Squire (1954), the transition region is still relatively long and the flow does not become fully developed for large dimensionless curvature 90° elbows.

The conclusion obtained from the above consideration is that the secondary flow starts at the portion of the elbow cross-section where the curvature is the largest (close to the inner curvature). When two successive pipe elbows are located to form "S" shape ($\Psi = 180°$), the influence of the second elbow on the flow in the spacer is strongest close to its inner curvature, making the streamlines in the spacer almost parallel to the pipe axis on the inner side closer to the second elbow center of curvature (Figure 10) and pushing the secondary flow circulation to the outer side.

Another conclusion will be illustrated in Chapter VI: when the flow with the secondary circulation enters a second elbow, the transverse flow occurs from the outside of the second elbow towards the inside. This flow exists in a thin layer along the elbow walls and is independent of the secondary circulation inside the flow core.

5.2 Separation

During the experiment, the phenomenon of boundary layer separation has been observed. In order to explain this phenomenon, let us consider first the flow about a infinitely long circular cylinder (Figure 11, by Schlichting, 1968). In the case of potential flow, for particles moving along DE, there is a transformation of pressure into kinetic energy, the reverse taking place along EF, so that a particle arrives at F with the same velocity as it had at D. In the actual case of a viscous flow, the boundary layer forms and a fluid particle which moves in the immediate vicinity of the wall in the boundary layer remains under the influence of the same pressure field as that existing outside and impressed on the b.l. However, owing to the large friction forces in the thin boundary layer such a particle consumes so much of its kinetic energy on its path from D to E that the remainder is too small to surmount the "pressure hill" from E to F. Such a particle can not move far into the region of increasing pressure between E and F and its motion is eventually arrested. The external pressure causes it then to move in the opposite direction. This reverse motion gives rise to a vortex whose size is increased until it becomes separated and moves downstream in the fluid. Flow in the boundary layer near a point of separation is shown diagrammatically in Figure 11 - B.

The above example, although it gives the explanation of separation, is not an analogy of the fluid flow inside

the elbow. To make an approach to such analogy, consider now the flow in the duct shown in Figure 12, assuming it is infinitely wide. Such a duct is the two dimensional model of the 90° large dimensionless curvature, constant radius elbow.

Inside this elbow model the kinetic energy of a particle at point E is relatively high, also the outer wall changes the direction of the flow and keeps the point of maximum velocity closer to the center of curvature. In this situation the separation occurs due to adverse pressure gradient existing between the inner curvature and the area downstream from the elbow. Inside the elbow the centrifugal force creates a pressure difference between the inner and the outter curvature of the elbow, with the lower pressure closer to the inner curvature. This moves the maximum velocity point outward and the flow at the inner curvature decelerates . Downstream from the elbow, the point of the maximum velocity moves again to the center of the pipe and pressure measured at the inner curvature, along the pipe, increases. The separation ends with the reattachment point when pressure starts to decrease again.

The two-dimensional elbows can be combined in the two basic configurations: "U" shape and "S" shape with or without a spacer between them. The "S" configuration, especially without or with a short spacer, gives an interesting contribution to the above considerations: the centrifugal force inside the second elbow causes a relatively high pres-

sure increase in the flow between the inner curvature of the first elbow and the outer curvature of the second one. This pressure gradient promotes the separation and as expected moves the separation line upstream. The strength of the centrifugal force depends on the flow velocity, therefore the length of the separation zone also depends on it. On the other hand, for the "U" configuration without spacer the separation is expected to be reduced due to the direction of the second elbow centrifugal force. This is related to the "first" separation, which originates in the first elbow, or the spacer, or the second elbow when there is no spacer, but a separation also can be expected in the second elbow and the outlet pipe, called the second separation.

The described phenomena of the first and second separation and the influence of the flow velocity, are even better expressed for the three-dimensional case of the elbows with the circular cross-section (Figures 13, 14, and 15), due to the secondary circulation which is changing the character of the flow. Instead of the steady circulatory motion inside the separation zones, as in the two-dimensional case, the presence of the secondary flow can create backflow supplied by the secondary circulation boundary layer flow and discharged in the plane dividing two vortices of the secondary flow, as shown schematically in Figure 16 (see also Figures 17 through 20 inclusive). This backflow has been observed over the whole investigated range of the flow in the first elbow, where the two-coil structure of the

secondary flow is always well-defined. The phenomenon also occurs in the second elbow for Re > 1400, where the secondary flow structure depends on a mutual position of the elbows (Figure 21).

The results of the separation measurements are graphically presented in Figures 22 through 39 inclusive. For the constant pressure tank the first separation line position is shown in Figures 22 through 25, the first separation reattachement line position in Figures 26 through 29 and the second separation line position in Figures 30 through 33. The same measurements for the fully developed flow for selected apparatus settings are presented in Figures 34 through 39.

These graphs (for numerical results see Appendix) show the similar relationships as previously concluded to the two-dimensional case observations. For angle $\Psi = 180°$ the high pressure region present on the outer side of the flow in the second elbow moves the first separation line upstream. When angle $\Psi < 180°$ this effect is weaker; when $\Psi = 0°$, the low pressure region present on the inner side of the flow in the second elbow moves the separation line downstream and for the case without spacer ($L' = 0$) prevents the separation from occurring in the first elbow.

The influence of the angle Ψ on the first separation line position is observed even for the longest spacer ($L' = 3.15$), but the influence of the spacer length is weak for $L' > 1.8$ due to the weaker influence of the second elbow

on the flow upstream.

The first separation reattachment line position is weakly affected by the angle Ψ - the curves shown in Figures 26 through 29 inclusive are located close one to another except the curve plotted for $\Psi = 180°$ in Figure 26. This one is located more downstream, due to the action of the backflow, already described. The influence of the spacer length is observed only for $L' = 0$ and $L' = 0.85$, where the presence of the second elbow limits the first separation. In other cases, $L' > 0.85$, the length of the separation, measured between the cross-section number 1 and the reattachment line, is almost the same.

The second separation line position as a function of the angle Ψ and the spacer length L' can be probably explained in terms of the secondary flow patterns. In the case of the "U" configuration ($\Psi = 0°$), the pressures measured perpendicularly to the axial velocity direction between a point located at the inner curvature of the second elbow and a point located directly downstream on the wall of the outlet pipe, should show relatively small difference with the lower pressure being in the elbow. This would be due to the relatively strong secondary cross-flow at the outlet of the second elbow, directed from the inside to the outside of the elbow (see Section 5.1). Finally the adverse pressure gradient is weak and the separation is relatively small. In the case of the "S" configuration ($\Psi = 180°$) the secondary circulation in the outlet pipe is

more complicated and forms a four coil structure featuring the two upper coils created by the first elbow, and the two lower coils created by the second one. The pressures measured perpendicularly to the flow direction between a point located at the inner curvature of the second elbow and a point located directly downstream on the wall of the outlet pipe, should show significant difference with the lower pressure being in the elbow. The adverse pressure gradient is strong and the separation line is located upstream, relative to the case of "U" configuration. For any other values of the angle Ψ, the separation line occupies intermediate positions.

The relationship between the second separation line position and the spacer length L' is probably associated with the strength of the two upper vortices created by the first elbow. These vortices in the second elbow are weaker, when the spacer is longer, which allows the second elbow to develop stronger lower vortices and reduces the adverse pressure gradient.

The influence of the Reynolds (Dean) number has been observed as the rapid change of the separation lines positions, which is associated with the transition from laminar to turbulent flow in the boundary layer. This position change is well-defined for the first separation and weaker for the second one. The possible explanation is that the flow approaching the second separation zone is already partially turbulent. The relationship between the reattachment

point position and the Reynolds (Dean) number also shows, for the spacers lengths L' = 0.85 and L' = 1.8, a similar rapid change of the position.

The fully developed velocity profile at the elbows entrance has introduced significant differences (compared with the uniform velocity profile) for the first separation line position only. Due to the lower velocity near the wall, this type of flow is more sensitive to the pressure changes and, for example, for the "S" configuration the first separation line position moves upstream very rapidly as the Reynolds number is increased.

5.3 Turbulence

The fact that separation in steady flow occurs only in decelerated flow, leads directly to the conclusion that there must exist a point of inflection of the velocity profile in the boundary layer (Schlichting 1968). The existence of such a point is important for the transition from laminar to turbulent flow. It provides a necessary and sufficient condition for the amplification of disturbances, as has been deduced from the frictionless Orr-Sommerfeld (stability) equation. This equation was obtained by omitting the viscous terms in the full Orr-Sommerfeld equation, as compared with the inertia terms, and the influence of viscosity changes the preceding conclusion only very slightly. The inflection point stability criterion means that a favourable pressure gradient stabilizes the flow, whereas an

adverse pressure gradient enhances instability; this statement helps to explain the basic difference between White's (1929) experiment, where the critical value of the Reynolds number for transition to turbulence was found to be Re=6000, and the present experiment, where the first turbulent instabilities were observed for Re=1407. The White experiment was conducted for a long pipe of relatively small dimensionless curvature, a/R=0.02, where no separation was observed and the centrifugal force efficiently stabilizes the flow. In the present experiment the flow was observed to be fully laminar for Re=796 (Figure 40) and for Re=938 (Figure 41) when the laminar vortices produced by the first separation were visible. For Re=1407 the flow center remained fully laminar (figure 42) but the first separation started to produce instabilities which are probably turbulent (Figure 43). This is based on the data from Figure 22 through 25 inclusive, showing a rapid change of the first separation line position which is characteristic for the boundary layer transition from laminar to turbulent conditions. This boundary layer transition, when the center of the flow still remains laminar, is likely to be associated with the presence of the separation in the entrance cross-section of the inlet pipe. For the higher Reynolds numbers the laminar vortices also occur at the outer curvature of the first elbow (Figure 44) and instabilities are produced by the second separation (Figure 45). Further increase of the Reynolds number shows that the flow center still remains laminar

(Figure 46), but outside the laminar center the instabilities are growing (Figure 47).

Although, as has been shown, White's experiment may not be directly compared with the present ones, both of them have given almost the same Dean numbers for the transition to turbulence, if the instabilities observed in this experiment for Re=1407 are assumed to be turbulent. These Dean numbers are 2400 and 2378, respectively.

The results obtained also show no contradiction with the Nerem et al (1972) measurements, showing only the laminar flow up to Re=5000 in the aortic arch. In the present experiment, the presence of the laminar center for Re=2221 confirms that result, but further comparisons are impossible due to the different entrance conditions. The sharp edge of the inlet pipe in the inlet tank (see Figures 4 and 6) may not be used as a model of the inlet to the aortic arch, due to the ring-shaped separation, which appears inside the inlet pipe, immediately downstream from the edge. This separation produces observable instabilities which disturbs the flow downstream. This is so even for "U" configuration, when there is no first separation (Figures 48 and 49).

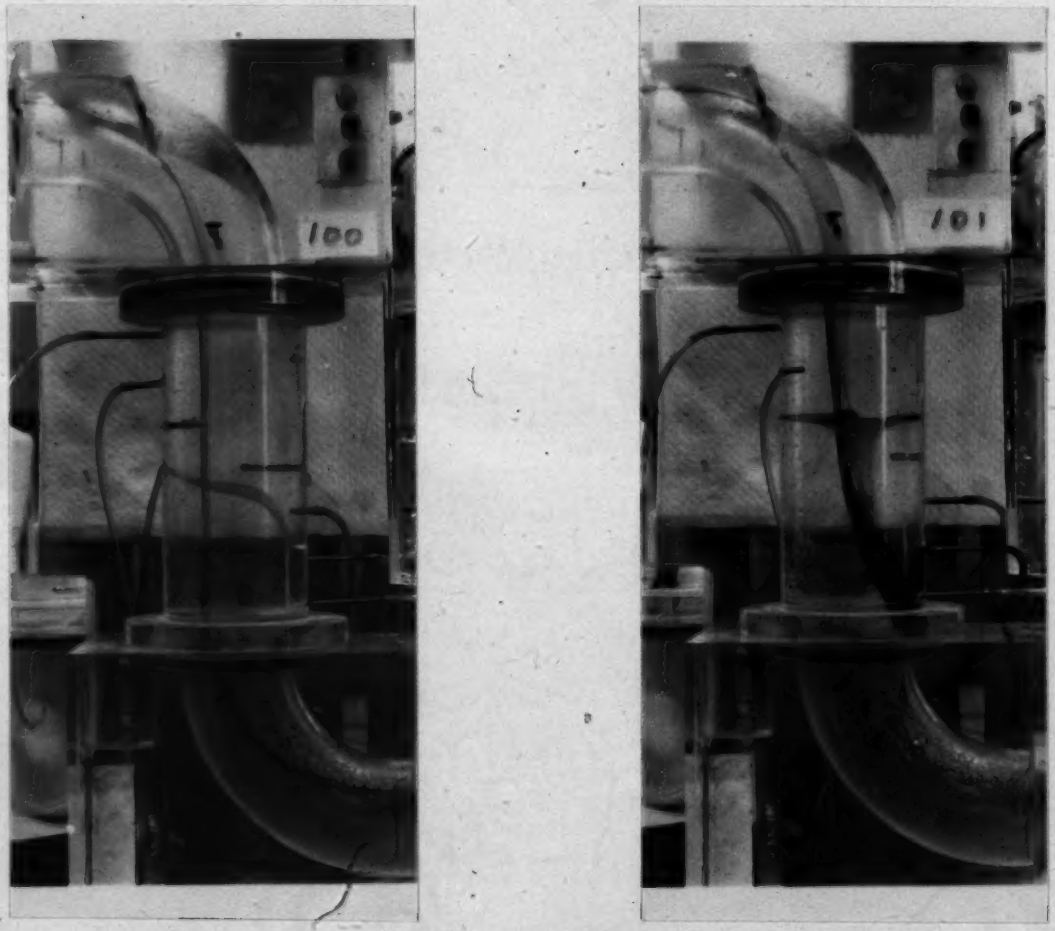

Figure 10 Influence of the Second Elbow on the Flow in the Spacer
(left fig.: Re = 767, Ψ = 180°, L'= 3.15, DP-A ⊙)
(right fig.: Re = 767, Ψ = 180°, L'= 3.15, DP-E ⊙)

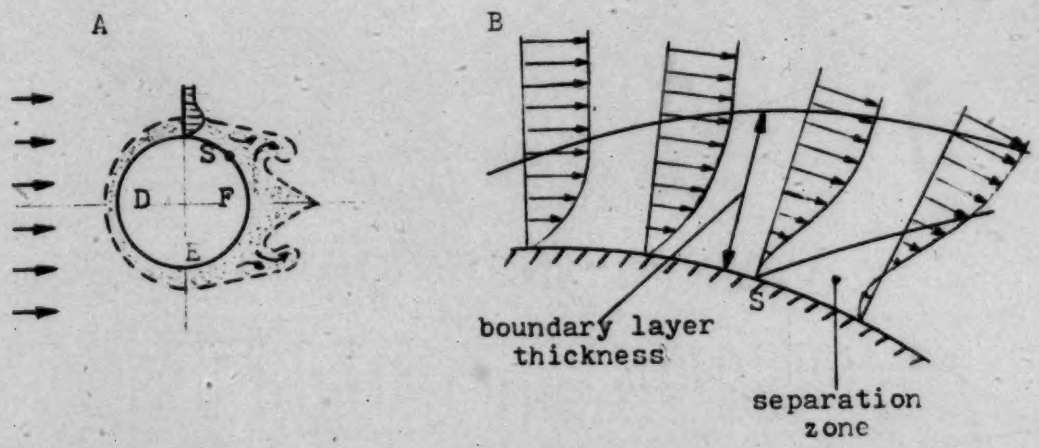

Figure 11 Separation and Vortex Formation on a Circular Cylinder and Flow in the Boundary Layer Near a Point of Separation (S - point of separation)

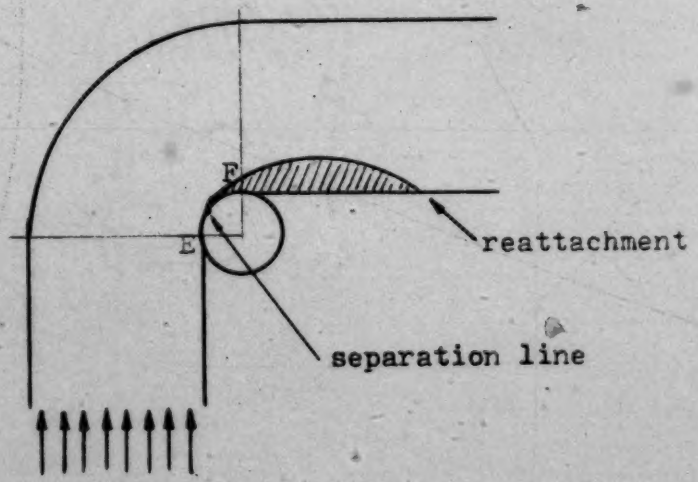

Figure 12 Separation in a Two - Dimensional Elbow

Figure 13 First Separation as a Function of Reynolds Number
(upper fig.: Re = 400, Ψ = 180°, L'= 0, DP - C1)
(lower fig.: Re = 650, Ψ = 180°, L'= 0, DP - C1)

Figure 14 Vortices Due to the Second Separation
(Re = 1055, Ψ = 180°, L'= 0, DP-A and Mi,
ΔT = 0.33s)

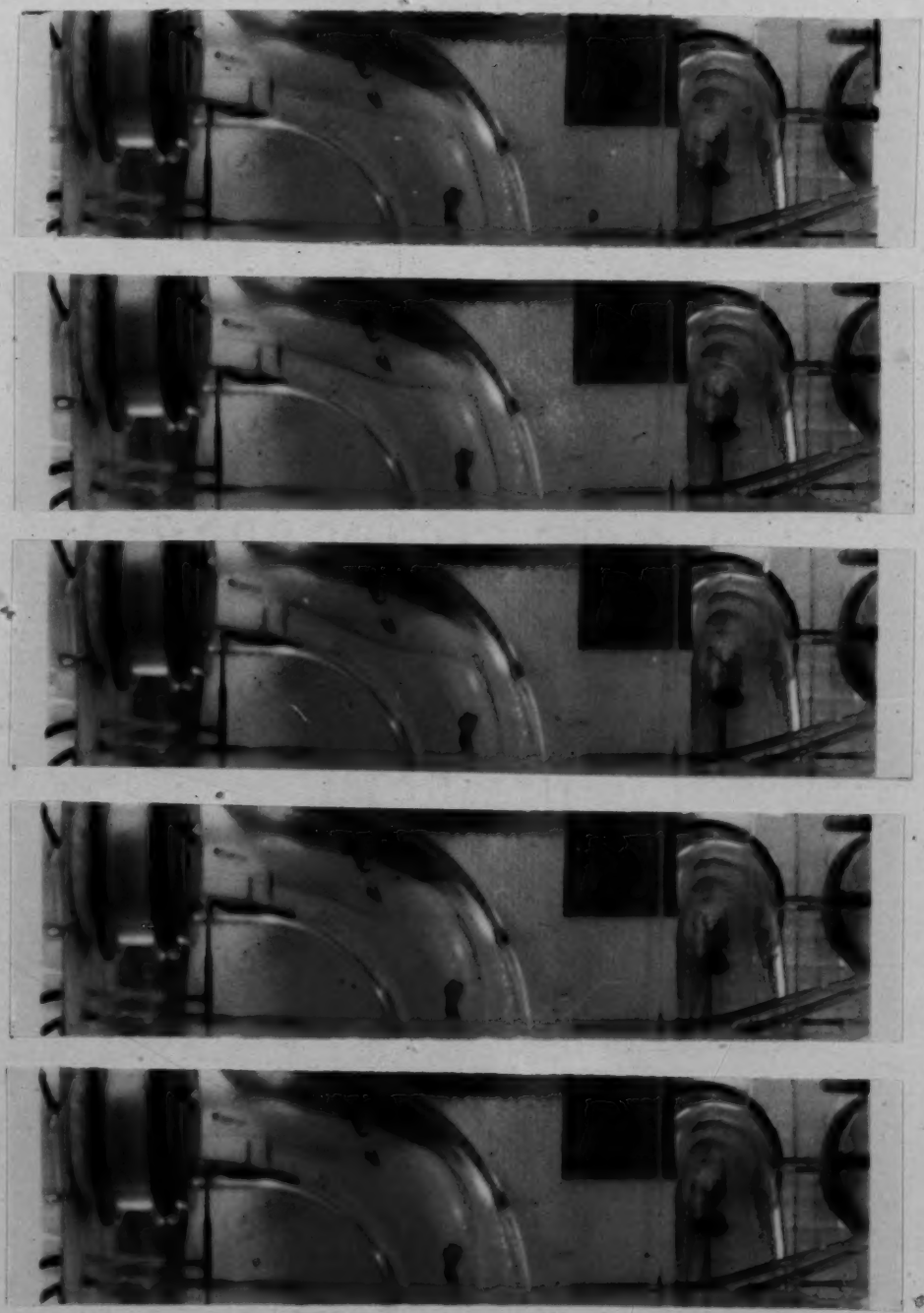

Figure 15 Second Separation - Dye Motion
(Re = 403, Ψ = 180°, L'= 0, DP-Mi, ▲T = 2s)

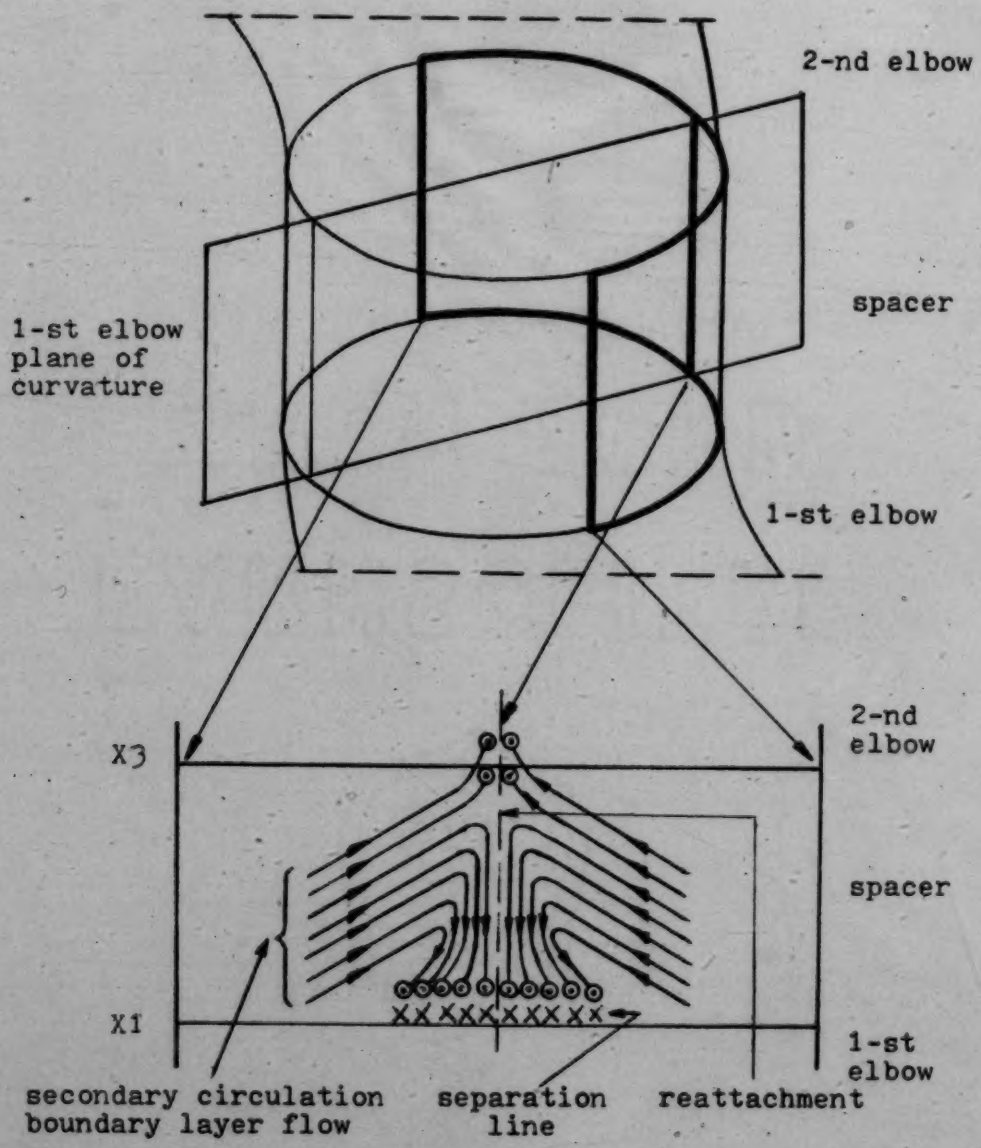

Figure 16 Backflow Streamlines in the First Separation

Figure 17 Backflow in the Spacer
(Re = 938, Ψ = 180°, L'= 3.15, upper fig. DP-D0°,
lower fig. DP-E20°)

Figure 18 First Separation - Dye Motion Due to the Backflow
(see mirror image on the right, Re = 403, Ψ =180°
L'= 0, DP-A⊙, Δ T = 0.5s)

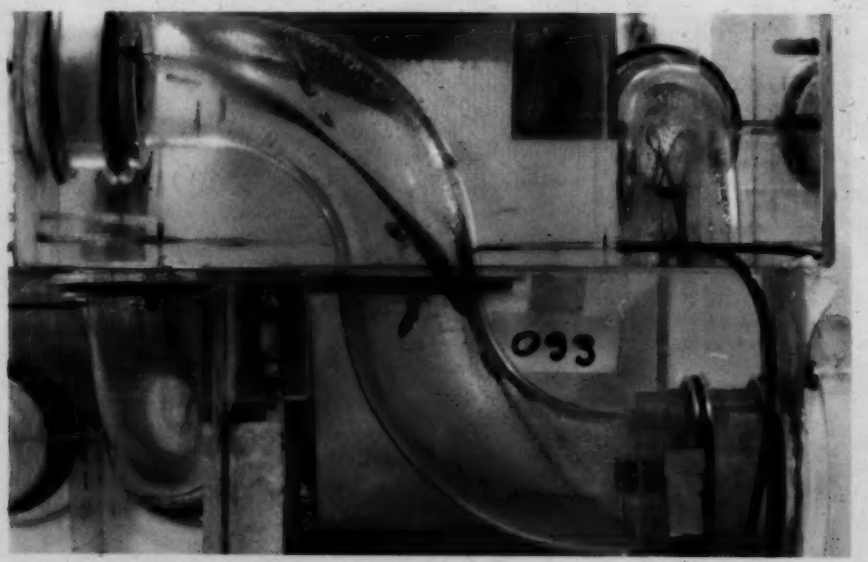

Figure 19 Backflow in the First Elbow
(Re = 420, Ψ = 180°, L'= 0, DP-Ko)

Figure 20 First Separation - Reattachment Line
(Re = 414, Ψ = 180°, L'= 3.15, DP-E0°)

Figure 21 Second Separation as a Function of Reynolds Number ($\Psi = 0°$, L'= 0, DP-Mi, upper fig. Re = 1530, lower fig.Re = 2400)

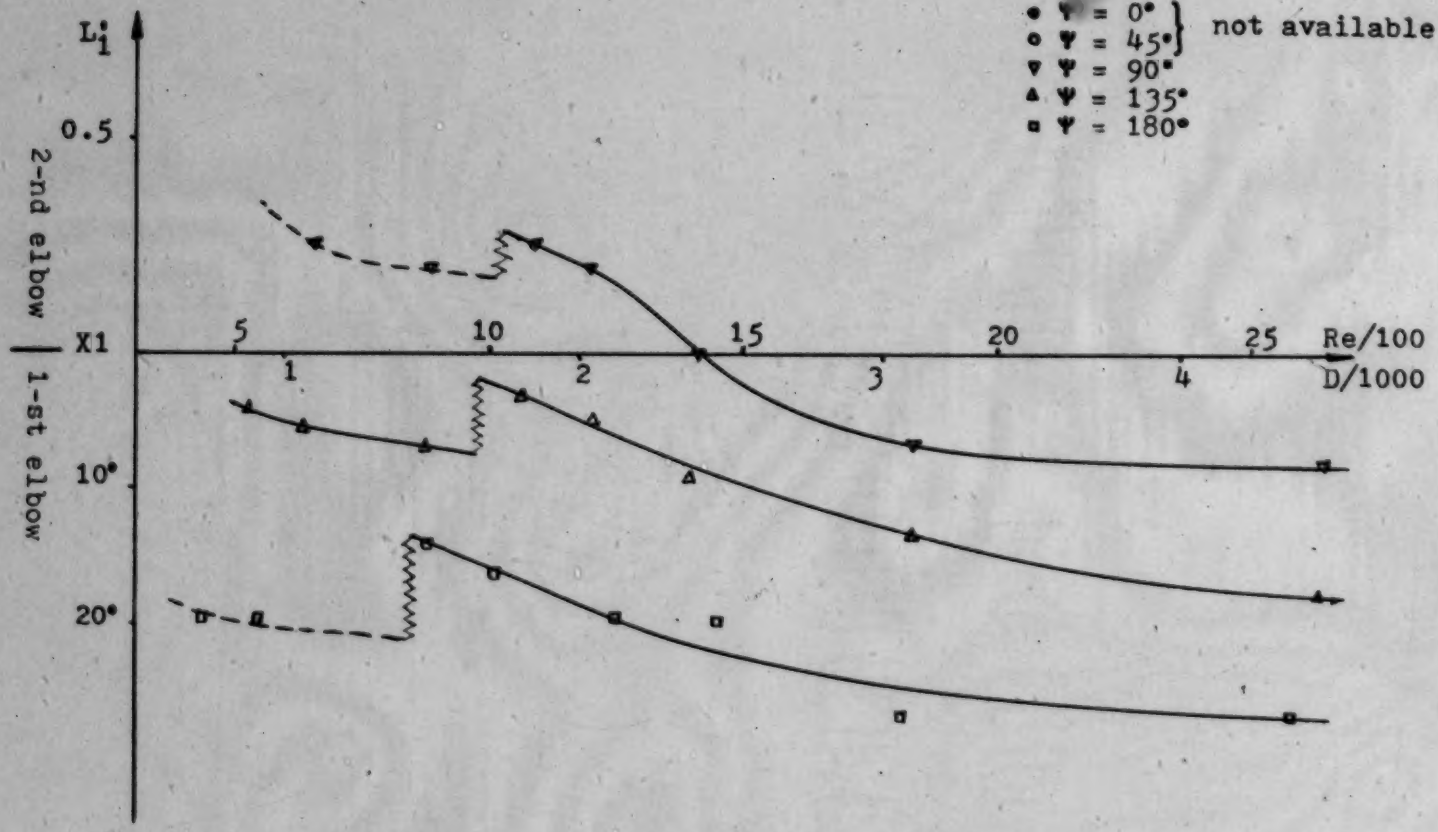

Figure 22 First Separation Line Position versus Reynolds (Dean) Number as a Function of Angle Ψ for a Uniform Velocity Profile and L' = 0

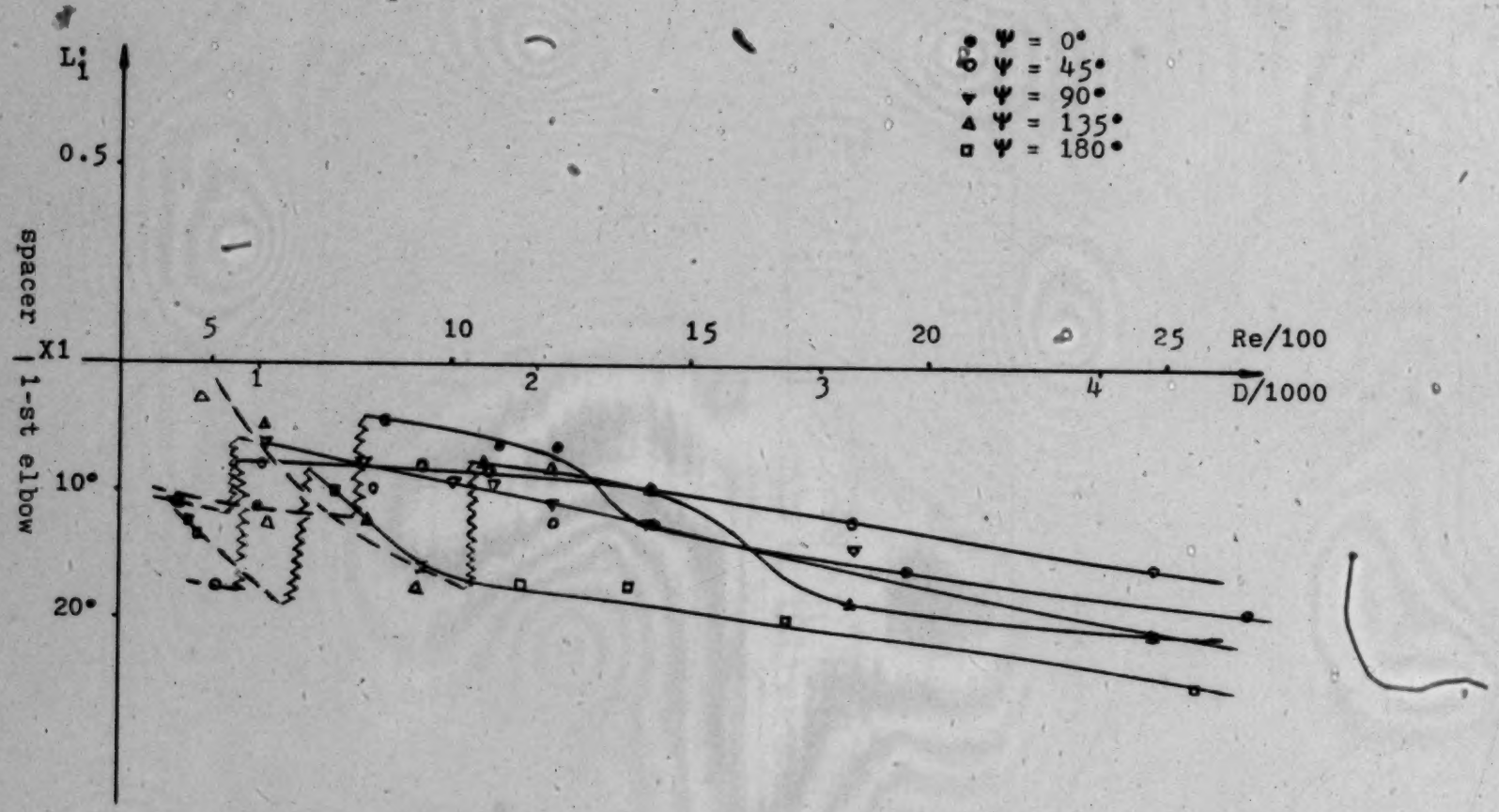

Eigure 23 First Separation Line Position versus Reynolds (Dean) Number as a Function of Angle Ψ for a Uniform Velocity Profile and L' = 0.85

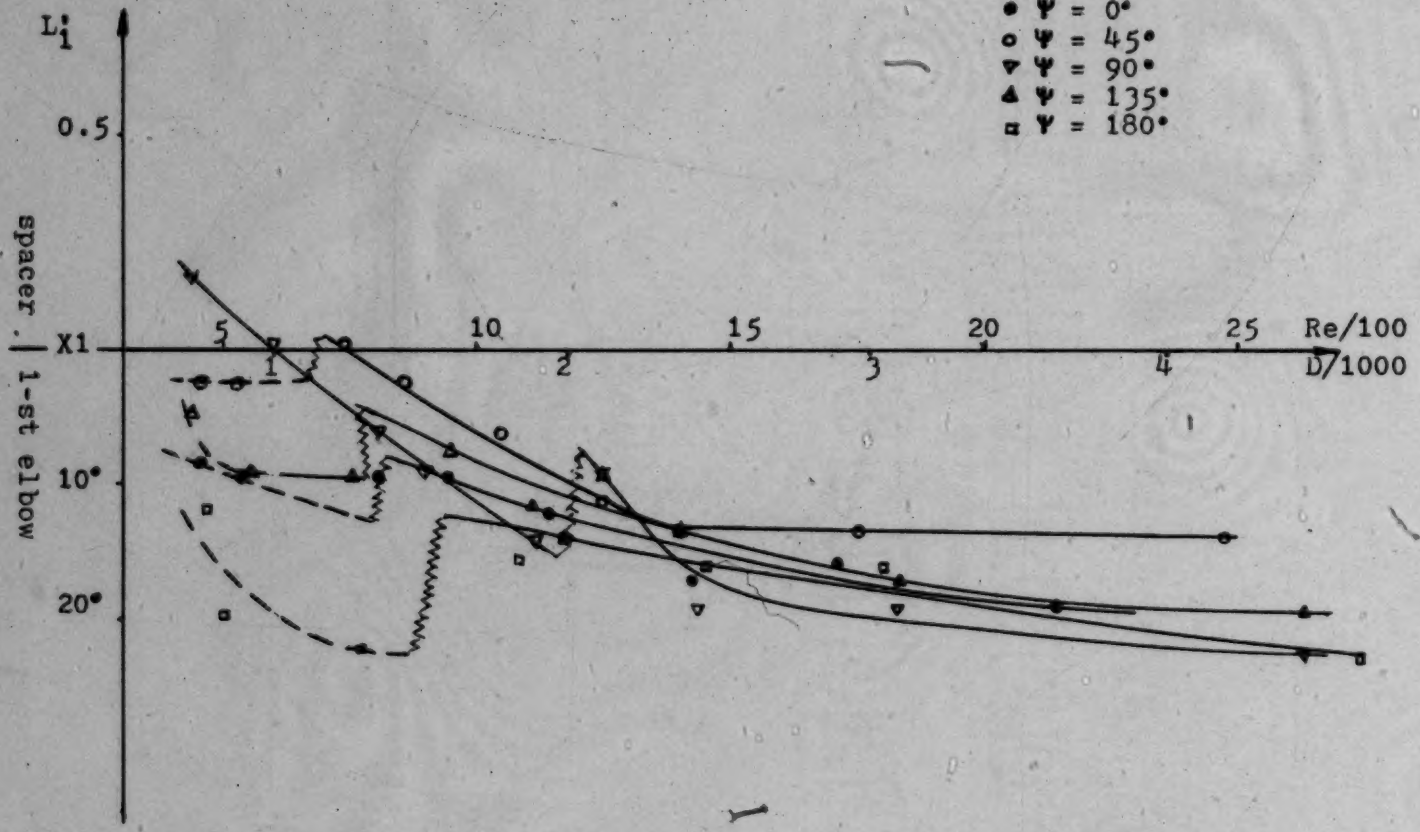

Figure 24 First Separation Line Position versus Reynolds (Dean) Number as a Function of Angle Ψ for a Uniform Velocity Profile and L' = 1.8

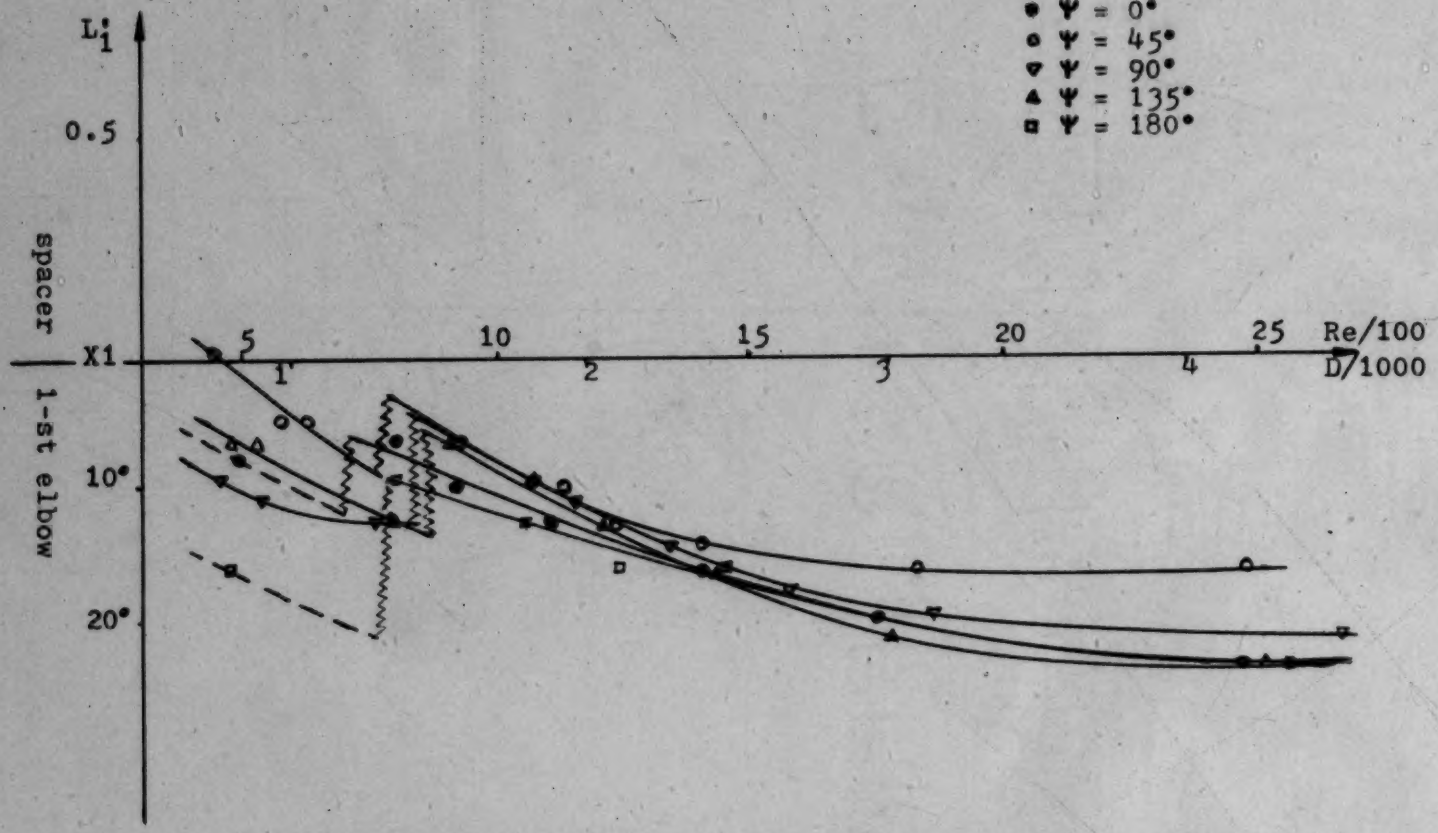

Figure 25 First Separation Line Position versus Reynolds (Dean) Number as a Function of Angle Ψ for a Uniform Velocity Profile and L' = 3.15

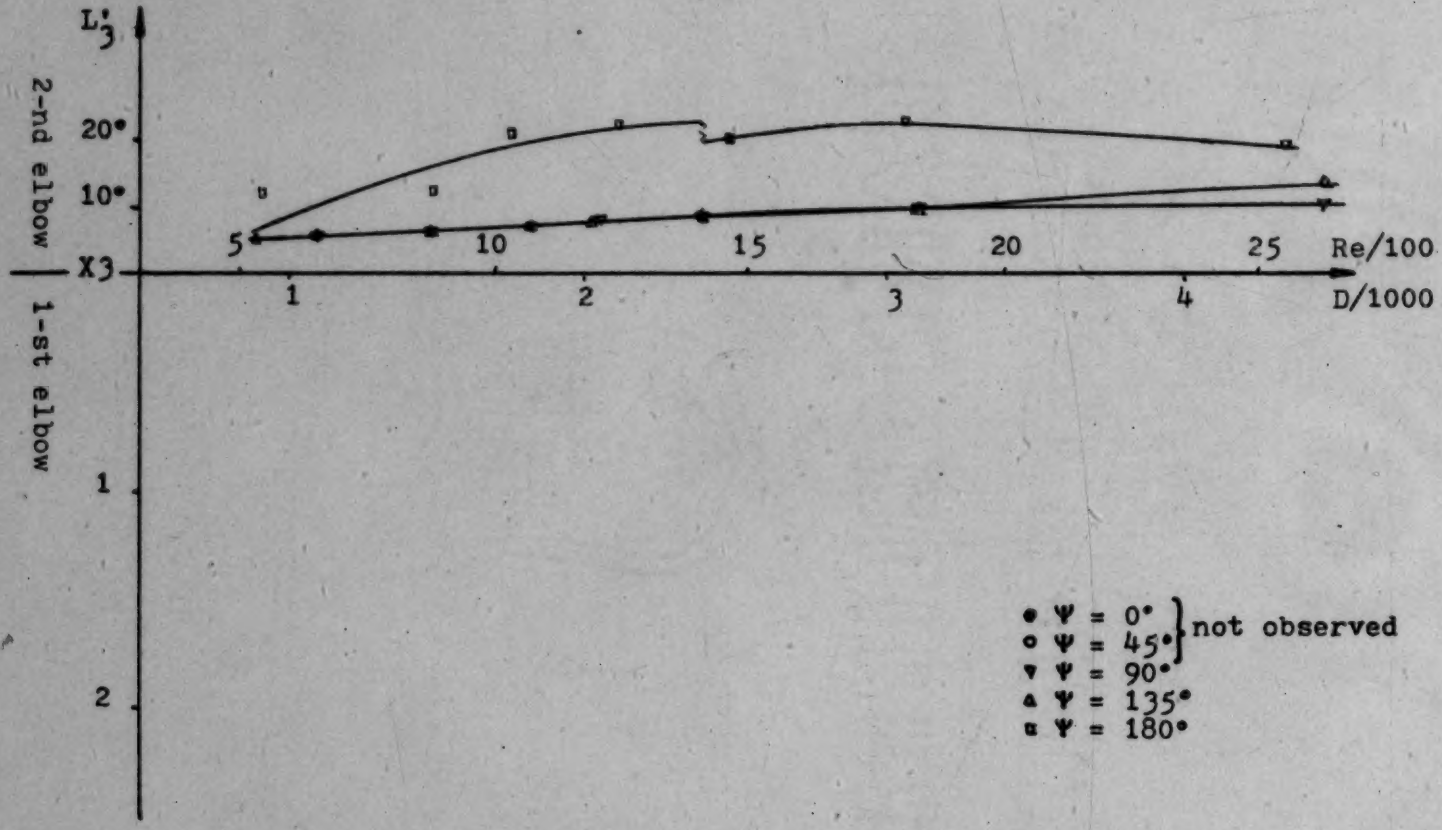

Figure 26 First Separation - Reattachment Line Position versus Reynolds (Dean) Number as a Function of Angle Ψ for a Uniform Velocity Profile and L' = 0

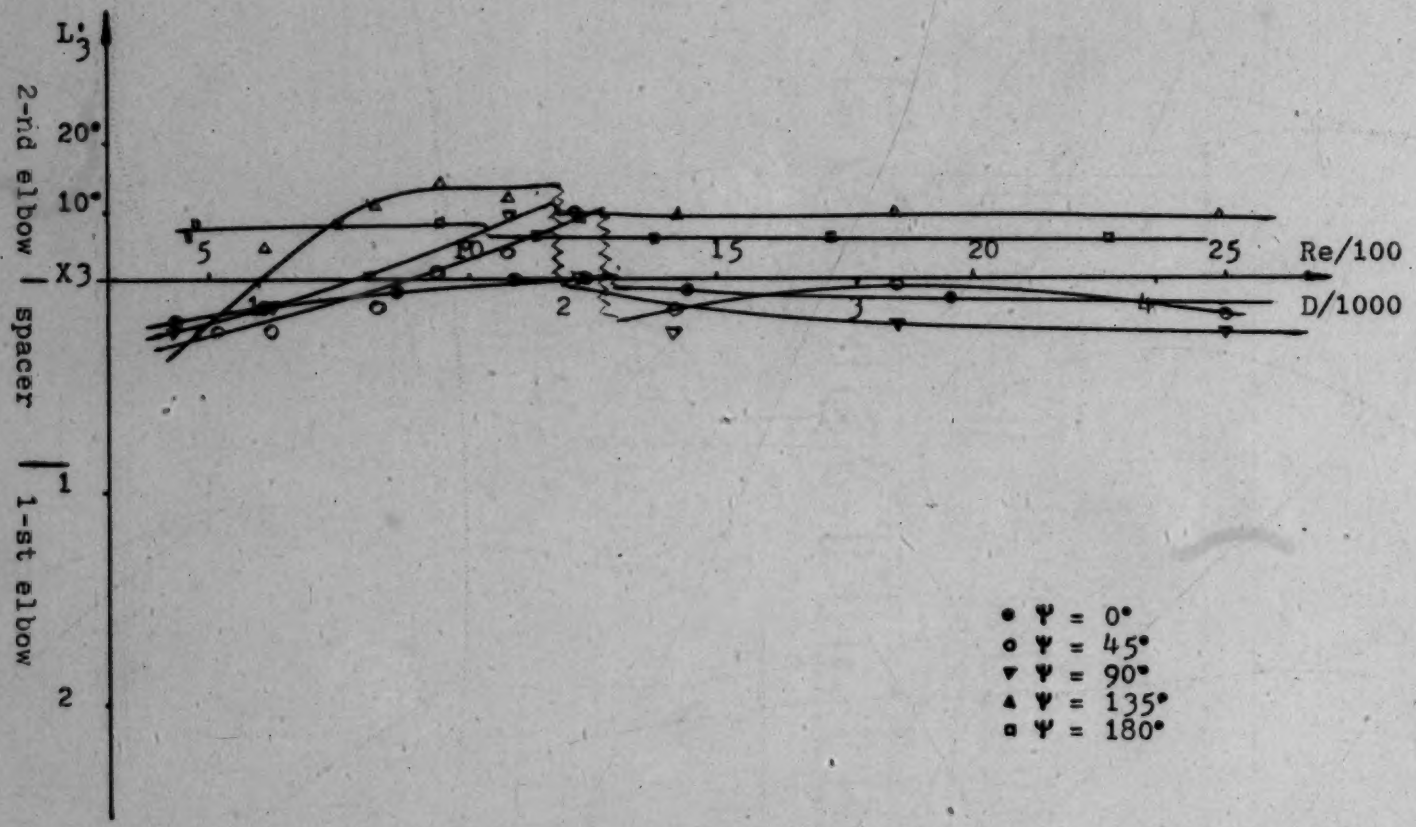

Figure 27 First Separation - Reattachment Line Position versus Reynolds (Dean) Number as a Function of Angle Ψ for a Uniform Velocity Profile and L' = 0.85

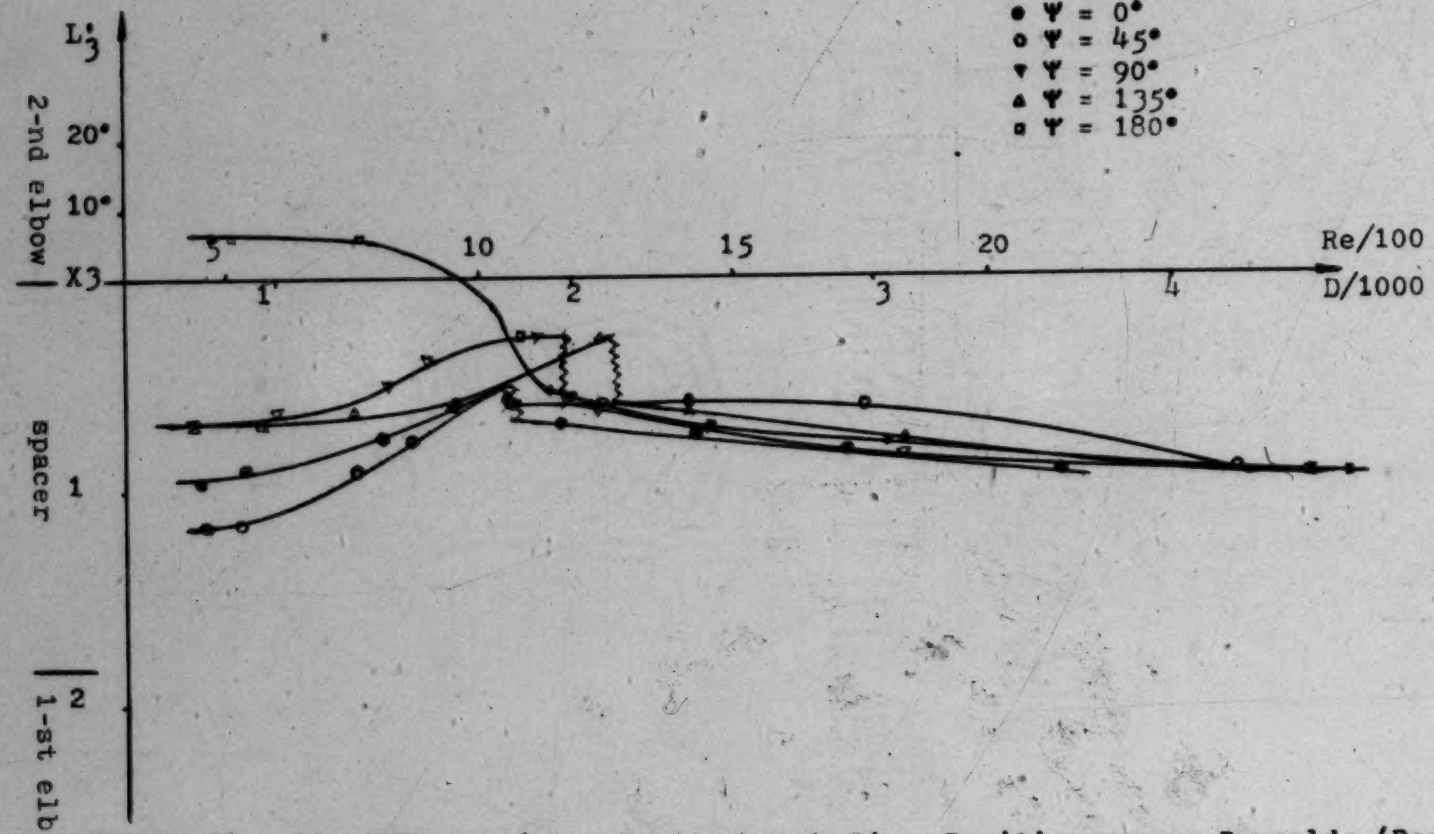

Figure 28 First Separation - Reattachment Line Position versus Reynolds (Dean) Number as a Function of Angle Ψ for a Uniform Velocity Profile and L' = 1.8

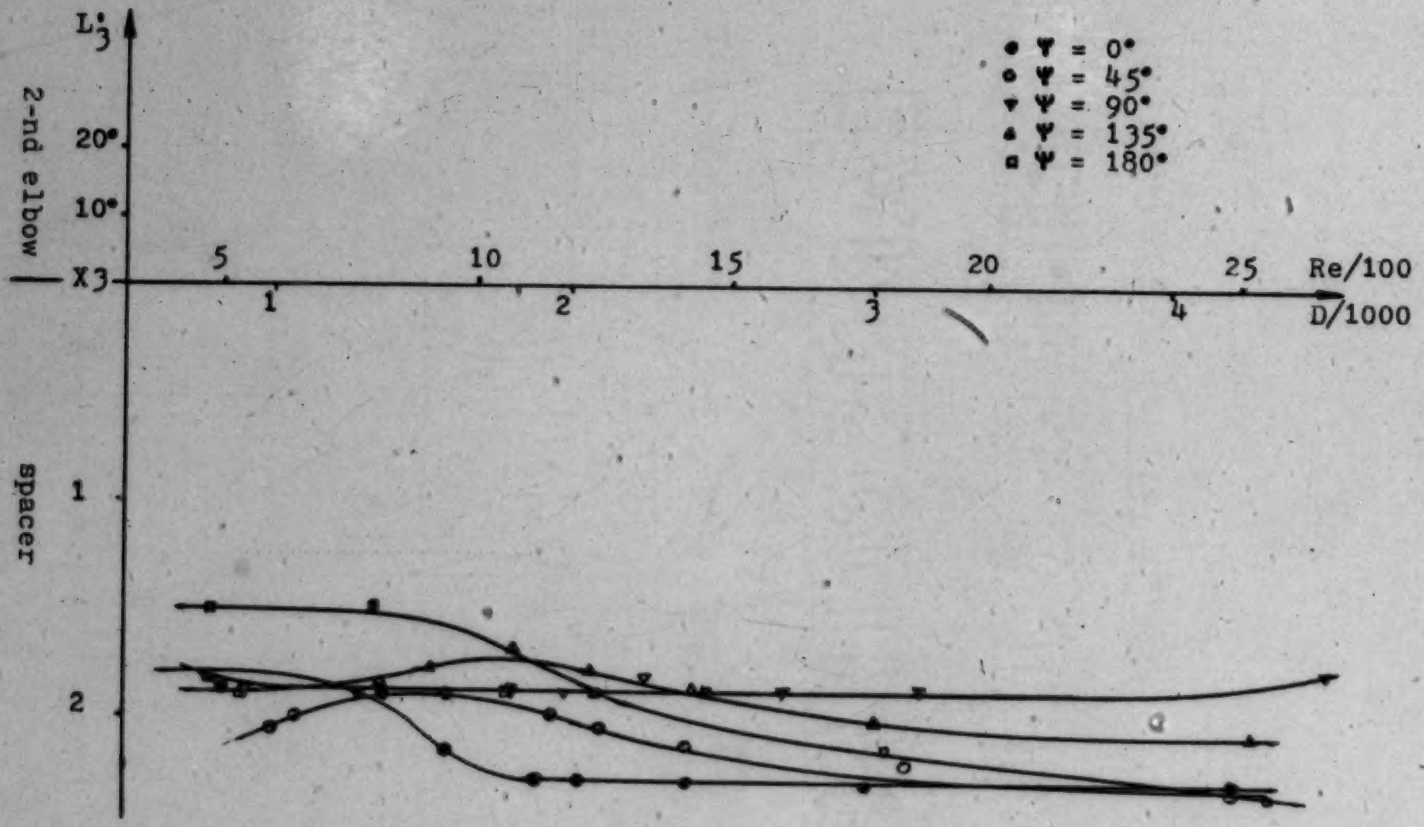

Figure 29 First Separation - Reattachment Line Position versus Reynolds (Dean) Number as a Function of Angle Ψ for a Uniform Velocity Profile and L' = 3.15

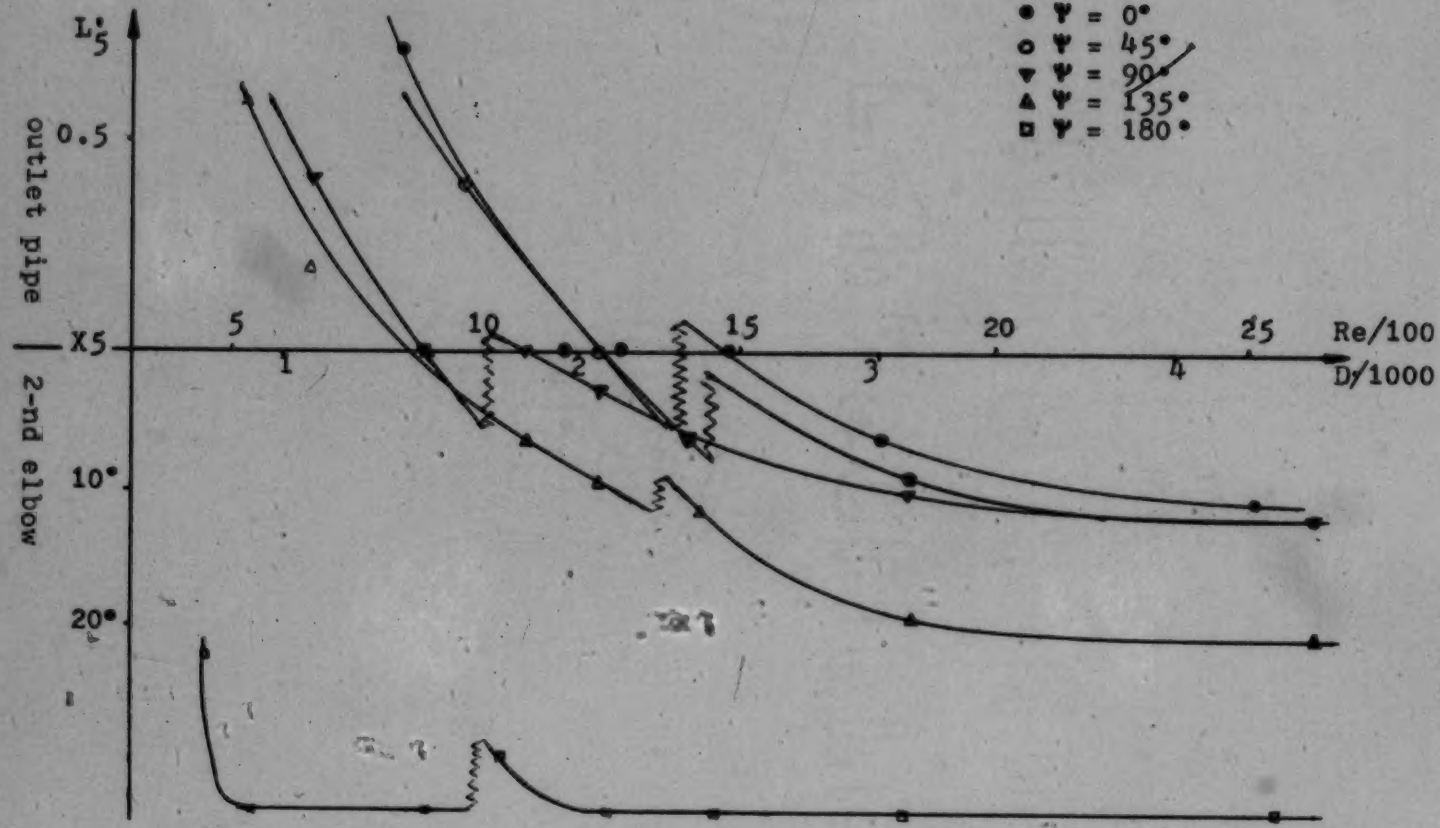

Figure 30 Second Separation Line Position versus Reynolds (Dean) Number as a Function of Angle Ψ for a Uniform Velocity Profile and L' = 0

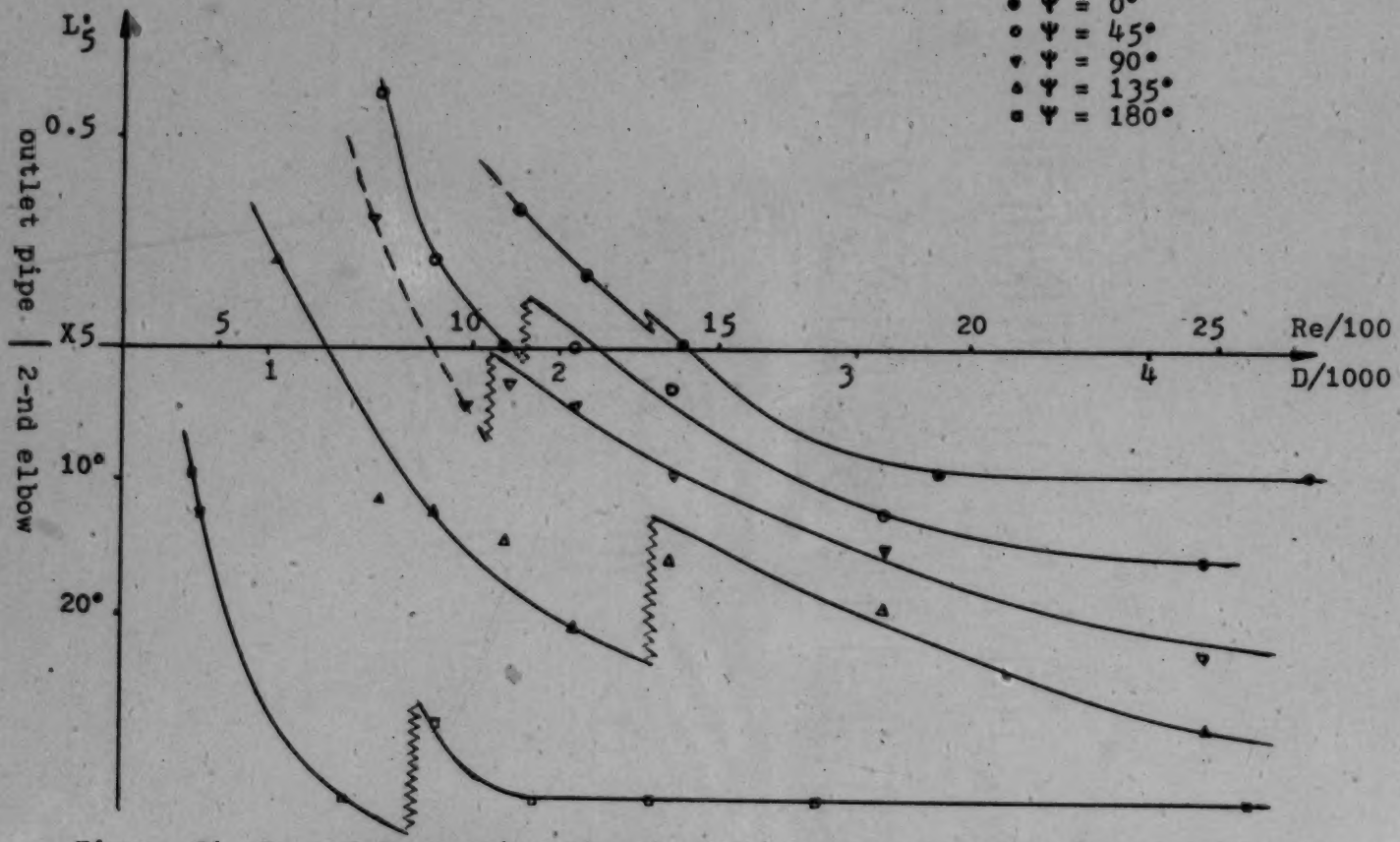

Figure 31 Second Separation Line Position versus Reynolds (Dean) Number as a Function of Angle Ψ for a Uniform Velocity Profile and L' = 0.85

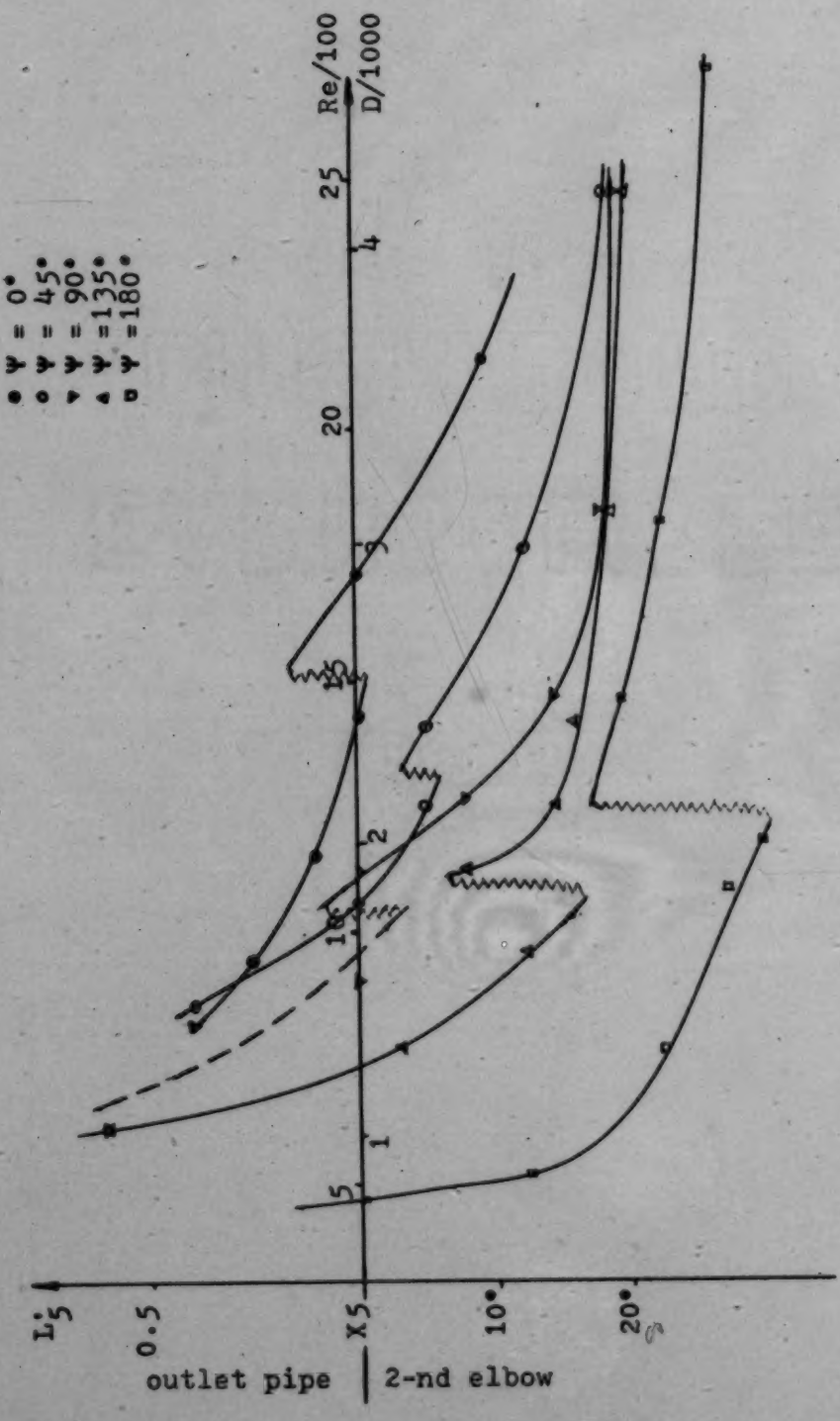

Figure 32 Second Separation Line Position versus Reynolds (Dean) Number as a Function of Angle Ψ for a Uniform Velocity Profile and L' = 1.8

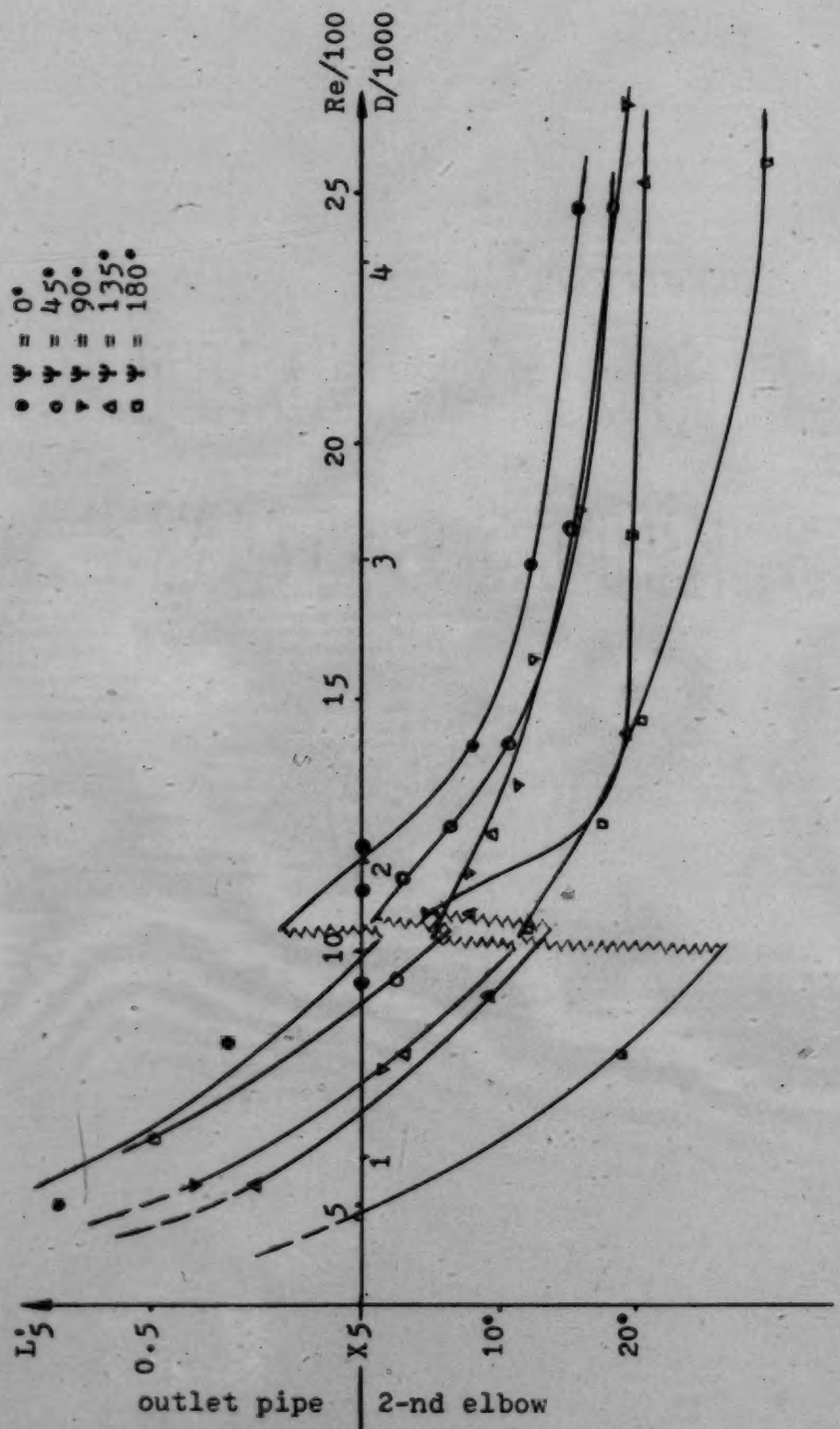

Figure 33 Second Separation Line Position versus Reynolds (Dean) Number as a Function of Angle Ψ for a Uniform Velocity Profile and L' = 3.15

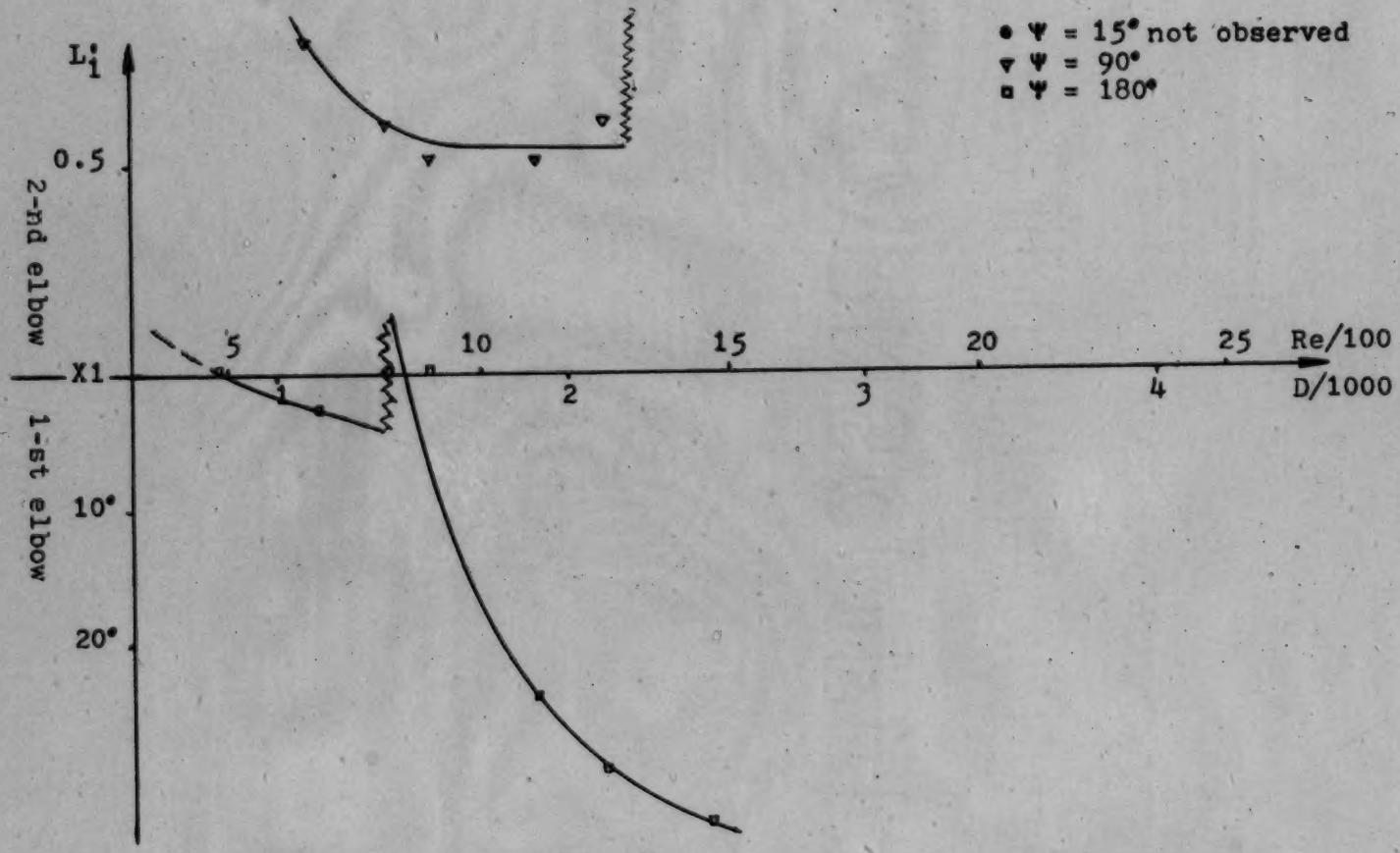

Figure 34 First Separation Line Position versus Reynolds (Dean) Number as a Function of Angle Ψ for a Fully Developed Velocity Profile and L' = 0

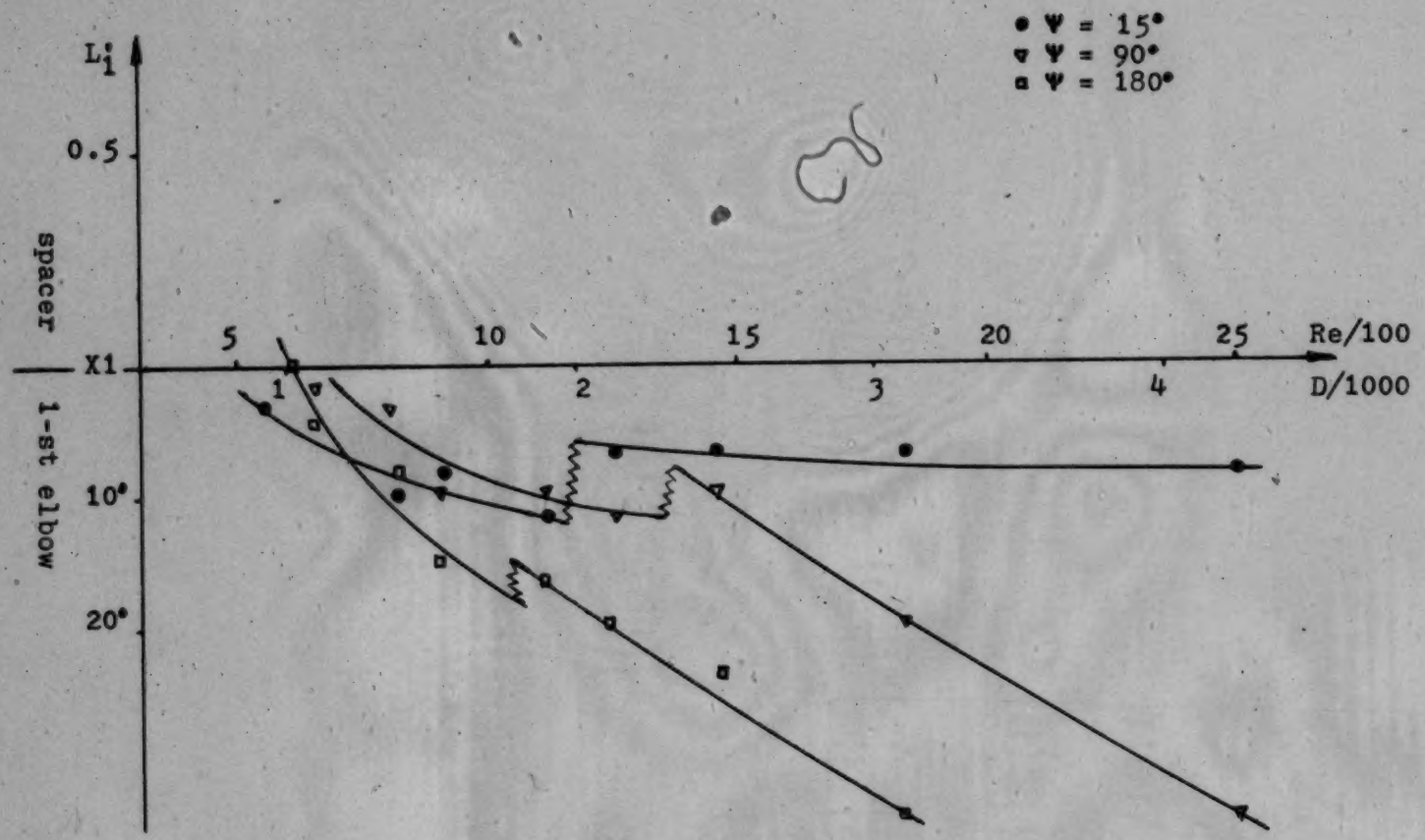

Figure 35 First Separation Line Position versus Reynolds (Dean) Number as a Function of Angle Ψ for a Fully Developed Velocity Profile and $L^* = 3.15$

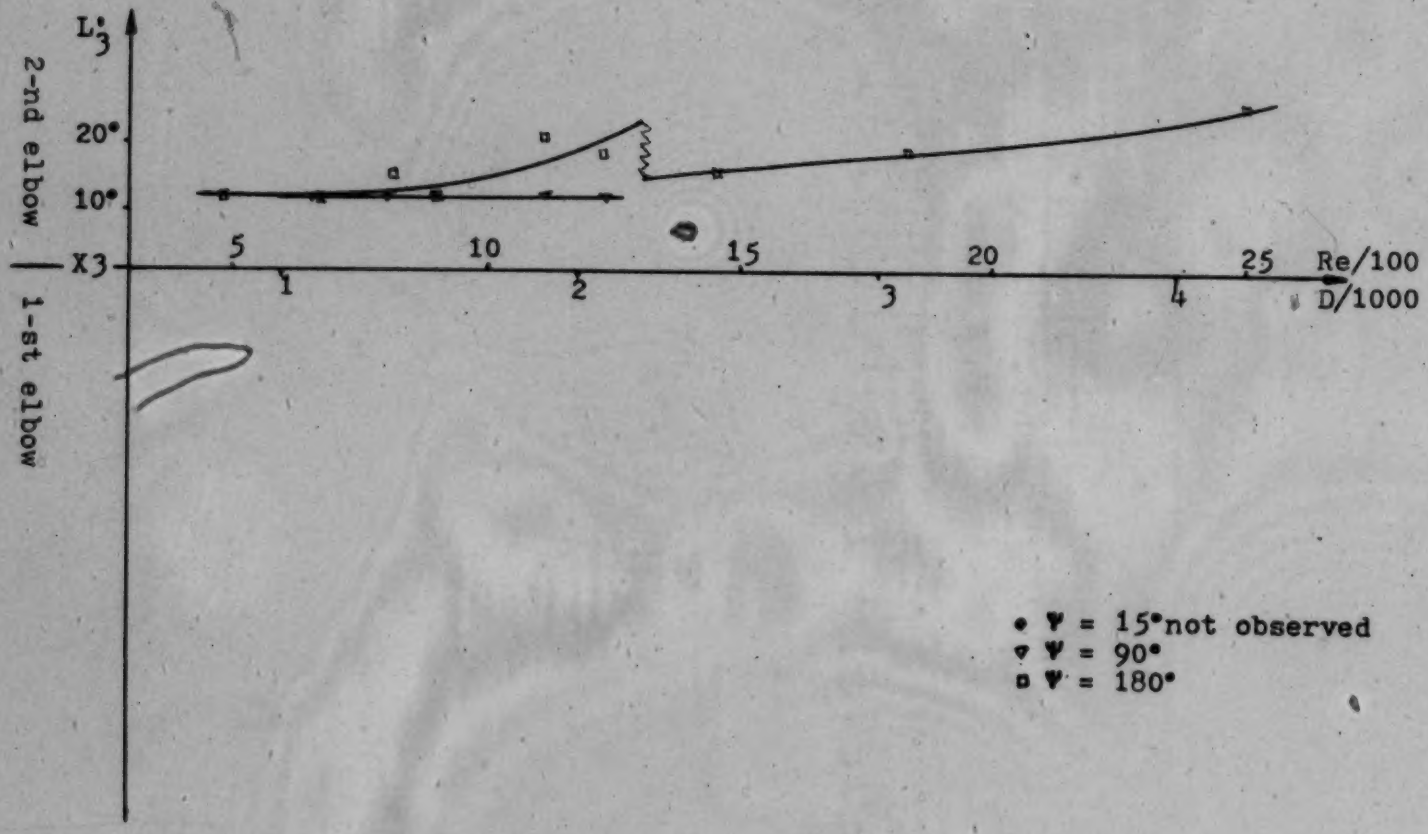

Figure 36 First Separation - Reattachment Line Position versus Reynolds (Dean) Number as a Function of Angle Ψ for a Fully Developed Velocity Profile and L' = 0

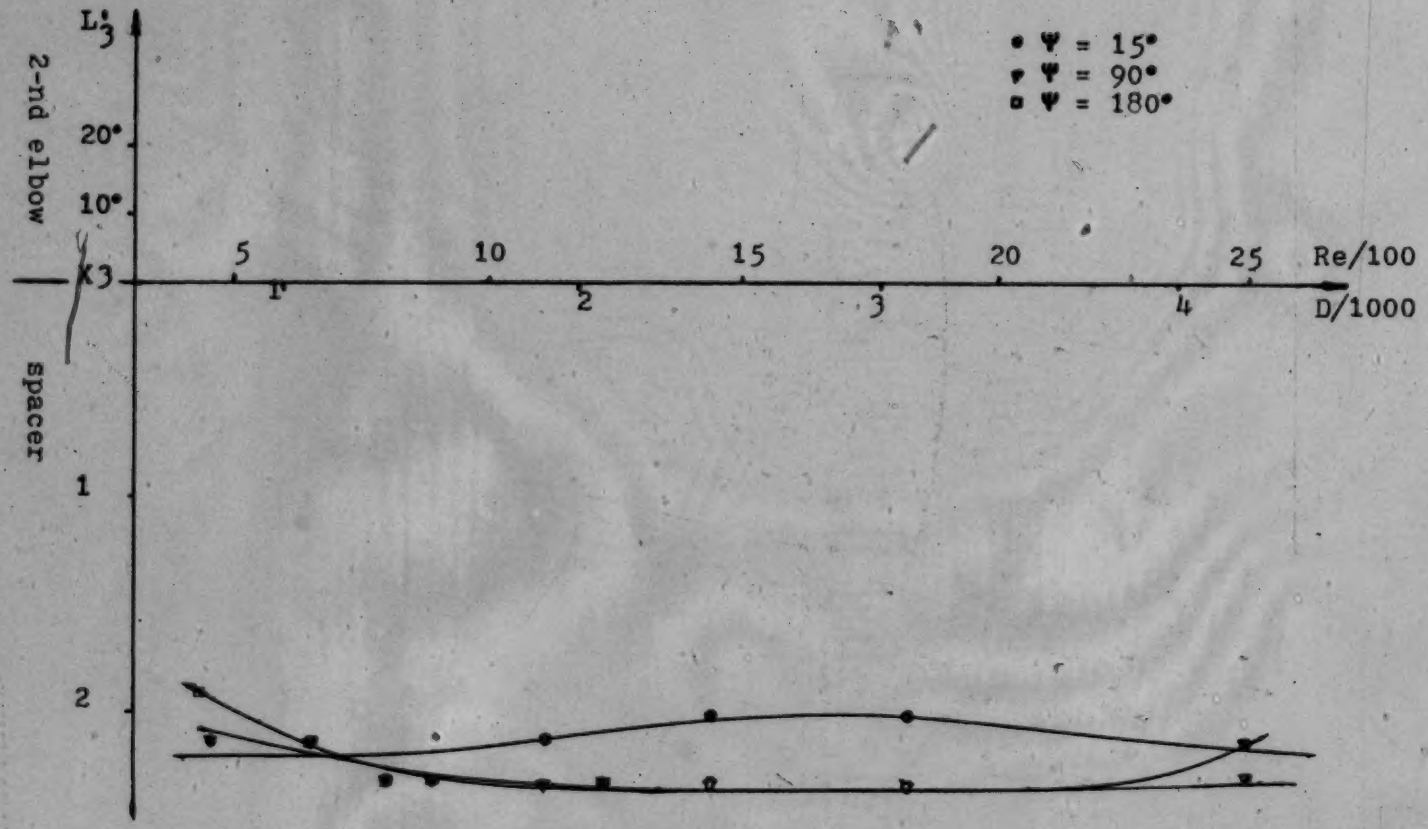

Figure 37 First Separation - Reattachment Line Position versus Reynolds (Dean) Number as a Function of Angle Ψ for a Fully Developed Velocity Profile and L' =3.15

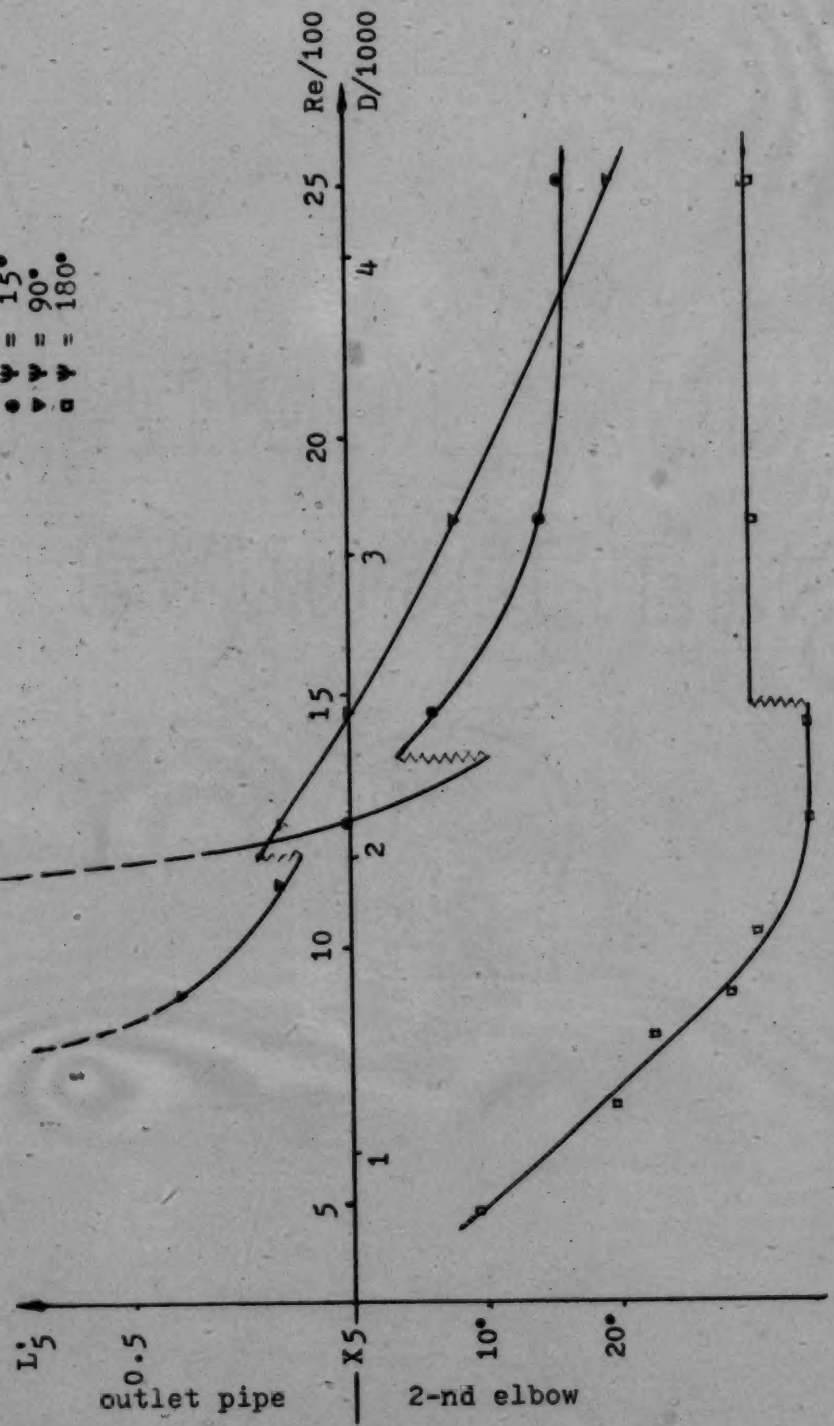

Figure 38 Second Separation Line Position versus Reynolds (Dean) Number as a Function of Angle Ψ for a Fully Developed Velocity Profile and L' = 0

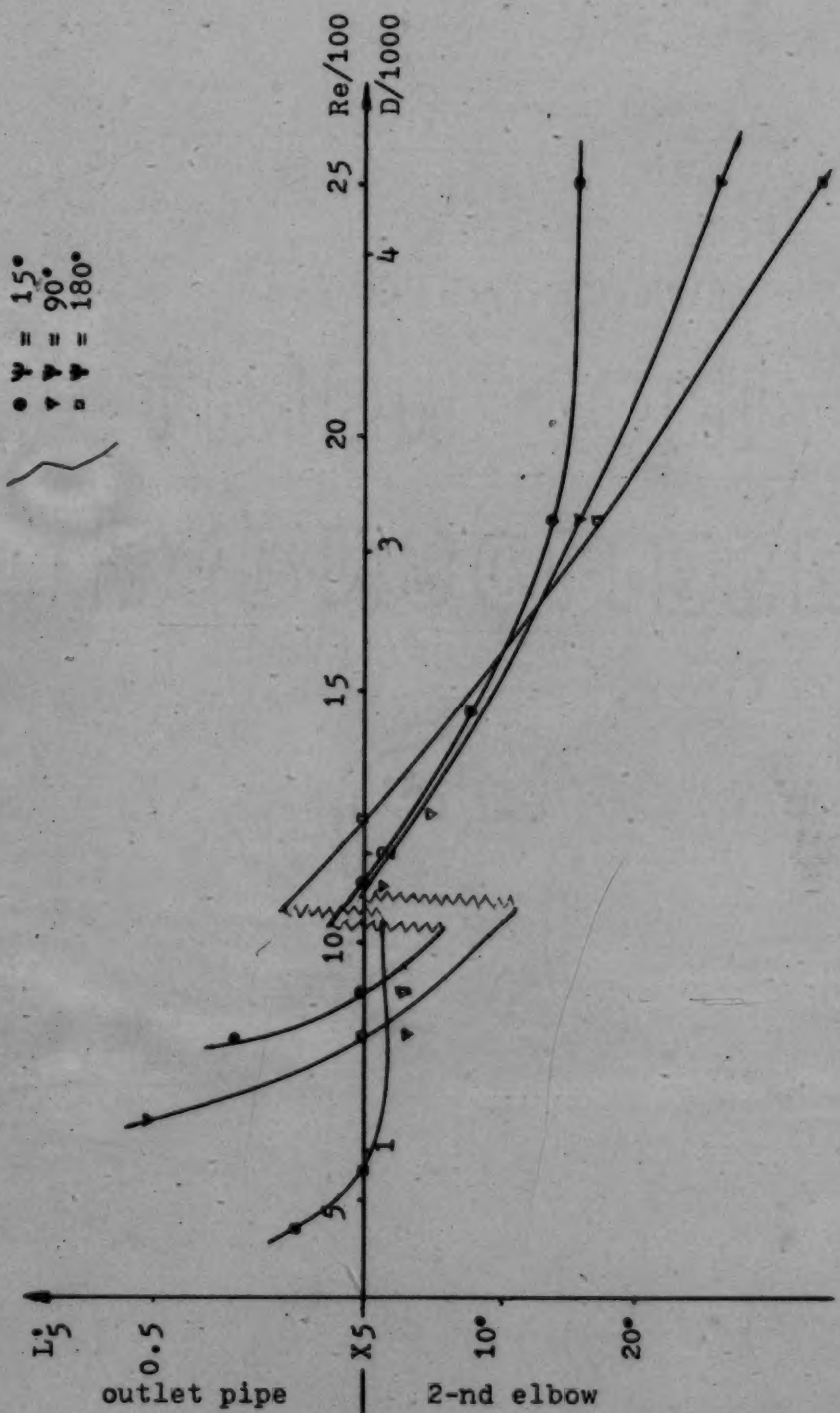

Figure 39 Second Separation Line Position versus Reynolds (Dean) Number as a Function of Angle Ψ for a Fully Developed Velocity Profile and L' = 3.15

Figure 40 Fully Laminar Flow with the Backflow
(Re = 796, Ψ = 180°, L'= 0, DP-A⊙)

Figure 41 Laminar Vortces Produced by the First Separation
(Re = 938, Ψ = 180°, L'= 0, DP-A⊙)

Figure 42 Laminar Flow Center
(Re = 1407, Ψ = 180°, L'= 0, DP-A⊙)

Figure 43 Instabilities Produced by the First Separation
(Re = 1407, Ψ = 180°, L'= 0, DP-A⊙)

Figure 44 Laminar Disturbances at the Outer Curvature of the First Elbow (Re=1835, Ψ = 180°, L'= 0, DP-A ⊙)

Figure 45 Instabilities Produced by the Second Separation (Re = 1835, Ψ = 180°, L' = 0, DP-A ⊙)

Figure 46 Laminar Flow Center
(Re = 2221, Ψ = 180°, L'= 0, DP-A⊙)

Figure 47 Instabilities Outside the Laminar Center
(Re = 2221, Ψ = 180°, L'= 0, DP-A⊙)

Figure 48 "U" Configuration Instabilities
(Re = 1507, Ψ = 0°, L'= 0, DP-A ⊙)

Figure 49 "U" Configuration Instabilities
(Re = 2200, Ψ = 0°, L'= 0, DP-A ⊙)

CHAPTER VI

SECONDARY FLOW PATTERNS

6.1 Introductory Remarks

The purpose of this chapter is to present the results of the qualitative observations of the secondary flow patterns. Although these patterns depend strongly on the spacer length and the angle Ψ, the following remarks are valid for all flow types, presented in Tables 3 and 4.

- Except for a very few cases, there is no observable influence of the Reynolds (Dean) number on the secondary flow patterns.
- The secondary flow velocities were found by the dye-motion observations to be at least one order of magnitude smaller than the main flow velocity U.
- The secondary flow always occurs first at the inner side of the elbow cross-section.
- The secondary flow in the first elbow always forms the symmetrical two coil structure, as described in Section 5.1. In certain cases (low Reynolds number) this structure may be disturbed by the influence of the second elbow, but the effect is not significant.
- Regardless of the flow in the core, in the thin layer along the walls of the second elbow there always exists flow directed inward, called the boundary layer flow of the second elbow secondary circulation. The velocity of this flow, compared with the mean velocity of the flow, U, is very slow and the layer is very thin, therefore even a minimal outward

motion inside the flow center is sufficient to supply enough fluid to meet continuity requirements. This flow has been observed in the elbow only.

- The second elbow magnifies the secondary flow patterns generated by the first elbow when $\Psi = 0°$. When enhancement is impossible, for example when the first elbow secondary flow patterns don't match the second elbow plane of curvature, the second elbow produces its own secondary flow patterns starting from the inner curvature.

- In the outlet pipe, downstream from the second elbow, for all practical purposes, only inertia and viscosity forces are acting on the secondary flow. On the distance not larger than approximately 10 diameters, these forces change the structures of the two, three or four vortices, present in the cross-section number 5, as follows:

* the smaller vortices combine with the larger one, if they are in the same direction,
* the stronger vortex overwhelms the weaker ones if are in the opposite directions, and in addition the weaker ones are more quickly damped by the viscous force,
* the two or four vortex structures remains unchanged in the flow, when the neighboring vortices are in opposite directions and equally strong they are equally damped by the viscous force and have been observed even in the outlet tank.

- Due to the apparatus construction, results have been obtained for the values of angle $0° \leq \Psi \leq 180°$, but symmetry allows the extrapolation of these results to cover $180° \leq \Psi \leq 360°$.

6.2 "U" Configuration ($\Psi = 0°$)

This configuration (angle $\Psi = 0°$) produces the secondary flow type A0, presented in Tables 3 and 4. The second elbow amplifies the two coil structure which has been observed as far as the outlet tank. Two additional outer vortices, reported by Rowe (1970) for high Reynolds number flow, Re = 2.36×10^5 have not been observed (Figures 50, 51 and 52).

6.3 "S" Configuration ($\Psi = 180°$)

This configuration produces secondary flow types B0 or B1 depending upon the flow velocity. In this case, the secondary circulation of the second elbow starts at the inner curvature of the second elbow, and at the outlet of this elbow the final, symmetrical four coil structure is observed. This structure consists of two upper vortices which are produced by the first elbow and two lower ones which are produced by the second elbow, and persists along the outlet pipe when the Reynolds number is higher than, approximately, 450. For lower values of Re, the vortices produced by the second elbow are weak and disappears before the cross-section number 7.

The presence of a spacer allows the second elbow to influence the flow between the elbows. This influence moves the two vortices produced by the first elbow to the spacer wall located directly upstream from the outer curvature of the second elbow (see points "0" in Figure 8). At this

time, the streamlines located closer to the opposite side of a spacer and upstream from the inner curvature of the second elbow, are almost parallel (points "I" in the spacer in Figure 8). This area without vortices grows, when proceeding from the cross-section 1 to the cross-section 3, where the two vortices of the second elbow appear. Figures 54 through 57 inclusive.

6.4 Flow Patterns for $0° < \Psi < 180°$

The three-dimensional configuration of the elbows centerline allows the observation of more complicated flow patterns than described in Sections 6.2 and 6.3. Slowly changing the angle Ψ from 0° to 180° and observing the secondary flow behavior between the elbows, for example, in the spacer in Figure 58, it can be seen that up to a certain critical value of the angle Ψ, the flow maintains the two coil structure, characteristic for the "U" configuration. To do this, the flow acts this way: the plane of symmetry of the two coil structure is twisted spirally along the flow axis, in order to match the second elbow plane of curvature, where the centrifugal force is acting. This type of flow, associated with the "U" configuration, is called "A" (A1 - A3 when $\Psi \neq 0°$) and is discussed later.

The opposite situation is observed, when the angle Ψ is slowly reduced from 180° to 0° . This time, down to a certain, critical value of the angle Ψ, the flow maintains the four coil structure, characteristic for the "S" configu-

ration. The flow behaves such that the plane of symmetry of the first elbow coils (Figure 58) is spirally twisted to match the four coil structure observed at the outlet of the second elbow when the angle $\Psi = 180°$. This type of flow, associated with the "S" configuration is called "B" type (B2 when $\Psi \neq 180°$) and the plane of symmetry is twisted in opposite direction than for flow type "A". The critical values of the angle Ψ for the flow type A and the flow type B are not equal and $\Psi_{\text{crit A}} < \Psi_{\text{crit A}}$ when $0° \leq \Psi \leq 180°$ or, as can be concluded $\Psi_{\text{crit A}} > \Psi_{\text{crit B}}$ when $180° \leq \Psi \leq 360°$. Additionally, there is no direct switch from the type A to the type B, except in the case when $L' = 0$; the intermediate type, called "AB" has been observed, featuring no twist of the plane of the two coil structure symmetry in the spacer, (Figures 58 and from 69 to 71 inclusive). This type has been observed to be unstable, expecially for small L' values and readily changes to either type A or type B. The area between the $\Psi_{\text{crit A}}$ and $\Psi_{\text{crit B}}$ is the same where the flow type AB has been observed. The critical values of the angle Ψ are likely to depend strongly on random, external vibrations and the rate at which the angle Ψ is changed. Therefore, results of the measurements have had a significant scatter and in Figure 59 the more consistent data have been collected.

As has been mentioned previously for the flow patterns type A and B, the flow in the spacer or in the second elbow when there is no spacer, acts such that the plane, div-

viding the two symmetrical vortices produced by the first elbow, is twisted in order to match it to the second elbow plane of curvature. But such twist, expecially when L' is small, disturbs the symmetry of the two vortices, making one of them stronger and the second-weaker, adds a rotation to the whole structure and the twist can not be completed before the second elbow entrance. Finally, under the forces in the second elbow, the flow patterns are still changing downstream from this elbow entrance (see Tables 3 and 4).

An interesting confirmation of the above can be given by the observation of the flow type A when there is no spacer between the elbows. For such case the flow type A has been observed up to $\Psi = 165°$. In the range of the $0° < \Psi \leq 135°$ the two coil structure of the first elbow is twisted inside the second elbow, as described previously and this is the version A1 (Tables 3 and 4, Figures 60, 61 and 62). When the angle Ψ is larger, approximately 120° to 160°, some of the fluid particles are not able to make such a long turn, due to the presence of the backflow zone on the outer side of the second elbow (Section 5.2). These particles make the smaller turn, dividing the larger coil in two, as shown in Table 4 and Figures 63, 65 and 67). For the largest Ψ allowable for the flow type A (from 155° to 165°) the two vortices obtained from the larger one, as described above , are smaller. The additional space in the fifth cross-section is occupied then by the small vortex created by the shear stress (Table 4, Figures 64,66 and 68). The

differences between the two versions of flow (called A2 and A3 respectively) are shown in Figures 65 through 68 inclusive. The versions A2 and A3 have not been observed for spacer lengths greater than $L' = 0.85$ and for the Reynolds number $Re<450$ which confirms the association of these versions of flow with the backflow in the second elbow.

The details of the flows types AB and B2 are shown in Figures 69 through 77 inclusive.

One of the most important features of the flows described in this section is the final effect observed downstream from the cross-section number 7. This effect is always (qualitatively) the same, regardless of the angle Ψ and the type of the flow inside the second elbow, and has the form of the single vortex, turning counterclockwise, when $0 < \Psi < 180$ and, concluding by the symmetry, clockwise, when $180 < \Psi < 360$. This is shown in Figure 78 (due to the observation point, the motion on the photographs is clockwise), where all pictures show the same direction of rotation, except one of the pictures taken for $\Psi = 30°$, where the second vortex (the flow is type A1) has been too strong to be overwhelmed or damped by the viscosity.

Table 3 Secondary Flow Patterns - Flow Types with a Long Spacer ($L' > 0.85$)

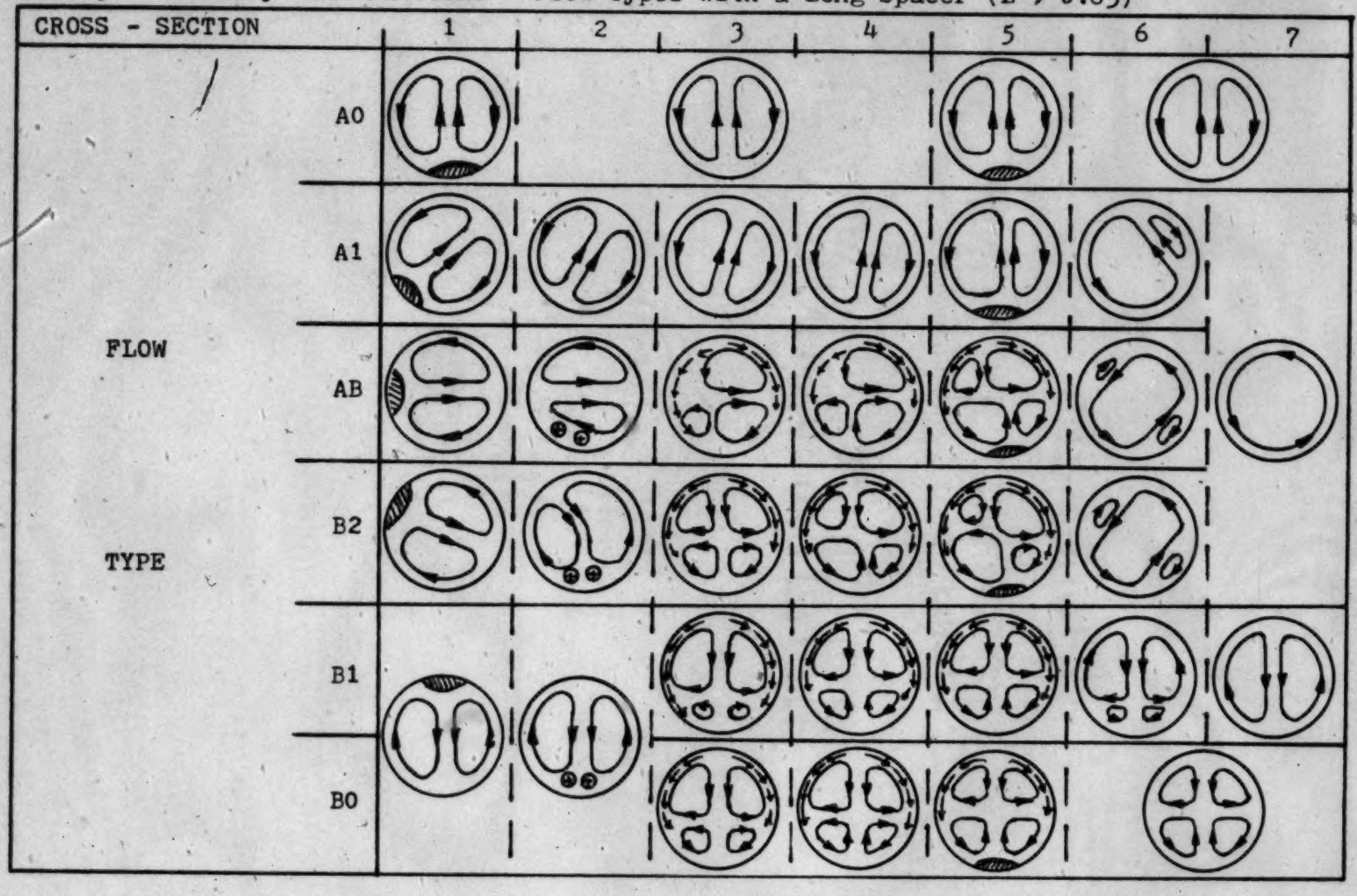

Table 4 Secondary Flow Patterns

Flow Types with a Short Spacer ($L' \leq 0.85$)

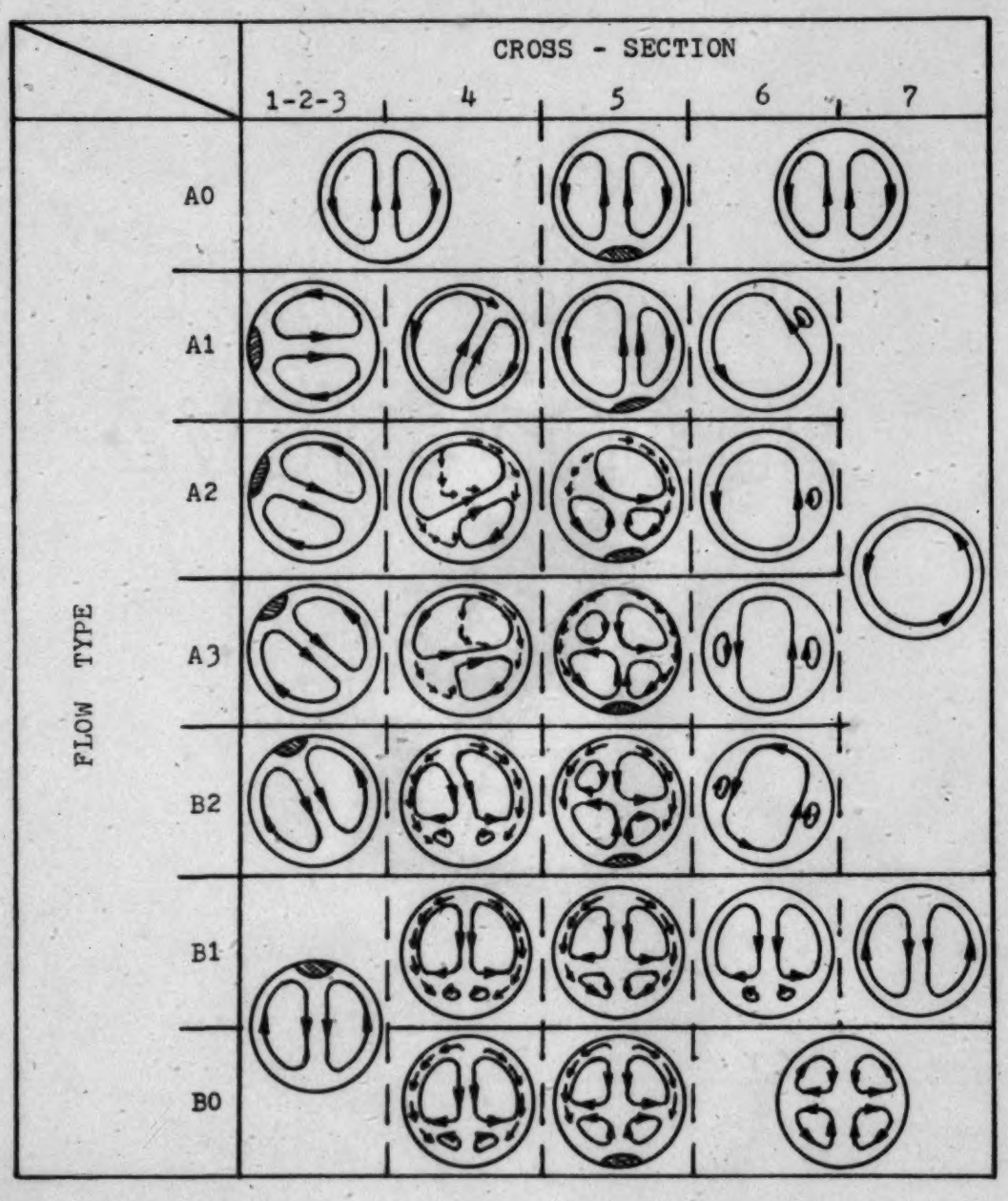

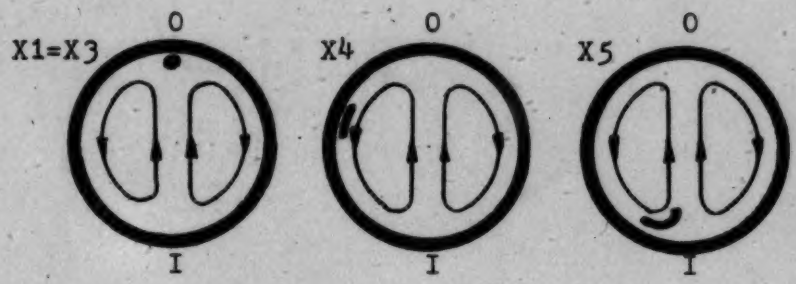

Figure 50 Flow Type A0 - Left Coil
(Re = 403, Ψ = 0°, L'= 0, DP-Ko)

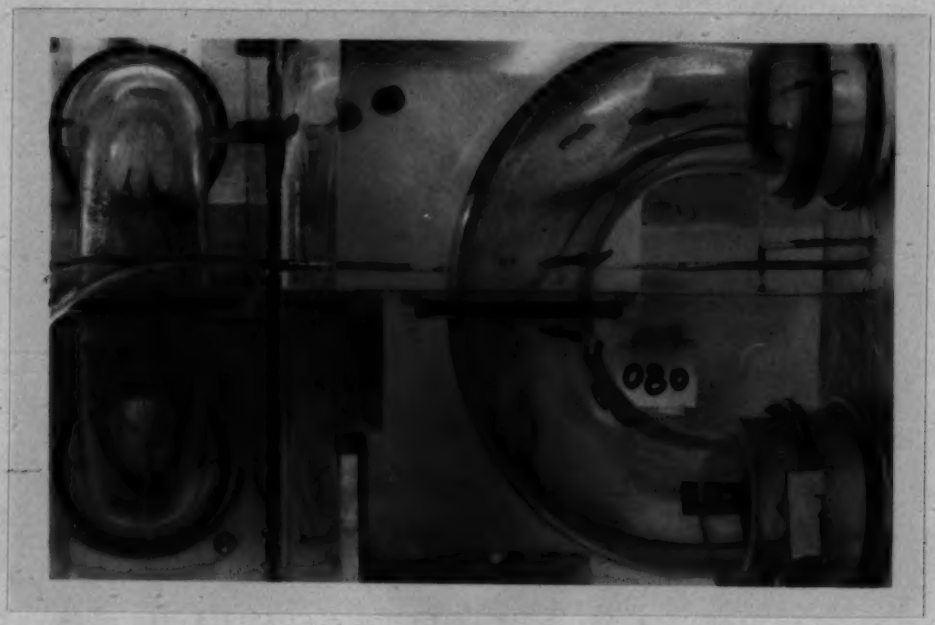

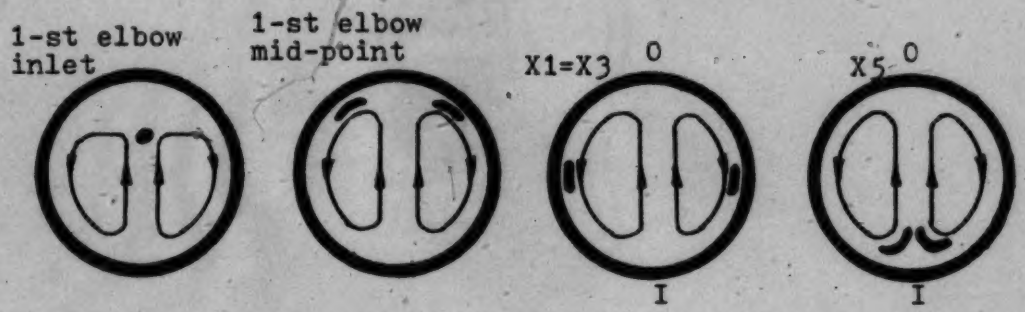

Figure 51 Flow Type A0 - Two Coil Structure
(Re = 403, Ψ = 0°, L'= 0, DP-A Ω)

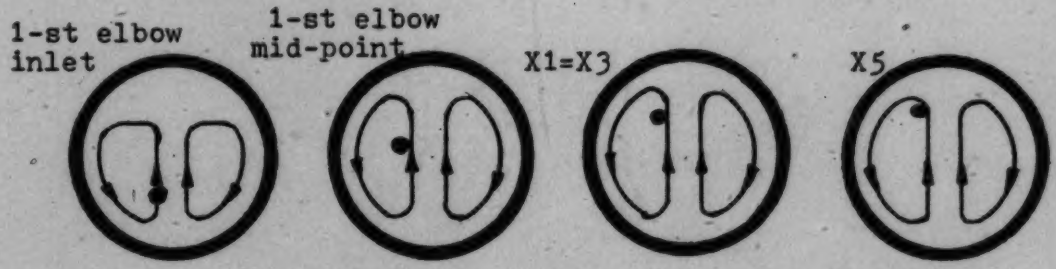

Figure 52 Flow Type A0 - Left Coil
(Re = 403, Ψ = 0°, L'= 0, DP-A○)

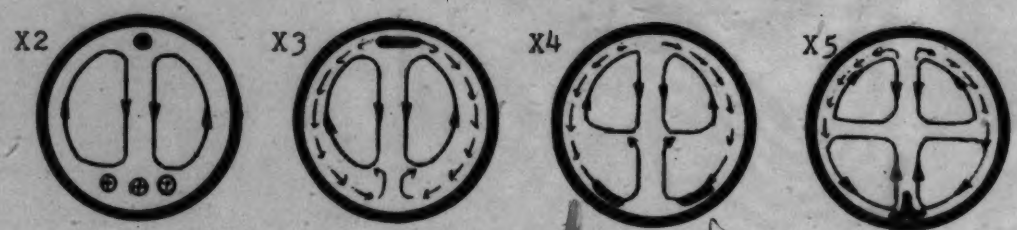

Figure 53 Flow Type B0 - Lower Coils
(Re = 681, ♥ = 180°, L'= 3.15, DP-H0-)
low initial momentum)

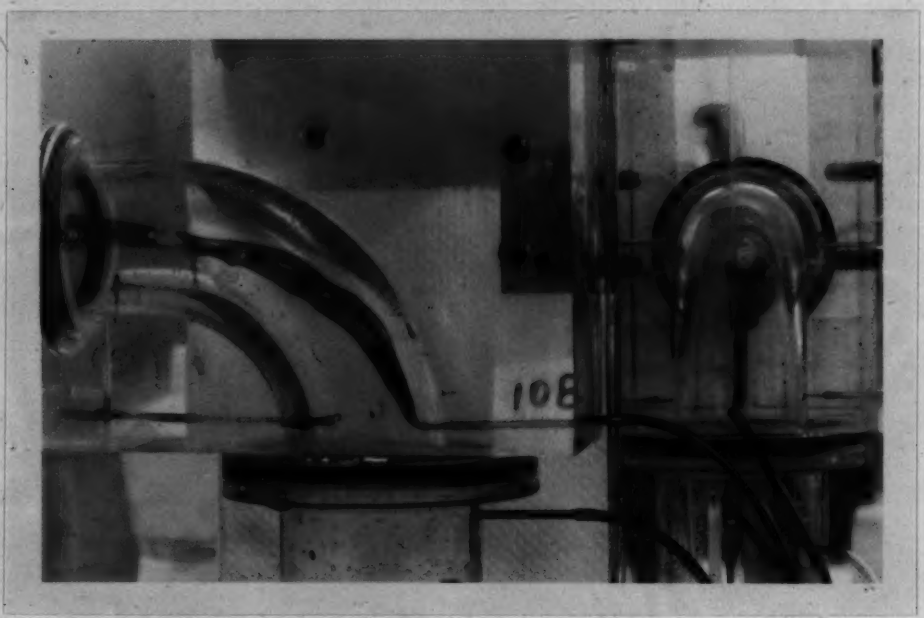

Figure 54 Flow Type B0 - Upper Coils
(Re = 812, Ψ = 180°, L'= 3.15, DP-Ko-high initial momentum)

Figure 55 Flow Type B1 - Upper Coils
(Re = 380, Ψ = 180°, L'= 0, DP-Ko-high
initial momentum)

Figure 56 Flow Type B1 - Lower Coils
(Re = 380, Ψ = 180°, L'= 3.15, DP-10°)

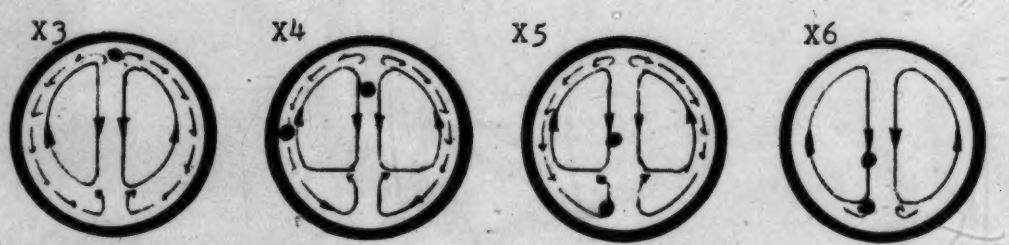

Figure 57 Flow Type B1 - Right Coils
(Re = 380, Ψ = 180°, L'= 3.15, DP-I0°)

A AB B

Figure 58 Basic Flow Types
(Re = 422, L'= 3.15, DP-A ⊙, left fig. Ψ = 90°,
central fig. Ψ = 65°, right fig. Ψ = 90°)

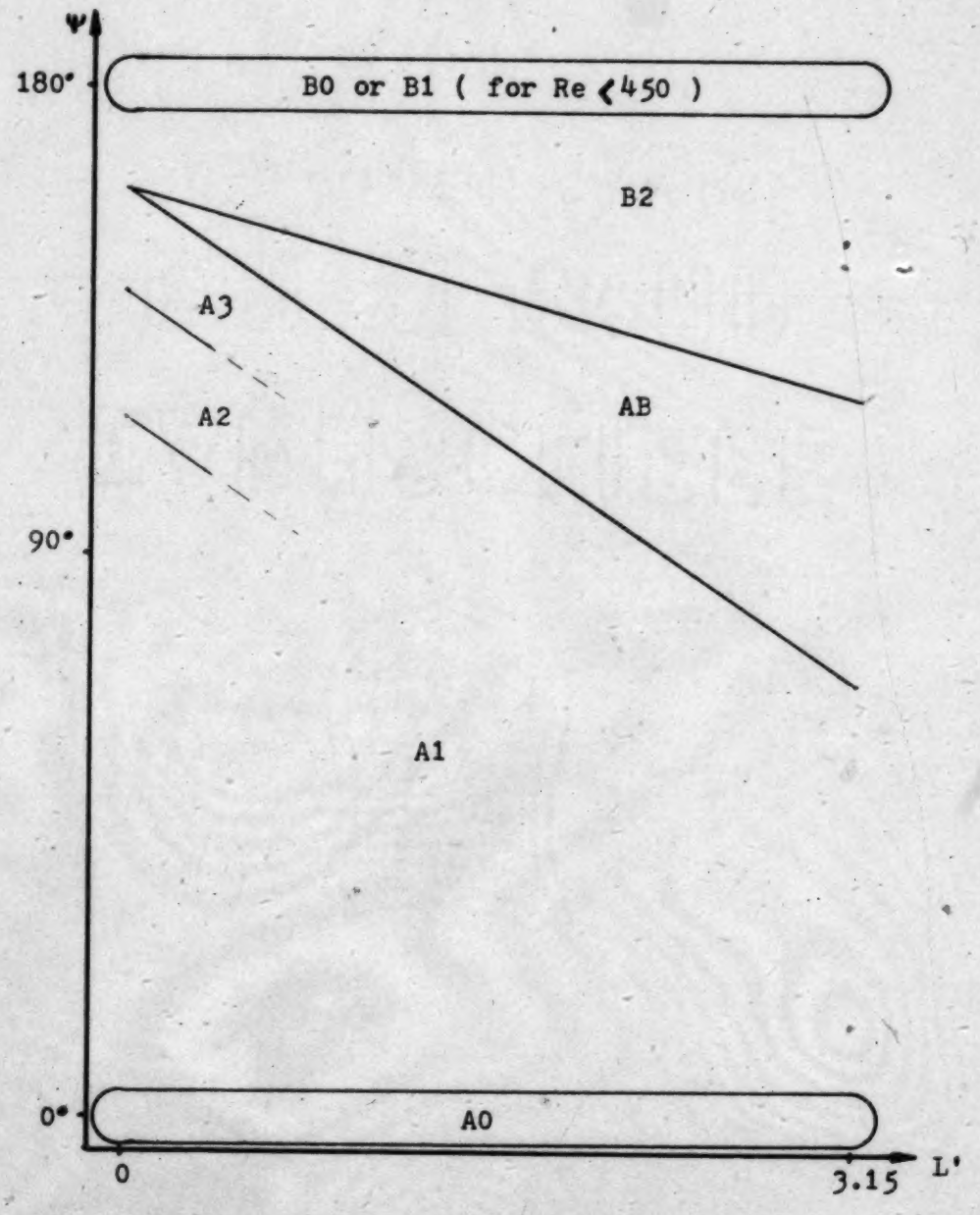

Figure 59 Area of the Flow Types Existence

Figure 60 Flow Type A1 - Left Coil
(Re = 659, Ψ = 135°, L'= 0, DP-C1)

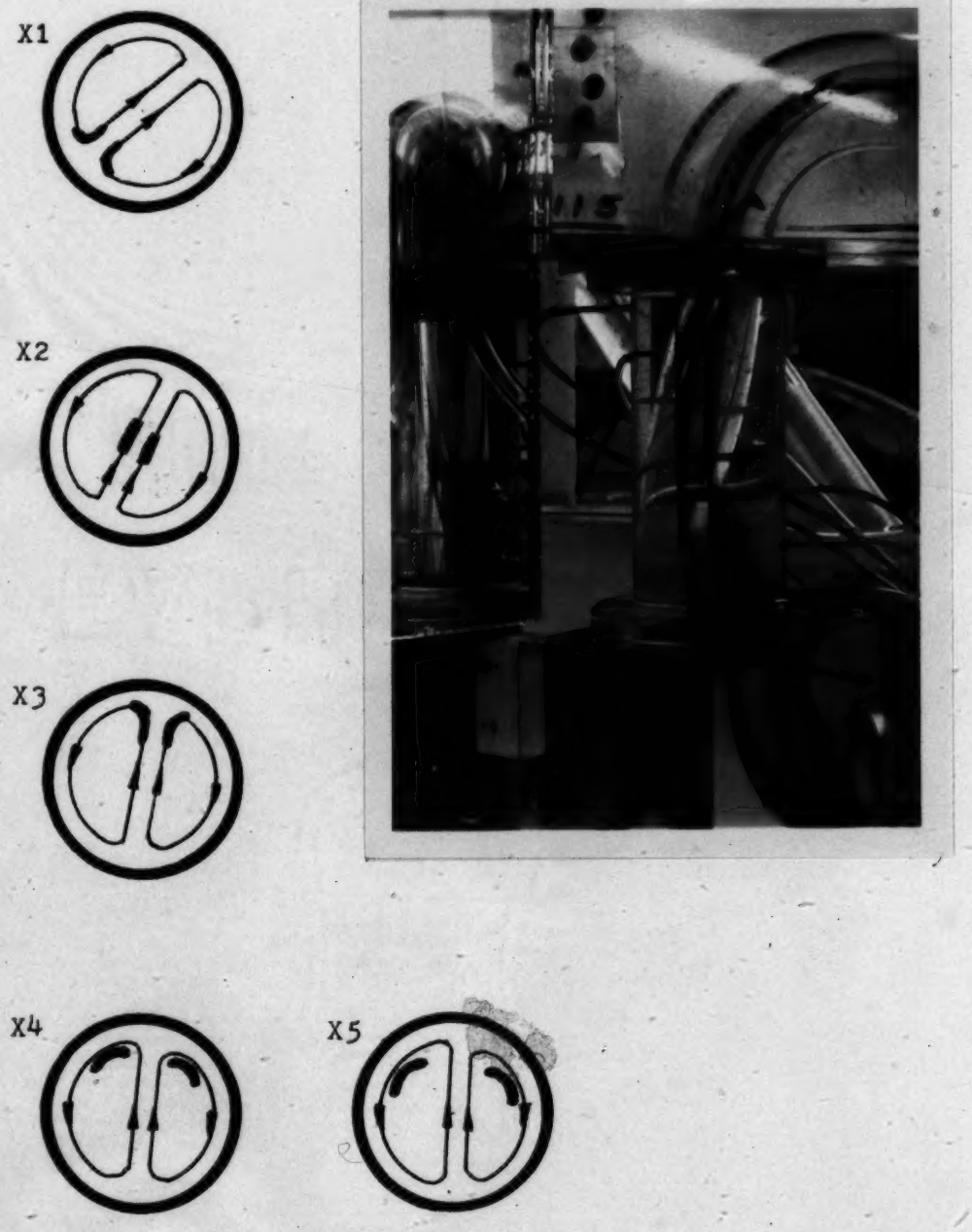

Figure 61 Flow Type A1 - Two Coil Structure
(Re = 485, Ψ = 45°, L'= 3.15, DP-A ⊙)

Figure 62 Flow Type A1 - Left Coil and Final Vortex
(Re = 659, Ψ = 90°, L'= 0, DP-Cr)

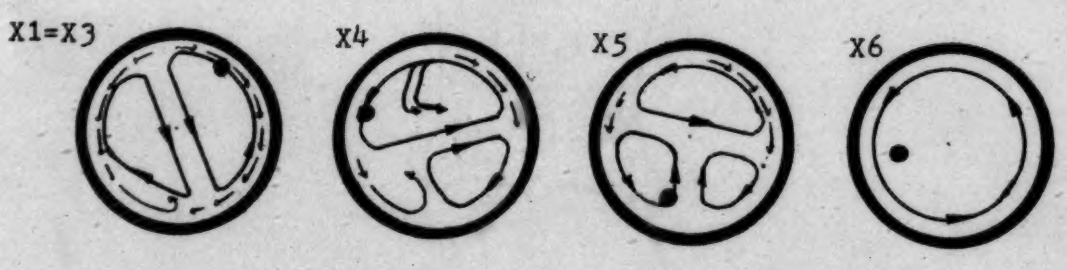

Figure 63 Flow Type A2 - Lower Left Coil and Backflow
(Re = 659, Ψ = 160°, L'= 0, DP-C1)

Figure 64 Flow Type A3 - Upper Right and Lower Left Coils
(Re = 508, Ψ = 150°, L'= 0, DP-Cr)

Figure 65 Flow Type A2 - Upper and Lower Right Coils, Final Vortex (Re = 508, Ψ = 120°, L'= 0, DP-Lr-high initial momentum)

Figure 66 Flow Type A3 - Right Coils and Final Vortex (Re = 508, Ψ = 150°, L'= 0, DP-Lr-high initial momentum)

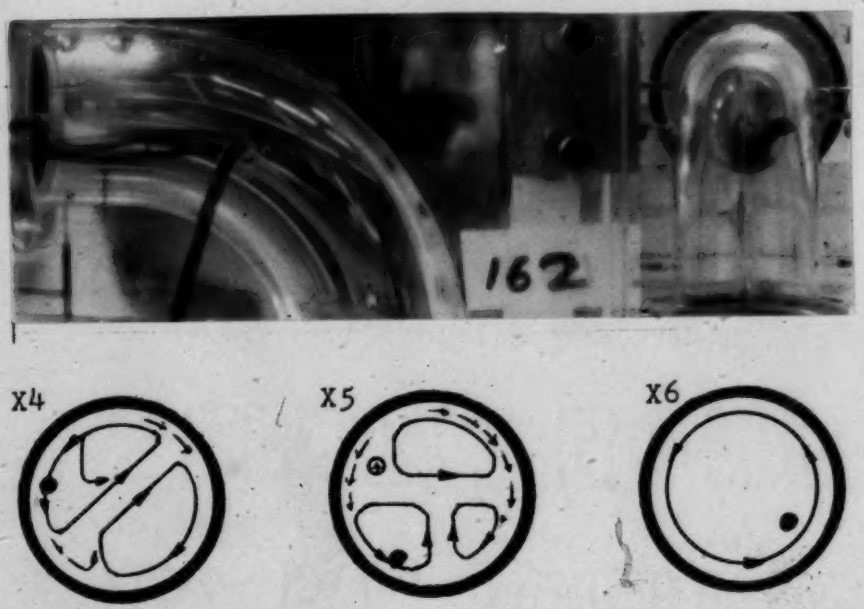

Figure 67 Flow Type A2 - Lower Left Coil and Final Vortex
(Re = 508, Ψ = 120°, L'= 0, DP-L1-high initial momentum)

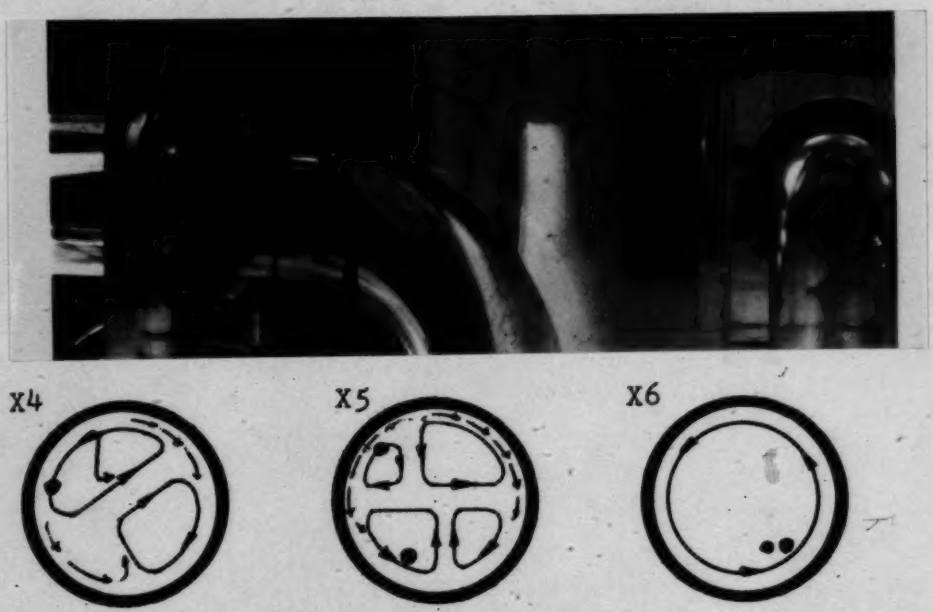

Figure 68 Flow Type A3 - Left Coils and Final Vortex
(Re = 400, Ψ = 155°, L'= 0, DP-L1-high initial momentum)

Figure 69 Flow Type AB - Lower Coils

(Re = 422, Ψ = 90°, L'= 3.15, DP-Ki-
upper fig. high initial momentum
lower fig. low initial momentum)

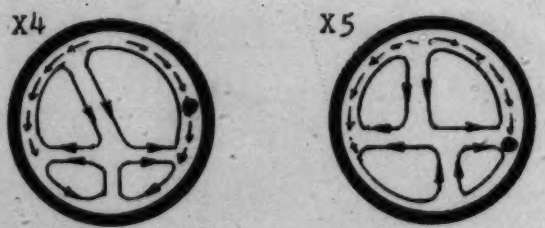

Figure 70 Flow Type AB - Lower Right Coil
(Re = 414, Ψ = 90°, L'= 3.15, DP-Lr)

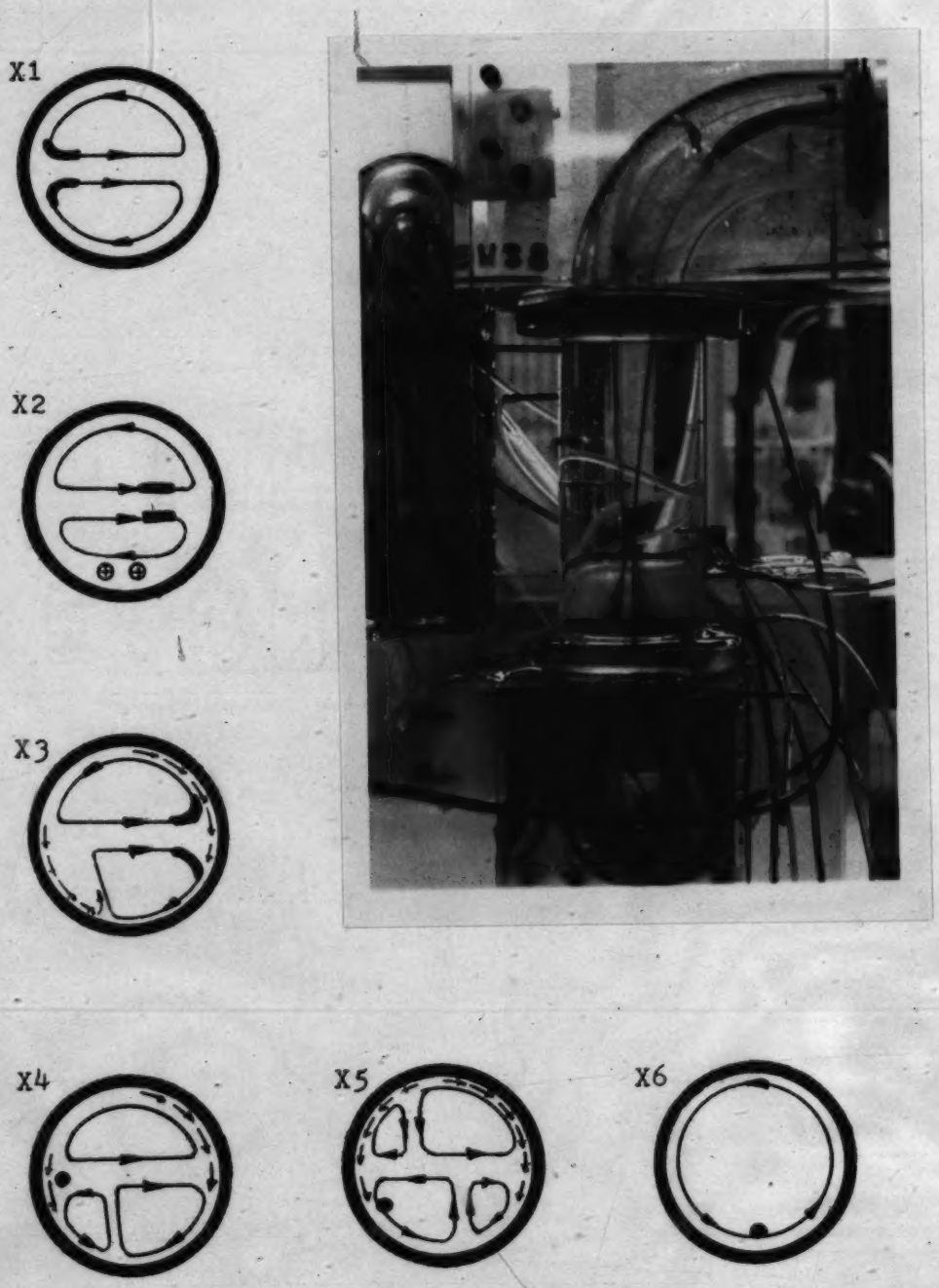

Figure 71 Flow Type AB - Lower Left Coil, Two Coil Structure in the Spacer and Final Vortex
(Re = 414, Ψ = 90°, L'= 3.15, DP-L1 and A⊙)

Figure 72 Flow Type B2 - Large Ψ
(Re = 422, Ψ = 45°, L'= 3.15, DP-A ⊙)

Figure 73 Flow Type B2 - Lower Right Coil and Final Vortex
(Re = 414, Ψ = 90°, L'= 3.15, DP-Lr)

Figure 74 Flow Type B2 - Lower Left Coil
(Re = 414, Ψ = 90°, L'= 3.15, DP-L1 and A⊙)

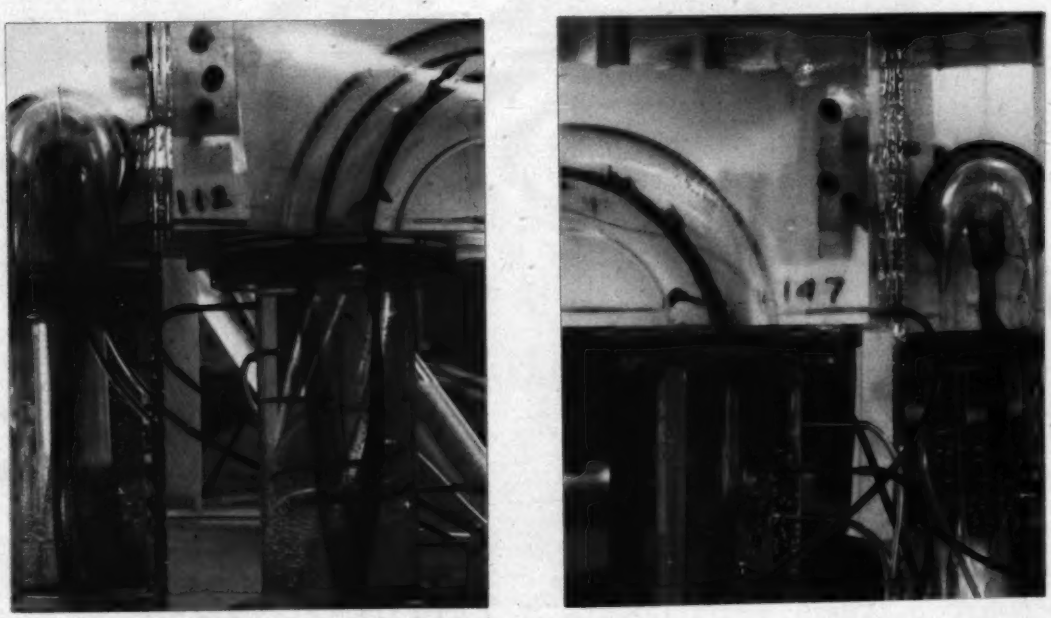

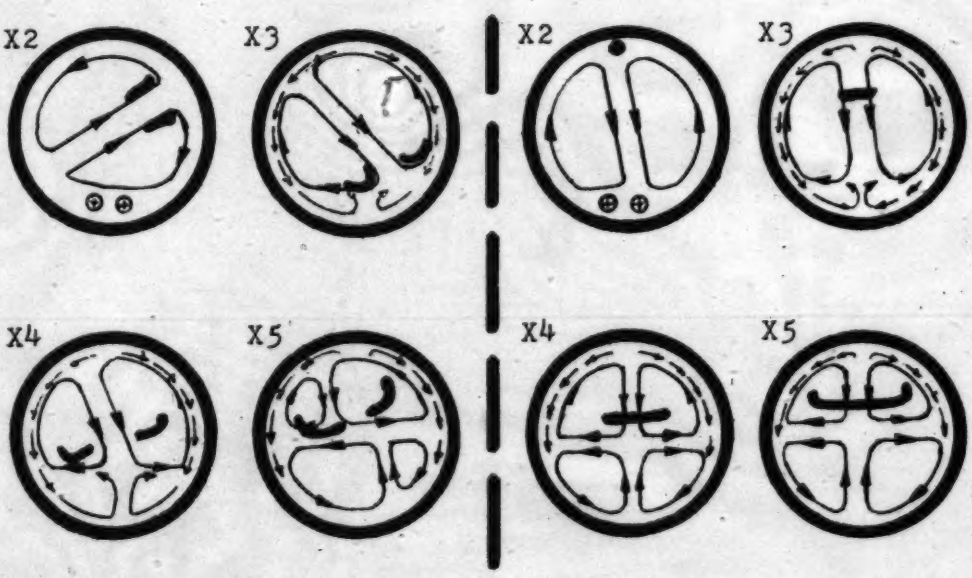

Figure 75 Flows Type B2 - Different Ψ

(left fig. Re = 485, Ψ = 45°, L'= 3.15, DP-A ⊙)
(right fig. Re = 340, Ψ =135°, L'= 3.15, DP-H0° - high initial momentum)

Figure 76 Flow Type B2 - Lower Left Coil and Final Vortex
(Re = 340, Ψ = 135°, L'= 3.15, DP-K1)

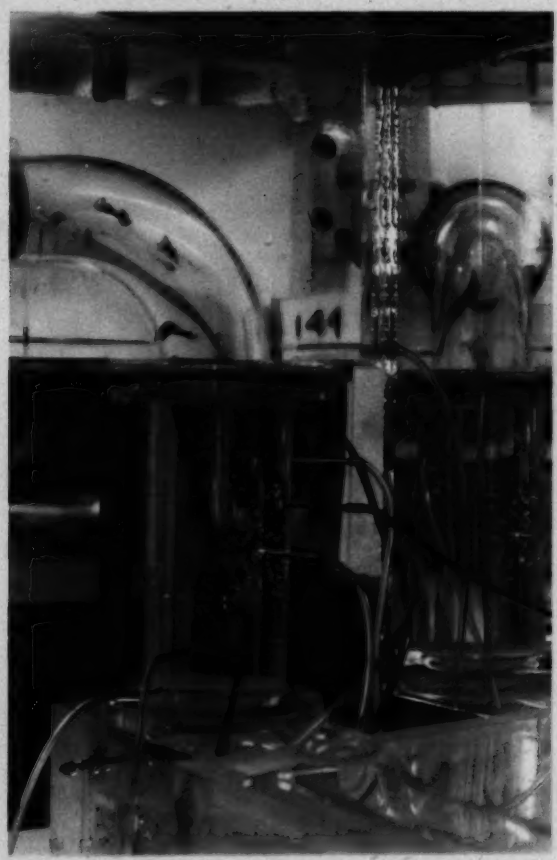

Figure 77 Flow Type B2 - Lower Right Coil
(Re = 340, Ψ = 135°, L'= 3.15, DP-Kr)

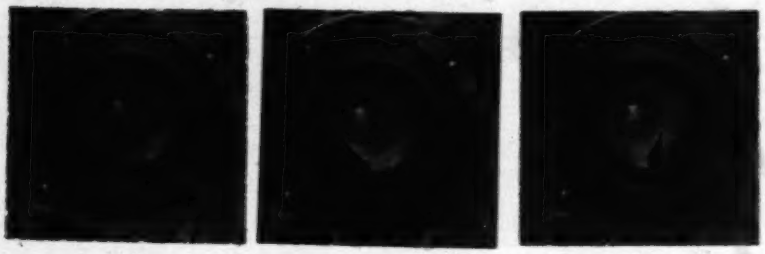

Ψ = 30°
L'= 3.15

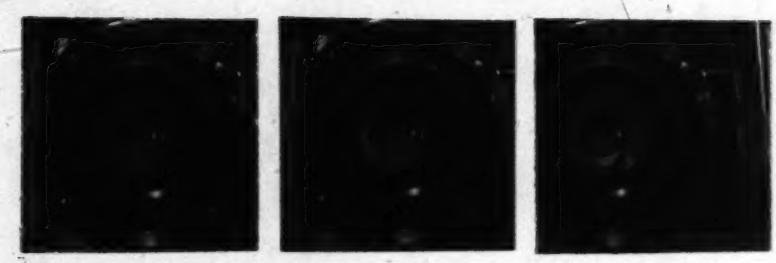

Ψ = 90°
L'= 0

Ψ = 135°
L'= 3.15

Ψ = 150°
L'= 0

Figure 78 Final Vortex
(Re = 450, DP-0)

CHAPTER VII

CONCLUSIONS

7.1 Summary

In conclusion, for the investigated range of variables, the experimental findings can be summarized as follows:

1. For "U" configuration, there exists a two vortex structure, symmetrical with respect to the plane of curvature of the elbows.
2. For the "S" configuration, there exists the four vortex structure (for $Re \geq 450$), symmetrical with respect to the plane of curvature of the elbows.
3. For the angles $0 < \Psi < 180$ there exist three basic types of flow, identified on the basis of the two coil structure at the inlet to the second elbow.
4. For the three-dimensional configuration, there is a single vortex in the outlet pipe at points sufficiently downstream from the second elbow.
5. There exists only one (second) separation region when both L' and Ψ are small, and there exist two independent separation regions, one in each elbow, for all other cases.
6. There exists backflow inside the first separation zone and for the higher Reynolds numbers also in the second one.
7. The backflow in the first elbow is amplified by the centrifugal force in the second elbow (especially for $\Psi = 180$).
8. The backflow in the second elbow changes the flow patterns downstream.

7.2 Suggestions for Further Work

As has been previously explained, the apparatus has been found inadequate to give valuable quantitative as well as qualitative pitot tube confirmation of the flow patterns investigation results obtained in this work. Because it is doubtful if such confirmation can be obtained for the low range of Reynolds numbers, the more advanced measurement techniques are required. Both the laser and the hot wire anemometry seem to be suitable, but are very laborious and require the specially designed apparatus and/or measuring devices (Nerem et al 1972, Agrawal et al 1978).

For better modelling of the human aortic arch, is is suggested to change the shape of the inlet to the first elbow in order to avoid the separation at the sharp edge. Such re-designed apparatus would allow to investigate the transition to turbulence using, for example a hot wire anemometer.

The experiments using the dye technique should be carried out with a larger apparatus in order to make the observations easier and to obtain more precise quantitative results, but if city water is used, also an efficient method of air bubbles removal should be developed and adequate warm water source should be provided.

For better control of the low-Reynolds number flow (below 400), it is suggested to use a precise by-pass valve at the inlet to the inlet tank.

REFERENCES

Adler, M., (1934) "Stromung in gekrummten Rohren", Zeit f. ang. Math. u. Mech., 14,257.

Agrawal, Y., Talbot, L., Gonk, K., (1978) "Laser Anemometry Study of Flow Development in Curved Circular Pipes", J. Fluid Mech., 85,497.

Akiyama, M., Cheng, K.C., (1971) "Boundary Vorticity Method for Laminar Forced Convection Heat Transfer in Curved Pipes", Int. J. Heat a. Mass Transf., 14,1659.

Barua, S.N., (1963) "On Secondary Flow in Stationary Curved Pipes", Q.J. Mech. Appl. Math., 16,61.

Beij, K.H., (1938) "Pressure Losses for Fluid Flow in 90 Pipe Bends", J. Res. Nat. Bur. St., 21,1.

Collins, W.M., Dennis, S.C.R., (1975) "The Steady Motion of a Viscous Fluid in a Curved Tube", Q.J. Mech. Appl. Math., 28,133.

Crane Ltd., (1942) "Flow of Fluids through Valves, Fittings and Pipe", Technical Paper No. M-409.

Dagherty, R.L., Ingersoll, A.C., (1954) "Fluid Mechanics with Engineering Applications", 5-th ed., McGrow-Hill.Co.

Dean, W.R., (1927) "Note on the Motion of Fluid in a Curved Pipe", Phil. Mag., 4,208.

Dean, W.R., (1928) "The Stream-Line Motion of Fluid in a Curved Pipe", Phil. Mag., 5,673.

Eustice, J., (1911) "Flow of Water in Curved Pipes", Proc. Roy. Soc., A84,107.

Greenspan, D., (1973) "Secondary Flow in a Curved Tube", J. Fluid Mech., 57,167.

Hawthorne, W.R., (1951) "Secondary Circulation in Fluid Flow", Proc. Roy. Soc., A206,374.

Horlock, J.H., (1956) "Some Experiments on the Secondary Flow in Pipe Bends", Proc. Roy. Soc., A234,335.

Ito, H., (1959) "Friction Factors for Turbulent Flow in Curved Pipes", Trans. ASME, D81,123.

Ito, H., (1960) "Pressure Losses in Smooth Pipe Bends", Trans ASME, D82,131.

Ito, H., (1969) "Laminar Flow in a Curved Pipe", Zeit. f. ang. Math. u. Mech., 49,653.

Lyne, W.H., (1971) "Unsteady Viscous Flow in a Curved Pipe", J. Fluid Mech., 45,13.

McConalgue, D.J., Srivastava, R.S., (1968) "Motion of a Fluid in a Curved Tube", Proc. Roy. Soc., A307,37.

McDonald, D.A., (1960) "Blood Flow in Arteries", London, Arnold.

Murakami, M., Shimizu, Y., (1977) "Hydraulic Losses and Flow Patterns in Pipes with Two Bends Combined", Bull. JSME, 20,1136.

Murakami, M., Shimizu, Y., (1978) "Asymmetric Swirling Flows in Composite Pipe Bends", Bull JSME, 21,1144.

Murata, S., Miyake, Y., Inaba, T., (1976) "Laminar Flow in a Curved Pipe with Varying Curvature", J. Fluid Mech., 73,735.

Nerem, R.M., Seed, W.A., Wood, N.B., (1972) "An Experimental Study of the Velocity Distribution and Transition to Turbulence in the Aorta", J. Fluid Mech., 52,173.

Patankar, S.V., Pratap, V.S., Spalding, D.B., (1974) "Prediction of Laminar Flow and Heat Transfer in Helically Coiled Pipe", J. Fluid Mech., 62,539.

Patankar, S.V., Pratap, V.S., Spalding, D.B., (1975) "Prediction of Turbulent Flow in Curved Pipes", J. Fluid Mech., 67,583.

Pigott, R.J.S., (1950) "Pressure Losses in Tubing, Pipe, and Fittings", Trans. ASME, 72,679.

Sankaraiah, M., Rao, Y.V.N., (1973) "Analysis of Steady Laminar Flow of an Incompressible Newtonian Fluid through Curved Pipes of Small Curvature", Trans. ASME, 95,75.

Schlichting, H., (1968) "Boundary-Layer Theory", 6-th ed., McGraw Hill Co.

Squire, H.B., Winter, K.G., (1949) Roy. Aeron. Estab., Rep. Aero 2317.

Squire, H.B., Winter, K.G., (1951) "The Secondary Flow in a Cascade of Airfoils in a Nonuniform Stream", J. Aeron. Scie., 18,271.

Singh, M.P., (1974) "Entry Flow in a Curved Pipe", J. Fluid Mech., 65,517.

Singh, M.P., Sinha, P.C., Aggarwal M., (1978) "Flow in the Entrance of the Aorta", J. Fluid Mech., 87,97.

Smith, F.T., (1975) "Pulsatile Flow in a Curved Pipe", J. Fluid Mech., 71,15.

Smith, F.T., (1976) "Fluid Flow into a Curved Pipe", Proc. Roy. Soc., A351,71.

Taylor, F.R.S., (1929) "The Criterion of Turbulence in Curved Pipes", Proc. Roy. Soc., A124,243.

Topakoglu, H.C., (1967) "Steady Laminar Flows of an Incompressible Viscous Fluid in Curved Pipes", J. Math. Mech., 16, 1321.

Truesdell, L.C., Adler, R.J., (1970) "Numerical Treatment of Fully Develope Laminar Flow in Helically Coiled Tubes", AIChEJ., 16,1010.

White, C.M., (1929) "Streamline Flow through Curved Pipes", Proc. Roy. Soc., A123,645.

Yao, L.S., Berger, S.A., (1975) "Entry Flow in a Curved Pipe", J. Fluid Mech., 67,177.

Zalosh, R.G., Nelson, W.G., (1973) "Pulsating Flow in a Curved Tube", J. Fluid Mech., 59,693.

APPENDIX

TABLES OF RESULTS FOR

SECTION 5.2

Table A.1 Dependance of L_1 on Ψ and Re for a Uniform Velocity Profile and L' = 0

Ψ = 0°	
Re	L_1/mm/
from 2517 to 450	not obs.

Ψ = 45°	
Re	L_1/mm/
from 2637 to 450	not obs.

Ψ = 90°	
Re	L_1/mm/
2637	-4.0
1835	-3.2
1407	0
1206	+3.2
1082	+4.0
879	+3.2
645	+4.0
527, 450	not obs.

Ψ = 135°	
Re	L_1/mm/
2637	-8.7
1835	-6.8
1407	-4.8
1206	-2.3
1082	-1.6
879	-3.2
649	-2.8
527	-2.3
450	not obs.

Ψ = 180°	
Re	L_1/mm/
2559	-12.7
1812	-12.7
1450	- 9.5
1242	-9.5
1012	-7.9
870	-7.1
544	-9.5
444	-9.5

Table A.2 Dependance of L_1 on Ψ and Re for a Uniform Velocity Profile and L' = 0.85

Ψ = 0°		Ψ = 45°		Ψ = 90°	
Re	L_1 (mm)	Re	L_1 (mm)	Re	L_1 (mm)
2675	-9.5	2482	-7.9	2482	-10.3
1945	-7.9	1835	-6.3	1835	-8.7
1427	-6.3	1407	-4.8	1407	-6.3
1223	-3.2	1206	-6.3	1206	-5.6
1097	-3.2	1082	-4.0	1082	-4.8
856	-2.4	938	-4.0	981	-4.8
594	-5.6	812	-4.8	796	-4.0
428	-5.6	603	-4.0	603	-3.2
		496	-8.7	422	-5.6

Ψ = 135°		Ψ = 180°	
Re	L_1 (mm)	Re	L_1 (mm)
2482	-10.3	2562	-11.9
1835	-10.3	1208	-9.7
1407	-4.8	1367	-8.7
1206	-4.0	1139	-8.7
1082	-4.0	932	-7.9
938	-8.1	745	-4.8
812	-6.3	466	-6.8
603	-2.4	450	-6.3
469	-1.6		

Table A.3 Dependance of L_1 on Ψ and Re for a Uniform Velocity Profile and L' = 1.8

Ψ = 0°		Ψ = 45°		Ψ = 90°	
Re	L_1(mm)	Re	L_1(mm)	Re	L_1(mm)
2140	-9.5	2482	-7.1	2637	-11.1
1712	-7.9	1758	-6.8	1835	-9.5
1427	-8.7	1407	-7.1	1455	-9.5
1157	-6.3	1241	-5.6	1241	-4.8
951	-4.8	1055	-3.2	1111	-2.1
608	-4.8	861	-1.6	898	-4.8
535	-4.8	740	0	812	-3.2
441	-4.0	527	-1.6	603	0
		457	-1.6	444	-2.5

Ψ = 135°		Ψ = 180°	
Re	L_1(mm)	Re	L_1(mm)
2637	-9.5	2718	-11.1
1835	-8.7	1812	-7.9
1407	-7.1	1450	-7.9
1241	-4.8	1176	-7.1
1111	-6.3	1087	-7.9
959	-4.0	763	-11.1
754	-4.8	512	-9.8
563	-4.8	473	-6.3
435	-2.4		

Table A.4 Dependance of L_1 on Ψ and Re for a Uniform Velocity Profile and L' = 3.15

Ψ = 0°	
Re	L_1 (mm)
2482	-11.1
1758	-9.5
1407	-7.9
1206	-6.3
1110	-6.3
938	-4.8
812	-3.2
496	-3.2
206	-3.2

Ψ = 45°	
Re	L_1 (mm)
2482	-7.9
1835	-7.9
1407	-7.1
1241	-6.3
1141	-5.0
938	-3.2
639	-2.4
586	-2.4
449	0

Ψ = 90°	
Re	L_1 (mm)
2675	-10.3
1861	-9.5
1585	-8.7
1337	-7.5
1157	-5.6
1070	-4.8
764	-6.3
542	-5.6
460	-4.8

Ψ = 135°	
Re	L_1 (mm)
2517	-11.1
1783	-10.3
1427	-7.9
1223	-6.3
1070	-4.8
911	-3.2
793	-6.3
535	-3.2
476	-3.2

Ψ = 180°	
Re	L_1 (mm)
2559	-11.1
1812	-7.9
1450	-7.9
1242	-7.9
1061	-6.3
791	-4.8
473	-7.9

Table A.5 Dependance of L_3 on Ψ and Re for a Uniform Velocity Profile and L' = 0

Ψ = 0°	
Re	L_3/mm/
from 2517 to 450	not obs.

Ψ = 45°	
Re	L_3/mm/
from 2637 to 450	not obs.

Ψ = 90°	
Re	L_3/mm/
2637	+9.5
1835	+9.5
1407	+8.2
1206	+7.8
1082	+6.9
879	+6.3
649	+5.6
527	not obs.
450	

Ψ = 135°	
Re	L_3/mm/
2637	+12.7
1835	+8.7
1407	+7.9
1190	+7.9
1082	+6.9
879	+6.3
649	+5.6
527	+5.6
450	not obs.

Ψ = 180°	
Re	L_3/mm/
2559	+19.0
1812	+22.2
1450	+19.9
1242	+22.2
1012	+20.8
870	+12.7
544	+12.7
444	not obs.

Table A.6 Dependance of L_3 on Ψ and Re for a Uniform Velocity Profile and L' = 0.85

Ψ = 0°	
Re	L_3/mm/
2675	-3.2
1945	-3.2
1427	-7.1
1223	0
1097	0
856	-1.7
594	-4.2
428	-6.4

Ψ = 45°	
Re	L_3/mm/
2482	-5.3
1835	-0.5
1407	-4.8
1206	+9.5
1082	+4.3
938	+1.2
812	-3.6
496	-7.9

Ψ = 90°	
Re	L_3/mm/
2482	-7.9
1835	-7.1
1407	-7.1
1206	0
1082	+9.0
981	+4.6
796	0
603	-3.9
422	-7.9

Ψ = 135°	
Re	L_3/mm/
2482	+9.5
1835	+9.5
1407	+9.5
1206	+9.5
1082	+12.1
938	+14.3
812	+11.1
603	+5.3
469	-7.9

Ψ = 180°	
Re	L_3/mm/
2562	+6.3
1708	+6.3
1367	+6.3
1139	+6.3
932	+7.9
745	+7.9
466	+7.9
450	+6.3

Table A.7 Dependance of L_3 on Ψ and Re for a Uniform Velocity Profile and L' = 1.8

Ψ = 0°	
Re	L_3/mm/
2140	-28.6
1712	-26.9
1427	-23.4
1157	-21.7
951	-19.1
808	-23.8
535	-28.6
441	-30.2

Ψ = 45°	
Re	L_3/mm/
2482	-28.6
1758	-19.0
1407	-19.0
1241	-19.0
1055	-19.0
861	-24.2
740	-28.6
527	-36.5
457	-36.5

Ψ = 90°	
Re	L_3/mm/
2637	-28.6
1835	-25.4
1455	-22.2
1241	-19.5
1111	-9.5
898	-12.5
812	-16.1
603	-19.5
444	-21.2

Ψ = 135°	
Re	L_3/mm/
2637	-28.6
1835	-24.1
1407	-19.5
1241	-9.5
1111	-9.5
959	-19.5
754	-19.5
563	-22.2
435	-22.2

Ψ = 180°	
Re	L_3/mm/
2712	-28.6
1812	-25.3
1450	-22.7
1176	-19.1
1087	-9.5
763	+6.3
512	+6.3
473	+6.3

Table A.8 Dependance of L_3 on Ψ and Re for a Uniform Velocity Profile and L' = 3.15

Ψ = 0°	
Re	L_3/mm/
2482	-73.2
1758	-73.2
1407	-73.3
1206	-73.2
1110	-73.2
938	-68.7
812	-60.4
496	-60.4
206	-47.7

Ψ = 45°	
Re	L_3/mm/
2482	-74.6
1835	-70.6
1407	-67.5
1241	-65.1
1141	-62.8
938	-60.3
639	-62.8
586	-65.1
449	not obs.

Ψ = 90°	
Re	L_3/mm/
2675	-58.3
1861	-59.4
1585	-60.3
1337	-57.6
1157	-60.3
1070	-60.3
764	-60.3
542	-60.3
460	-58.3

Ψ = 135°	
Re	L_3/mm/
2517	-66.7
1783	-63.4
1427	-60.3
1223	-57.0
1070	-53.5
911	-57.0
793	-58.3
535	-60.3
476	-57.7

Ψ = 180°	
Re	L_3/mm/
2559	-74.6
1812	-68.4
1450	-60.3
1242	-60.3
1061	-60.3
791	-47.7
473	-47.7

Table A.9 Dependance of L_5 on Ψ and Re for a Uniform Velocity Profile and L' = 0

Ψ = 0°	
Re	L_5/mm/
2517	-5.6
1783	-3.2
1476	0
1259	0
1157	0
839	+11.1
522	not obs.
450	

Ψ = 45°	
Re	L_5/mm/
2637	-6.3
1835	-4.8
1407	-3.2
1206	0
959	+6.3
767	not obs.
544	
450	

Ψ = 90°	
Re	L_5/mm/
2637	-6.3
1835	-5.2
1407	-3.2
1206	-1.6
1082	0
879	0
649	+6.3
527	not obs.
450	

Ψ = 135°	
Re	L_5/mm/
2637	-10.3
1835	- 9.5
1407	-5.6
1206	-4.8
1082	-3.2
879	0
649	+3.2
527	+9.5
450	not obs.

Ψ = 180°	
Re	L_5/mm/
2559	-15.9
1812	-15.3
1450	-15.9
1242	-15.9
1012	-14.3
870	-15.9
544	-15.9
444	-11.1

Table A.10 Dependance of L_5 on Ψ and Re for a Uniform Velocity Profile and L' = 0.85

Ψ = 0°	
Re	L_5/mm/
2675	-4.8
1945	-4.8
1427	0
1223	+2.4
1097	+4.8
856	not obs.
594	not obs.
428	not obs.

Ψ = 45°	
Re	L_5/mm/
2482	-7.9
1835	-6.3
1407	-1.6
1206	0
1082	0
938	+3.2
812	+9.5
603	not obs.
496	not obs.

Ψ = 90°	
Re	L_5/mm/
2482	-11.1
1835	-7.9
1407	-4.8
1206	-2.4
1082	-1.6
981	-2.4
796	+4.8
603	not obs.
422	not obs.

Ψ = 135°	
Re	L_5/mm/
2482	-13.5
1835	-9.5
1407	-7.9
1206	-10.3
1082	-7.1
938	-6.3
812	-5.6
603	+3.2
469	not obs.

Ψ = 180°	
Re	L_5/mm/
2562	-15.9
1708	-15.9
1367	-15.9
1139	-15.9
932	-13.5
745	-15.9
466	-6.3
450	-4.8

Table A.11 Dependance of L_5 on Ψ and Re for a Uniform Velocity Profile and L' = 1.8

Ψ = 0°	
Re	L_5/mm/
2140	-4.8
1712	0
1427	0
1157	+1.6
951	+4.0
808	not obs.
535	
441	

Ψ = 45°	
Re	L_5/mm/
2482	-8.3
1758	-6.3
1407	-2.4
1241	-2.4
1055	0
861	+6.3
740	not obs.
527	
457	

Ψ = 90°	
Re	L_5/mm/
2637	-9.5
1835	-8.3
1455	-7.1
1241	-4.0
1111	0
898	0
812	+6.3
603	+9.5
444	not obs.

Ψ = 135°	
Re	L_5/mm/
2637	-9.7
1835	-9.5
1407	-7.9
1241	-7.1
1111	-4.0
959	-6.3
764	-1.6
603	+9.5
435	not obs.

Ψ = 180°	
Re	L_5/mm/
2718	-12.7
1812	-11.1
1450	-9.5
1176	-14.3
1087	-13.3
763	-11.1
512	-6.3
473	0

Table A.12 Dependance of L_5 on Ψ and Re for a Uniform Velocity Profile and L' = 3.15

Ψ = 0°	
Re	L_5/mm/
2482	-7.9
1758	-6.3
1407	-4.0
1206	0
1110	0
938	0
812	+5.0
496	+11.1
206	not obs.

Ψ = 45°	
Re	L_5/mm/
2482	-9.3
1835	-7.8
1407	-5.6
1241	-3.2
1141	-1.6
938	-1.6
639	+7.9
584	not
449	obs.

Ψ = 90°	
Re	L_5/mm/
2675	-9.5
1861	-7.9
1585	-6.3
1337	-5.6
1157	-4.0
1070	-2.4
764	-0.8
542	+6.3
460	not obs.

Ψ = 135°	
Re	L_5/mm/
2517	-10.3
1783	-5.6
1427	-9.5
1223	-4.8
1070	-4.0
911	-4.8
793	-1.6
535	+4.0
476	not obs.

Ψ = 180°	
Re	L_5/mm/
2559	-14.3
1812	-8.9
1450	-10.3
1242	-8.5
1061	-6.3
791	-9.5
473	0

Table A.13 Dependance of L_1 on L', Ψ and Re for a Fully Developed Velocity Profile

L'= 0, Ψ = 15°	
Re	L_1/mm/
from 2500 to 453	not obs.

L'= 0, Ψ = 90°	
Re	L_1/mm/
2500	not obs.
1835	
1450	
1240	+10.3
1110	+7.9
900	+6.3
812	+9.5
650	+12.7
453	not obs.

L'= 0, Ψ = 180°	
Re	L_1/mm/
2500	-19.0
1835	-19.0
1450	-15.9
1240	-14.3
1110	-11.9
900	0
812	0
680	-1.6
485	0

L'=3.15, Ψ =180°	
Re	L_1/mm/
2500	-19.0
1835	-15.9
1450	-11.1
1240	-9.5
1110	-7.9
900	-7.1
812	-4.0
650	-2.4
612	0

L'=3.15, Ψ =90°	
Re	L_1/mm/
2500	-15.9
1835	-9.5
1450	-4.8
1240	-5.6
1110	-4.8
900	-4.8
812	-1.6
650	-0.8
453	-4.8

L'=3.15, Ψ =15°	
Re	L_1/mm/
2500	-4.0
1835	-3.2
1450	-3.2
1240	-3.2
1110	-5.6
900	-4.0
812	-4.8
550	-1.6
444	-3.2

Table A.14 Dependance of L_3 on L', Ψ and Re for a Fully Developed Velocity Profile

L'= 0, Ψ = 15°	
Re	L_3/mm/
from 2500 to 483	not obs.

L'= 0, Ψ = 90°	
Re	L_3/mm/
2500	not obs.
1835	
1450	
1240	+12.7
1110	+12.7
900	+12.7
812	+12.7
650	+12.7
453	not obs.

L'= 0, Ψ = 180°	
Re	L_3/mm/
2500	+25.4
1835	+19.0
1450	+14.9
1240	+19.0
1110	+20.6
900	+12.7
812	+15.9
680	+12.7
485	+12.7

L'=3.15, Ψ =15°	
Re	L_3/mm/
2500	-68.2
1835	-64.3
1450	-64.3
1240	-74.6
1110	-68.2
900	-74.6
812	-74.6
650	-68.2
453	-68.3

L'=3.15, Ψ =90°	
Re	L_3/mm/
2500	-73.2
1835	-74.6
1450	-74.6
1240	-74.6
1110	-74.6
900	-74.6
812	-74.6
650	-68.2
453	-68.2

L'=3.15, Ψ =180°	
Re	L_3/mm/
2500	-68.3
1835	-74.6
1450	-74.6
1240	-74.6
1110	-74.6
900	-74.6
812	-74.6
550	-68.2
444	-60.3

Table A.15 Dependance of L_5 on L', Ψ and Re for a Fully Developed Velocity Profile

L'= 0, Ψ = 15°	
Re	L_5/mm/
2500	-7.9
1835	-7.1
1450	-3.2
1240	0
1110	+19.0
900	not obs.
812	
650	
453	

L'= 0, Ψ = 90°	
Re	L_5/mm/
2500	-9.5
1835	-3.2
1450	0
1240	+2.4
1110	+2.4
900	+6.3
812	+9.5
650	not obs.
453	

L'= 0, Ψ = 180°	
Re	L_5/mm/
2500	-14.3
1835	-14.3
1450	-15.9
1240	-15.9
1110	+14.3
900	+13.5
812	-11.1
680	-9.5
485	-4.8

L'=3.15, Ψ =15°	
Re	L_5/mm/
2500	-7.9
1835	-7.1
1450	-4.0
1240	-1.6
1110	0
900	0
812	+4.8
650	not obs.
453	

L'=3.15, Ψ =90°	
Re	L_5/mm/
2500	-12.7
1835	-8.0
1450	-4.0
1240	-2.4
1110	-0.8
900	-1.6
812	-1.6
650	+7.9
453	not obs.

L'=3.15, Ψ=180°	
Re	L_5/mm/
2500	-15.9
1835	-8.5
1450	-4.0
1240	0
1110	0
900	-1.6
812	0
550	0
444	+2.4